Università degli Studi di Palermo
DIPARTIMENTO DI SCIENZE
DELLA TERRA E DEL MARE
(Di.S.Te.M)

Ph.D. in Geochemistry

PhD course in Geochemistry - XXIV Cycle (GEO/08)

BROMINE DEGASSING IN BASALTIC VOLCANIC SYSTEMS

Ph.D. thesis by

Michela Costa

Supervisors:

Prof. Alessandro Aiuppa

Dr. Antonio Paonita

PhD. Coordinator:

Prof. Francesco Parello

Jan 2011 – Dec 2013

Università degli Studi di Palermo
DIPARTIMENTO DI SCIENZE
DELLA TERRA E DEL MARE
(Di.S.Te.M)

Ph.D. in Geochemistry

PhD course in Geochemistry - XXIV Cycle (GEO/08)

BROMINE DEGASSING IN BASALTIC VOLCANIC SYSTEMS

Ph.D. thesis by

Michela Costa

Supervisors:

Prof. Alessandro Aiuppa

Dr. Antonio Paonita

PhD. Coordinator:

Prof. Francesco Parello

Reviewers:

Dr. Giada Iacono Marziano (Institut des Sciences de la Terre d'Orléans - ISTO))
Dr. Bruno Scaillet (Institut des Sciences de la Terre d'Orléans -ISTO)

Jan 2011 – Dec 2013

Abstract

Volcanic halogens play a central role not only in magmatic systems processes but also in atmospheric chemistry, since they have been shown to participate in several reactions implicated in tropospheric O_3 destruction. Unfortunately, relevant data (e.g., solubility, vapor–melt partitioning) required to model halogen behaviour have been in large part lacking, so that our current state of knowledge concerning Br is still rather poor. This work has been mainly aimed to develop a model to interpret bromine behaviour during degassing in basaltic volcanic systems. This goal was achieved through three different approaches: a) measurements of bromine contents in volcanic plumes by filter-packs techniques; b) measurements of initial bromine abundance in a set of olivine-hosted melt inclusions from Etna and Stromboli volcanoes by synchrotrone analysis; c) bromine melt/fluid partitioning coefficient ($D_{Br}^{m/f}$) experiments by rapid-quench in Internally Heated Pressure Vessel carried out at ISTO-CNRS of Orléans. This last was a fundamental step to experimentally investigate Br melt/fluid distribution between a basaltic melt (Mt. Etna) and a coexisting fluid phase containing H_2O and known concentrations of Br, which has not been investigated yet in basaltic melts.

The informations obtained by linking together results from both bromine measurements in volcanic gases and in melt-inclusions and from experimental runs, were used to extends the Aiuppa (2009) model approach to bromine to interpret S-Cl-Br compositions that could explain the large variability of volcanic S-Cl-Br gas compositions and so, the mechanism through which bromine is fractionated relative to other volatiles during volcanic degassing. In spite of the mechanism of Br release upon magma ascent and degassing remain a puzzling matter, and further data are extremely required, our study contributes to achieve an advance in the current state of knowledge, since no experimental data on $D_{Br}^{melt/fluid}$ in basaltic melts have ever been obtained so far.

1. Introduction

1.1 The importance of halogens in volcanic emissions context p 7
1.2 Aim and strategy of this work " 9
1.3 Focus on ozone depletion: the role of BrO " 11

2. Halogen contents in terrestrial reservoirs

2.1 General properties of halogen p 15
2.2 Signs on the role of D in distribution of Br " 16
2.3 Halogens contents in terrestrial reservoirs " 17

3. Melt inclusions: description and preparation

3.1 The importance of melt inclusion " 23
3.2 Melt inclusions set analysed " 24
3.2.1 Stromboli MIs set " 25
3.2.2 Etna MIs set " 30
3.3 Samples preparation " 31

4. Experimental and analytical techniques

4.1 Gas measurements
4.1.1 filter packs technique " 34
4.2 Experiments by IHPV
4.2.1 Introduction " 37
4.2.2 Starting material " 38
4.2.3 Preparation of solutions " 38
4.2.4 Preparation of capsules " 39
4.2.5 Experiments by IHPV " 41
4.2.6 Creation of a set of Br synthetic standard glasses " 43

4.2.7 Partitioning experiments " 44
4.1.8 Opening capsules and preparation of the mounts " 45

4.3 Analytical methods
4.3.1 Homogeneity of the glasses " 47
4.3.2 Major elements analyses on standards glasses: EMP " 48
4.3.3 Br mesurements on high-concentrated synthetic glasses: INAA " 50
4.3.4 Measurements on low concentrated glasses: Sy-XRF " 53
4.3.5: Laser Ablation – ICP-MS " 58

5. Results and discussion
5.1: Gas data set " 69
5.2: Partitioning experiments " 79
5.3: Melt inclusions " 85
5.3.1: Br abundances in MIs " 85
5.3.2 Br vs MI differentiation indexes " 88
5.3.3 Br vs other volatiles in MIs " 91
5.3.4: Br in Etna and Stromboli MIs in a broader context " 94

6. Bromine degassing model
6.1: Br degassing model " 102

7 Summary and conclusions " 111

8 References " 115

9 Acknowledgements " 126

Chapter 1
Introduction

1.1. The importance of halogens in volcanic emission context:

Understanding the chemistry of atmospheric volcanic plumes is important for evaluating eruption hazards and for measuring the atmospheric and environmental impacts of volcanic emissions (Kelly et al., 2012). In fact emissions of volcanic gases provide valuable information to understand volcanic processes giving both a warning sign and an indication of the nature of the corresponding lava (Bobrowski et al., 2003). They exert significant effects on properties of melts (e.g., diffusion, viscosity, phase equilibria), trigger volcanic eruptions and control the eruptive style (Baker et al., 2008).

Also, volcanic emissions are persistent and significant sources of reactive volatiles to the Earth's atmosphere that can have local, regional and global effects, both on short and longer time scales (Bobrowski et al., 2003; Bobrowski et al., 2007).

Among the gaseous volatile emitted by volcanoes, halogens have been a matter of growing interest in the last decades. Their chemical group is only the fourth most abundant type of volatile component in volcanic emissions, after water, sulphur and carbon dioxide but however, in spite of their low concentrations in volcanic gases and plumes, halogens play a central role in studying the evolution of magmatic systems. They have been shown to contain useful information on volcanic subsurface processes contributing to volcanic hazard assessment (Aiuppa, 2009). The reason lies in the different solubilities of halogens respect to other major species, resulting in a progressive compositional changes of the gas phase in function of the depth and the dynamics of magma degassing. Halogens, in fact, because of their high solubility, remain in the melt after CO_2 and SO_2 have left and they start to separate and release from ascending magmas at relatively shallow depths (typically at pressures low than 50 MPa in basaltic magmas; (Aiuppa, 2009).

So, the increasing ratio between halogens and sulphur in volcanic gases is an indicator of changing activity of a volcano and can provide insights into pre-eruptive and syn-eruptive volcanic degassing, thus contributing to volcano monitoring (Aiuppa, 2009; Bobrowski et al., 2007; Alletti et al., 2007).

Recent and known examples occurred both at Etna and both at Stromboli volcano showing the close link between the variation in S/halogen ratio and the changes in eruption dynamics and degassing mechanisms. In the eruptive volcanic plume of the October 2002 – January 2003 eruption of Mount Etna, the recurrent sampling of plume acidic volatiles by filter-pack methodology revealed that plume S/Cl ratios increased by a factor of ~10 as volcanic activity drifted from paroxysmal lava fountaining to passive degassing and minor effusion, and then decreased to the low values (S/Cl = 0.1) typical of the final stages of the eruption (Aiuppa et l.,a 2004). Authors suggested that the increase in the S/Cl ratios was probably due to a new input of a magma body approaching the surface and consequent shallower degassing.

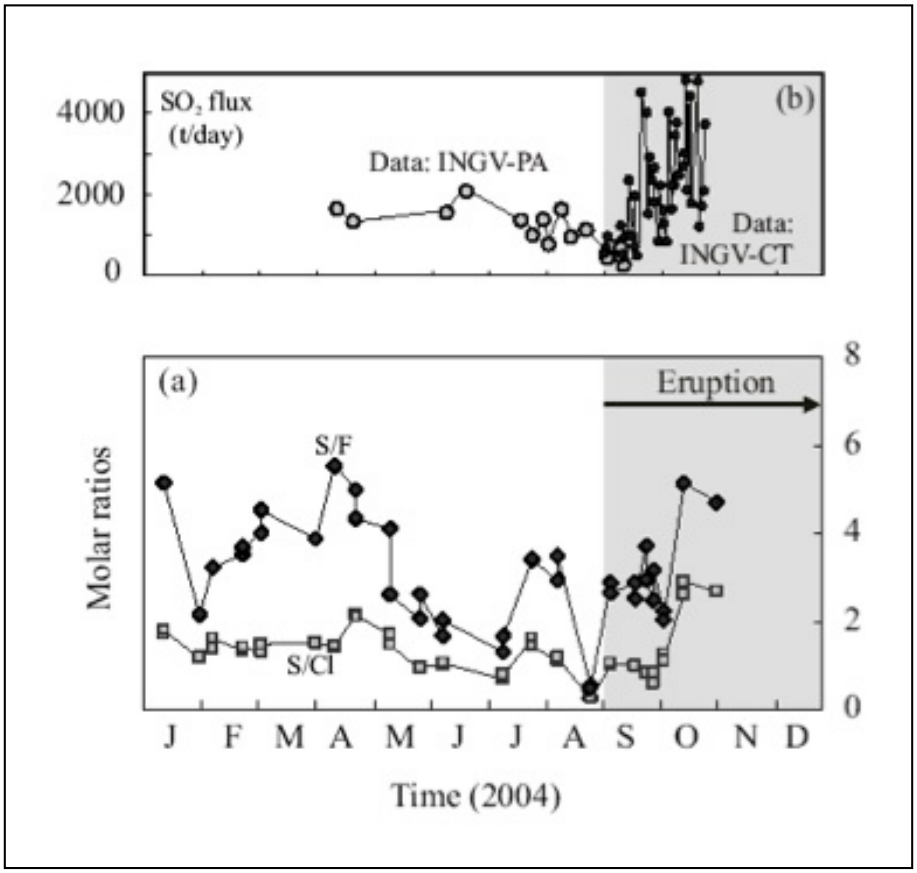

Figure 1.1: (a) Variations in sulfur to halogen molar ratios in Etna's North-East crater plume between January and October 2004 ; (b) SO2 fluxes, measured by differential optical absorption spectroscopy [Aiuppa et al. , 2004].

Also, reconstruction of the melt degassing history may be carried out by relating the halogen concentration in glass at different degassing steps. Since accurate measurements of H_2O concentrations in glasses of erupted material (melt inclusions, matrix glasses) is often a difficult task, halogens may represent a good helpful tool to identify and trace degassing processes(Balcone-Boissard et al., 2010).

Another essential aspect that emphasizes the importance of halogens is from an atmospheric point of view. For a long time, in fact, it was assumed that these gases would behave rather passively within the plume and in the atmosphere. But in the last decades several recent studies highlighted that tropospheric volcanic plumes are chemically active and that relatively non-reactive hydrogen halide gases (e.g. hydrogen bromide, HBr) emitted from volcanoes can be rapidly converted into reactive halogen species (e.g. bromine monoxide, BrO) by in-plume heterogeneous chemical processes (Bobrowski et al., 2003; Bobrowski et al., 2007; Kelly et al., 2012; Gerlach, 2004; Oppenheimer et al., 2006). So, halogens released from volcanoes can exert a deep impact on the atmosphere and hydrosphere, perturbing the tropospheric and stratospheric ozone budgets and contributing to the development of acid rain, volcanogenic air pollution or acidification of soils and surface waters (Aiuppa 2009).

1.2 Aim and strategy of this work

Considerations above highlights the importance of volcanic Br in tropospheric processes, and strongly suggest that volcanoes may seriously impact with dramatic effects the chemistry of the atmosphere by causing localized small ozone "holes" in the vicinity of active volcanoes (Aiuppa, 2009; Bobrowski et al., 2003a).

Unfortunately however, even though we have recognised the importance of halogens in magmatic processes and, more recently, their impact on atmospheric chemistry, our knowledge of halogen behaviour in magmatic systems (especially Br and I) is still rather poor (Baker et al., 2009; Aiuppa et al., 2009; Baker et a., 2009; Pyle and Mather, 2009), to the point that a quantitative knowledge of the mechanisms controlling Br degassing from subaerial volcanism is currently impossible.

Estimate of the nature and the extent of total Br degassing from volcanoes, in fact, is considerably less well constrained than other species due to its really low abundances (Bobrowski et al., 2003).

Many physical parameters are still largely unknown such as bromine solubility and diffusivity in silicate melts as a function of temperature, pressure and melt composition and their vapour/melt partitioning coefficients during volcanic degassing (Alletti et al., 2007; Alletti et al., 2009). As such, our understanding of the mechanisms of halogen degassing from volcanoes is still fragmentary.

The main purpose of this work is to develop an exhaustive quantitative halogens behaviour model in magmatic system, which attempt to interpret volcanic gas composition in terms of halogen partitioning between silicate melts and a magmatic vapour phase upon the ascent and degassing path of magma.

To achieve this goal, the improvement of our knowledge on pre-eruptive halogen concentrations in silicate melts is mandatory. So, since no comparable Br data in basaltic melt inclusions is currently existent in literature the first important step is to gain accurate information about initial Br abundances in basaltic magma. This would require to achieve reliable measurements of Br contents in primitive (basaltic) silicate melt-inclusions trapped in crystals, which have never been obtained since so far, due to the their extremely difficulties. In fact, microprobe techniques to determine Br by in-situ spot analyses in natural samples are not yet routinely used, due to concentrations near detection limits of most available techniques (EMP, LA-ICP-MS, PIXE) and/or lack of suitable reference materials (Wehrmann, 2005).

Once we have obtained information regarding magma pre-degassing composition, next step are the acquisition of more information as possible concerning Br parameters that are still unknown, especially bromine $D^{melt/fluid}$ partitioning coefficient. This has been carried on through melt-fluid partitioning experiments on a basaltic etnean melt and a coexisting fluid phase.

The final purpose is to link together analytical studies of natural systems with measurements of halogen transport in volcanic gases and partitioning between melt and fluid phases, that would open the way to constraints Br role in magmatic systems (aiuppa et al., 2009).

Sure, the goal of this study is to be not the ending but the starting point for developing empirical models that not only will predict the diffusion of halogens, but also the effect of halogens on the diffusions of major elements. Although further measurements on partition

coefficient and diffusion of heavier halogens (Br and I) in different melt compositions are required, we expect our results would have a high impact on the geochemical and petrologic communities.

In this study we focus on two important case of study: Etna and Stromboli volcanoes. Mount Etna, with its persistent open conduit degassing activity, the frequent eruptions and the impressive budget of emitted volatiles is a unique site to characterize volcanic degassing halogens (Aiuppa 2009). As well as Stromboli, its magmatic system can be reliably studied by combining crystal melt inclusion studies with data obtained by the multidisciplinary monitoring network developed by INGV (Spilliaert et al., 2006; Aiuppa et al., 2002).

1.3 Focus on ozone depletion: the role of BrO

Reactive halogen species (X, XO, X_2, XY, OXO, HOX, $XONO_2$, XNO_2, where X, Y=Cl, Br, or I), especially those that contain bromine, can rapidly destroy ozone (O_3), alter common atmospheric oxidation pathways, and increase the deposition of toxic metals like mercury to the surface (von Glasow et al., 2009; Kelly et al., 2012).

BrO, in particular, plays a key role in atmospheric chemistry, by participating in complex reactions in the troposphere implicated in ozone destruction (Bobrowski et al., 2007; von Glasow et al., 2009).

The idea that in-plume BrO formation and O3 destruction could be important aspects of volcanic plume chemistry was first proposed by Bobrowski et al., 2003, evaluated from a high-temperature thermodynamic perspective by Gerlach, 2004, and assessed from a kinetic standpoint by Oppenheimer et al., 2006.

BrO, a very reactive halogens compound, was detected at a volcanic site for the first time by Bobrowski et al., 2003 in the plume of Soufriere Hills volcano (Montserrat) in May 2002, by a ground-based passive optical absorption technique Multi-Axis Differential Optical Absorption Spectroscopy (MAX-DOAS). This first observation was followed by the detection of BrO at several other volcanoes (Lee et al., 2005; Oppenheimer et al., 2006; Boichu et al., 2012). This further demonstrates that Soufriere Hills is not an exceptional volcano with respect to emission of reactive bromine. Bobrowski et al., 2003 unexpectedly measured high mixing

ratios of about 1 ppb of BrO, the highest BrO mixing ratios measured so far in the atmosphere (Von Glasow et al., 2009).

BrO is not emitted directly from magma, but is formed from hydrogen halides (e.g., HCl and HBr) as a result of heterogeneous chemical reactions during plume transport and mixing with background air.

Many heterogeneous reactions are involved in formation of BrO in volcanic plumes and in the activation of ozone depletion mechanism. The whole process is known as "bromine explosion" and it is the result of a complex sequence of reactions taking place into the plume (Bobrowski et al., 2003; von Glasow, 2009; Kelly et al., 2012). The main chemical reaction sequence is summarized below:

1) $HOBr(gas) \rightarrow HOBr\ (aq)$

2) $HBr\ (gas) \rightarrow Br^-\ (gas) + H^+(aq)$

3) $HOBr(aq) + Br^-\ (aq) + H+(aq) \rightarrow Br_2\ (gas) + H_2O$

4) $Br_2 + hv \rightarrow 2Br$

5) $Br + O_3 \rightarrow BrO + O_2$

6) $BrO + BrO \rightarrow 2Br + O_2$

7) $BrO + BrO \rightarrow Br_2 + O_2$

8) $BrO + H_2O \rightarrow HOBr + O_2$ (Von Glasow et al., 2009)

First process involves gas phase reactions so that, for pH<6, gaseous HOBr and HBr are taken up onto acidic particles (1-2); HOBr interacts with acid aerosol through an acid-catalyzed aqueous-phase reaction to form Br_2 or BrCl gas species (3); further rapid photolysis of Br_2 (4) and subsequent reaction with O_3 sourced by entrainment of ambient air, generates BrO (5); O_3 destruction can be sustained by the BrO self-reaction and reaction of BrO with H_2O (8) allows the cycle to repeat (Boichu et al., 2011; Kelly et al., 2012). Each autocatalytic cycle doubles the BrO concentration which can lead to rapid, non-linear increases of BrO in volcanic plumes and significant O_3 destruction.

Several other reactions are involved in this complex process (including NOX interaction or

combined chlorine-bromine interaction that can be regarded as a synergetic effect of Br explosion (Halmer et al., 2002).

Evidences confirming that photochemical processes are a key for BrO formation are recent measurements with an active DOAS instruments at Masaya showing the presence of BrO only at daytime (Bobrowski et al., 2007).

In spite of the difficulty in measurements, several recent studies have reported observations of low O_3 in tropospheric volcanic plumes and have showed that their observations were a consequence of in-plume bromine chemistry (Oppenheimer et al., 2010; Boichu et al., 2011; Kelly et al., 2012). Their results highlight important aspects of in-plume chemical and dynamic processes and provide insights that will be useful for better understanding O_3 anomalies and reactive halogen chemistry in volcanic plumes.

The idea that BrO is not directly emitted by volcanoes but it is produced inside the plume, as a secondary gas, is strongly supported by BrO/SO_2 measurements of Oppenheimer et al., 2006 an Bobrowski et al., 2007). In fact they observed an increasing of BrO/SO_2 with distance from the crater and, being SO_2 a passive tracer, this indicates a chemical production of BrO in the plume (Von Glasow et al., 2009).

According to this, as BrO concentration increases, O_3 concentration decreases, due to its implication in the set of reactions summarised above.

Boichu et al., 2010 pointed out how the "Bromine explosion" process can be fast: the 15-30% of the total available Br at the crater rim (i.e., the sum of HBr gas phase and particulate Br, both sampled with filter packs) is converted in BrO in about 1-3 min.

Also, Bobrowski et al., 2003 reported that Br, despite being two orders of magnitude less abundant than chlorine, is several times more efficient in O_3 destruction: 1ppb of BrO can destroy about 10 ppb of O_3 per minute. So, if we consider that large-scale climatic eruptions (e.g. Pinatubo 1991, Agung 1963, El Cichòn 1982) can release, in a single event, amounts of bromine comparable to the total annual influx of bromine into the stratosphere from all other natural and anthropogenic sources (Bureau et al., 2002; Aiuppa et al., 2005) it is easy imagine how volcanoes may seriously impact the chemistry of the atmosphere.

Chapter 2

Halogen contents in earth reservoirs

2.1 General propierties of halogen

Halogens (F, Cl, Br, I, At) are nonmetals elements from group 17 of the periodic table (formerly VII, VIIA). They are rarely found in nature in their free elemental states, and are more usually combined as halide ions (X^-) in salts, solutions and gases (Pyle, Mather, 2008).
As a group, halogens exhibit highly variable physical properties. They are the only periodic table group ranging from solid state (I_2) to liquid state (Br_2) to gaseous state (F_2 and Cl_2) at room temperature. This is due to the increasing boiling points of halogens down the group since also strength of Van der Waals forces, size and relative atomic mass of the atoms increase too.
The chemical properties are more uniform. Due to their particular electronic shell configuration (1 electron missing from their outer shell) halogens are known to have very high degrees of electron affinity and low dissociation energies. As a result, their ability to gain electrons is very high so as their ability to easily break up, or dissociate, into atoms and then combine with other substances. This fact makes them extremely reactive group of elements, specially with alkali metals and alkaline earths. As their electronegativities and electron affinities decrease from fluorine (the smallest one) to iodine (the largest one) their reactivities also decrease, making F the most reactive of the halogens (Aiuppa et al., 2009).
Chlorine, bromine, and iodine are progressively less reactive but still form compounds with most other elements.

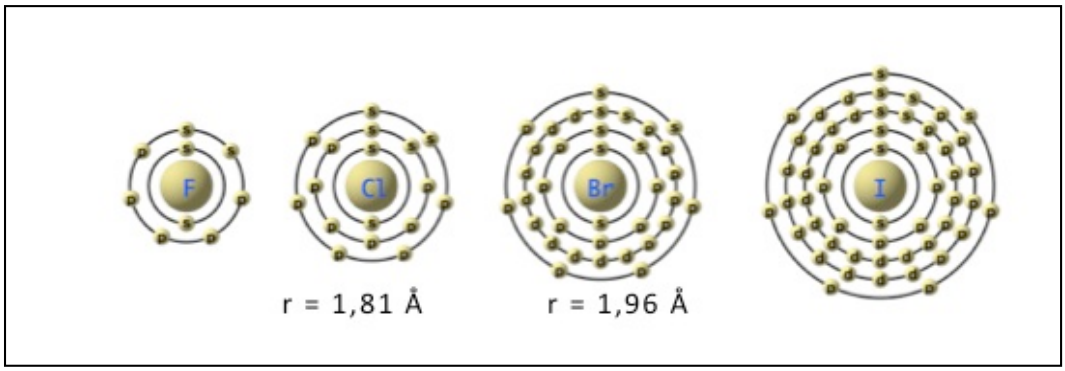

Figure 2.1: Sketch of compared halogen ionic radius.

2.2 Signs on the role of D in distribution of Br

There is a large lacking of information around halogens (specially the heaviest Br and I); several parameters in fact are still unknown and until this gap has not been filled, it will not be possible to reach any exhaustive understanding of the role played by halogens in volcanic processes.

A parameter which must absolutely be investigated is the melt-gas partition coefficient. This parameter is used to describe the behaviour of the volatile component in the fluid and in the melt during crystallization and partial melting. It is closely related to solubility and refers to the relative distribution of a component between two phases (usually at equilibrium). Partitioning is commonly quantified by the Henrian partition, or distribution, coefficient, $D^{melt/fluid}$, which is calculated by dividing the concentration of a species in one phase by its concentration in the other species (Baker and Alletti, 2012).

Dealing with halogens, it is known as they behave almost simply during magmatic differentiation and degassing because they generally have low mineral/melt partition coefficients and high H_2O vapour/melt partition coefficient (Balcone- Boissard et al., 2010).

Several studies have been focused on the Cl partitioning coefficient determination both in silicic magmas (e.g. Shinohara et al., 1989; Metrich and Rutherford, 1992; Signorelli and Carrol, 2000, 2001; Webster et al., 2009), both in basaltic melts (Alletti et al., 2009).

Experimental data show as in high differentiated melts generally halogens are high soluble and their volatile behaviour is mainly controlled by H_2O degassing (Balcone- Boissard, 2010).

Alletti et al., 2009 report a D fluid/melt for Cl in H_2O+Cl-bearing experiments ranging between 11–14 at 1 and 25 Mpa to 6 at 200 MPa at NNO. This value highlights the incompatible behaviour of Cl and confirms that Cl has a high affinity for the H_2O-bearing vapor phase exsolved by decompressing basaltic magmas upon ascent in the upper crust. Also, they demonstrated that Cl partitioning between fluid and melt ($D_{Cl}^{f/m}$) is highly dependent on the composition of the fluid phase and, on pressure and oxygen fugacity. So, their measurements provide the basis for a better understanding of the modes, timing and rates of Cl degassing in basaltic systems, which have been a matter of increasing interest in recent years (Spilliaert et al., 2006b, Aiuppa et al., 2009; Alletti et al., 2009). Considering Br, $^{fluid/melt}$ D has been determined by Bureau and Metrich, 200; Bureau et al., 2010, in synthetic glasses

from albitic ($NaAlSi_3O_8$) composition. They report a $D^{f/m}$ in the range of 44 up to >100. This is coherent with the incompatible behaviour the Br is expected to have, due to the ionic radius, even larger than Cl. In fact, the heavier is the halogen, the more incompatible is its behaviour, due to the big ionic radius (Pyle and Mather, 2009; Kendrick et al., 2012).
Unfortunately no analogue informations regarding basaltic composition have been produced for Br since so far. In order to draw at the best a complete degassing picture of halogens, scientific communities strongly need to achieve more information regarding Br behaviour in magmas especially at Mt. Etna that is the most active volcano in Europe and with a massive persistent degassing activity.

Even if this study can not be considered a goal, concerning Br partitioning investigation, it aims to give a first estimation of $D^{melt/fluid}$ and it could be a starting point for further considerations.

2.3 Halogen in terrestrial reservoirs

Little progress has been made in quantifying the distribution of halogens in the major terrestrial geochemical reservoirs (volcanic rocks, volcanic degassing fluxes, oceans, atmosphere). In part, this reflects the challenges of analysing species (such as Br, I) which are only present in very low concentrations (ppb) in the Earth's mantle (Pyle and Mather, 2009). Also, there is a still-open debate about halogens origin, if they are originated by mantle out-gassing, or accretion of a volatile-rich late veneer (Kendrick et al., 2012 and references therein). Generally, there is common agreement that halogens are strongly concentrated in Earth's surface reservoir (sediments, hydrosphere and atmosphere). Many halogen-bearing compounds are volatile (e.g. the halogen halides, HX, and halocarbons), while others are soluble in aqueous fluids. As a consequence, the halogens are distributed between the various terrestrial geochemical reservoirs, with distribution patterns that have been influenced by transport between these reservoirs over geological time (Pyle and Mather , 2009).
As we already focused, in spite of anthropogenic surface emission of halogen in atmosphere could be significant, volcanoes contribute considerably as punctual halogens sources.
Both the sustained "quiescent" degassing of volcanoes and sporadic explosive eruption

contribute significant quantities of reactive gases and aerosol to the atmosphere. Each year million of tons of volatiles are released into the atmosphere by volcanic activity either by active or passive degassing (Boichu, 2011). Specially the large-magnitude subaerial plinian eruptions are able to inject the plume high up to the stratosphere, where reactive halogens radicals will take part to several catalysts reactions. Once in the stratosphere, the plume can be dispersed around a whole latitude band within weeks (Von Glasow, 2009). So, the residence time of water-soluble gases emitted into the atmosphere strongly depends on the height of the eruption column (Halmer et al., 2002) so that higher is the input in the atmosphere, longer is the time until volcanic gases would be removed.

Solubility is a key parameter controlling the abundance of a compound in atmosphere. The magnitude of the volcanic HCl input into the stratosphere (the amount of HCl that reaches the atmosphere) has been suggested to be less than 1% of the emitted HCl. This is due to very efficient removal in precipitation because of the high solubility of HCl (Von Glasow et al., 2009). So, even being less abundant than Cl, Br stays longer in atmosphere because of its lower solubility and for this reason Br is considered to be about hundred times more efficient than Cl in ozone depletion reactions (Wehrmann, 2005;).

In addition, possible interactions between halogen species that intensify the effects cannot be ruled out, and little is yet know about residence times of the elements at the various stratospheric altitudes. The effect of heavy halogens on stratospheric chemistry might still be underestimated, and Br and I should be considered for hazard assessments that include climatic aspects (Wehrmann, 2005).

As revealed by their exceedingly high concentration in the crust (525 ppm F, 1900 ppm Cl, 6.95 ppm Br and 1.54 ppm I; Aiuppa, 2009 and reference therein) halogens are strongly incompatible element**.** Bromine, due to its huge ionic radius, was likely incorporated into the Earth during the late stage of accretion like other volatile elements and then it was extracted from the mantle during the process of continental crust formation and probably also during the early stages of the equivalent of present-day oceanic crust formation (Deruelle et al., 1992). In sedimentary environments, bromine and iodine are commonly associated with organic materials. Muramatsu and Wedepohl, 1998 and Martin et al., 1993 analysed a large series of samples from different part of the Earth's crust and their results show that crustal Br and I are greatly concentrated in the sedimentary shell of the Earth, and preferentially in organic-

bearing argillaceous sediments and marine sediments in general. Due to decay of organic materials on the ocean floor, marine sediments could be strongly Br enriched compared to terrestrial organic sediments (up to 205 ppm; Martin et al. 1993). Their contents generally decrease with increasing depth of burial, due to more complete decomposition of organic bromine and iodine compounds and the release of Br and I into pore fluids. Processes such as trapping of pore fluids in thick, organic-rich sediments can lead to extreme Br and I enrichment (Martin et al., 1993). As Br at the Earth surface is specifically concentrated in sediments, this elements could be a potential tracer of sediment recycling into the mantle (Déruelle et al., 1992).

Magmatic abundance of halogens, and other volatiles in general, are commonly determined through analyses of volcanic matrix glasses and silicate melt inclusions (Aiuppa et al., 2009). If Cl and F could be found sometimes even as "major" species in magma (ppm to % concentration) Br and I occur only as trace components given their ppb to ppm abundance ranges. Magmatic F concentrations vary widely depending on the tectonic environment and the type of volcanic system involved. The lowest abundances typically occur in glasses of basaltic rocks from oceanic island and ocean ridge environments. Most contain only from tens up to one thousand ppm F. The highest concentration (F > 5-7 %) was recorded in some felsic evolved volcanic and plutonic environments as in melt inclusions from highly differentiated granitic plutons (Aiuppa et al., 2009 and reference within). These elevated concentrations of F are atypical, but they can occur because F generally behaves as an incompatible element.

As fluorine, also chlorine in magmas shows significant variability depending on the tectonic environment and magma composition. Chlorine concentrations of most basalts and melt inclusion glasses from oceanic-rift and -island environments are generally low and similar to those of F. Chlorine in these environments is generally < 800 ppm. However felsic melt inclusions of continental high-silica rhyolites contain higher Cl abundances (≤3000 ppm), and dacitic to rhyolitic melt inclusions of subduction-related, calc-alkaline volcanoes contain up to 7500 ppm Cl. The highest abundances of magmatic Cl occur in intermediate to high-silica peralkaline magmas (Cl up to to 1.2 wt.%). Rare basaltic glasses from Hawaii containing nearly 1.7 wt.% Cl and basaltic melt inclusions of ocean islands containing up to 2.5 wt.% Cl have been reported (Aiuppa et al., 2009 and reference within).

Clearly, magmatic abundances of Br and I are typically lower than those of F and Cl for corresponding volcanic environments. Bromine, ranges from 0.1 to 0.8 ppm in crystalline basaltic to granitic rocks; and from 0.06 to 300 ppm in melt inclusions from basaltic, andesitic, rhyolitic, and phonolitic rocks (Aiuppa et al., 2009).

Bureau and Metrich, 2003 determined 10 to 28 ppm Br in natural matrix glasses and silicate melt inclusions from a series of trachytic, pantelleritic, rhyolitic, phonolitic, and shoshonitic eruptives. Wehrmann, 2005, measured 5 to 302 ppm Br in matrix glasses (although most analyses showed Br <150 ppm) and 4 to 250 ppm Br in melt inclusions from the Fontana basaltic-andesite tephra of the Masaya area of west-central Nicaragua. In these same samples Wehrmann, 2005 measured 1.7 to 18 ppm of Iodine in matrix glasses and 0.6 to 113 ppm in melt inclusions.

Current constraints on the concentrations of Br and I in magmas, however, are extremely limited and an important goal is to achieve a reasonable connection between concentration measured in melt inclusion and measured volcanic gas composition.

If we can achieve some information about halogens stored in Earth's outer reservoirs, concentrations and distributions of halogens in the mantle remain still unconstrained, since analytical studies of halogen concentrations in individual mantle minerals are very rare. Smith et al., 1981 found that the most common upper mantle minerals, olivine, orthopyroxene, clinopyroxene, and garnet, only contain halogens at or below their detection limit of 20 to 50 ppm. This estimate is similar to the range of values tabulated by Newsom 1995 for F and Cl, but much higher than the Br estimates that is expected to be very lower. The concentrations in the primitive mantle summarized by Newsom, 1995 vary from 19.4 to 28 ppm for F, from 8 to 38 ppm for Cl, from 0.456 to 0.09 ppm for Br f and from 0.0042 to 0.0133 ppm for I. These concentrations are consistent with whole mantle estimates of halogens, except that Cl may be more enriched (Aiuppa, et al., 2009).

This extremely low mantle content suggest that Br has probably been extracted from the mantle by liquids during partial melting (Déruelle et al., 1992).

A key role in the achievement of information about elements contents in the mantle are analysis of Mid Ocean Ridge Basalt (MORB) glasses. They are the first step in the cycle of oceanic crust formation and link the geochemical cycle of Earth's mantle with the surface reservoir, representing the closest available proxy for the composition of Earth's depleted-mantle (Kendrick et al., 2012).

Jambon et al., 1995 analysed Cl and Br in a set of glasses from the Mid-Atlantic Ridge and the East Pacific Rise. Cl concentrations range from 20 to 2800 ppm while Br from 62 to 1320 ppb. The significant (a factor of 140), variation of Cl contents, consistent with other published data from similar samples, may be the result of interaction with seawater (Ping, 2005). Burgess et al., 200 also estimated that the sub-continental mantle has 3 ppm Cl, 11 ppb Br, and 0.4 ppb I and that the bulk Earth has 27 ppm Cl, 108 ppb Br, and 7 ppb I; Ping, 2005).

More recently, Kendrick et al., 2012 reported first high precision simultaneous-measurements of Br, Cl and I with Cl and Br for a well documented suite of enriched glasses from Macquarie Island in the southwest Pacific. The Macquarie Island glasses have Cl concentrations that vary from 71 to 1356 ppm. This value is strongly correlated with the majority of trace elements, as well as the other halogens and K. They estimated mean depleted mantle concentrations of 10 ± 4 ppm Cl, 36 ± 16 ppb Br and 1.2 ± 1.1 ppb I. The Br inventory of the surface reservoir has been adjusted to include Br in marine sediments, which is estimated as 3 ± 2 times the sediments I content and 0.002 ± 0.001 times the Cl content. the final estimates for the Bulk Silicate Earth concentrations of 23 ± 4 ppm Cl, 82 ± 22 ppb Br and 7 ± 4 ppb I.

Chapter 3

Melt inclusion: description and preparation

3.1 The importance of melt inclusions

Silicate melt inclusions (MIs) are small (a few tens to a few hundred microns) droplets of silicate melt that are trapped within igneous phenocrystals growing in the magma. They are "primary" if containing any phase present at the time of crystal growth, or "secondary" if containing phases that enter crystals along fractures after primary crystal growth has ceased. They could be totally glassy, partially or totally crystalline, depending on the cooling-rate.

It is possible to obtain a range of unique information from primary melt inclusions since they are a kind of "geochemical fossils". In fact, because they can form at high pressures and are contained within relatively incompressible phenocrysts hosts, and assuming they become isolated from the surrounding system since the time of entrapment, MIs can preserve the pristine concentrations of volatile elements that normally escape from magmas during degassing.

As such, analysis of these inclusions, trapped at different stages of evolution of the melt, provides a detailed record about volatile contents and entrapping pre-eruptive conditions (P-T) of the bulk magma and are considered useful tools to monitoring the chemical evolution of the magmatic liquid with time (Roedder, 1984; Metrich et al., 2004; Spilliaert et al., 2006).

Sometimes MIs contain a gas-bubble (**shrinkage bubbles**) of variable volume, according with the cooling rate of the MI, as shown in figure 3.1. Shrinkage bubbles are formed during the last decompression stage of ascent when MI become saturated with a volatile phase. The contraction of the silicate melt (that has a greater thermal expansion coefficients than its host silicate crystals) generates a bubble inside the inclusion. This bubble is like a separate phase formed by immiscibility of the melt and vapor and it should contain a very little amount of gas. Its size is an important parameter for understanding cooling behaviour, composition and volatile content of the inclusion. In this study we considered both bubble-free MIs, both bubble-bearing MIs.

Since volcanic matrix glasses have normally undergone large degree of volatile loss during and after eruption, melt inclusions represent one of few practical means of sampling pre-eruption volatile chemistry in magmatic systems.

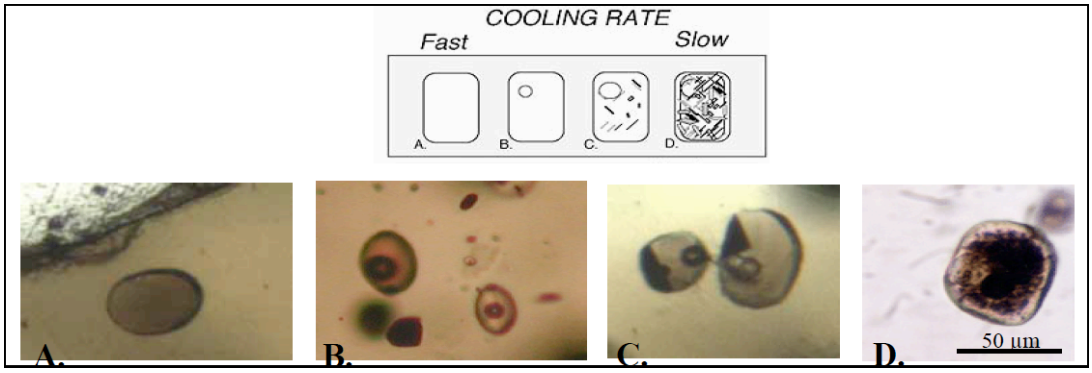

Figure 3.1: Schematic diagram and real photos of four olivine crystal-hosted MI that undergo different cooling rates. **(A)** During rapid cooling, neither crystals nor bubble form prior to cooling to the glass transition. **(B)** A bubble may nucleate during less-rapid cooling. **(C)** Diffusion during slow cooling allows the bubble to grow and the melt to partly crystallize. **(D)** Very slow cooling permits nearly full crystallization of the inclusion and growth of a layer of host mineral on the MI's wall (Modified from Rosciglione, 2008).

In this study, only MIs hosted in olivine crystals were selected. The host minerals provide important information about the forming conditions of MIs since they crystallize and trap fluids at different episodes. In basaltic systems, the most favourable conditions are offered by melt inclusion that are trapped in early formed olivine crystals and that are recovered in rapid quenched products from explosive volcanic activity (Spilliaert et al., 2006). The reason of choosing olivine as hosting phenocrysts where searching for MIs are several: (1) they are relatively abundant as phenocrysts in basaltic rocks; (2) since they crystallize earlier than the other mineral phases present in a mafic magma, olivine is is the most likely to trap primitive signature of the original parent fluids; (3) their imperfect cleavage make inclusions less subject to fracture and leakage (Rosciglione, 2008). Generally, olivines found in lapilli tephra from explosive eruptions, rather than lavas, are strongly preferred, due to their extremely fast cooling that minimize H_2O loss out of the olivine by diffusion or through cracks.

3.2 MIs set analysed

Our sample set includes Mis from different eruptions collected in two different sicilian volcanoes: Etna and Stromboli.

Concerning Stromboli we analysed Br on MIs kindly provided by N. Metrich (Institut de Physique du Globe de Paris) already analysed and studied by Metrich et al., 2001 (sample ST82) and by Metrich et al., 2010 (sample ST150307).
ST82 is a sample from pumice produced during the historical large scale paroxysm; sample ST150307 is from the last recent medium-scale paroxysm occurred on 15 March 2007.
About Etna, we selected a set of melt inclusion from recent activities (2001, 2002, 2006) both from lower and upper vent. Also, we analysed a historical eruption (sample FS, ~4 k.y. ago) kindly provided by E. Gennaro (Università degli Studi di Palermo).
We mainly focuses our measurements to inclusions that are dominated by glass and do not contain bubbles or titano-magnetite daughter crystals.

3.2.1 Stromboli MIs set

Stromboli products analysed both belong to a particular kind of eruption, so called **paroxysm**. Paroxysms are sporadic more energetic and short-lived explosive episodes(Bertagnini et al., 2008) that interrupt the typical normal Strombolian activity (a continuos streaming of gas from the crater area, low-intensity intermittent explosion). Depending on the intensitive of the event, during a paroxysm, an huge amount of magma is emitted, relative to normal strombolian activity (from 10^3 to 10^5 m^3; Bertagnini et al., 2003).
Typical signature of a paroxysm is the production of a deep-derived, low porphyritic golden pumice, rich in dissolved volatiles (>3 wt %), the so-called **LP magma** (Bertagnini et al., 2008; Francalanci et al., 2004; Metrich et al., 2001; Pichavant et al., 2009) in contrast with the shallow, crystal-rich and partially degassed black scoriae (HP magma) emitted during normal strombolian activity. In particoular sample ST82c is from a large-scale paroxysms and so it is especially suitable for MIs studies due to its rapid cooling upon eruption.
The investigated set is made of olivines grains usually tabular and nearly euhedral. Their common characteristic is their huge amount of inclusions and glass embayments, created during the growth of the crystal.
The average size of MIs range from 50 to 70 um with the largest inclusions about 200 um wide, having both sub-spherical both irregular shape and they are present as single individuals, randomly distributed in a given crystal, or as groups of inclusions. They show no signs of devitrification and no quench crystals.

These two set of MIs are well characterized by Metrich et al., 2001 and by Metrich et al., 2010. **ST82c** shows an high density of irregular, quite well-preserved MIs, inside olivine skeletal crystal with dendritic overgrowths. Mis are not crystallised and the most of them contain a shrinkage bubble. **ST150307** rapresents an intermediate-scale events occurred on 5 April 2003 and 15 March 2007.

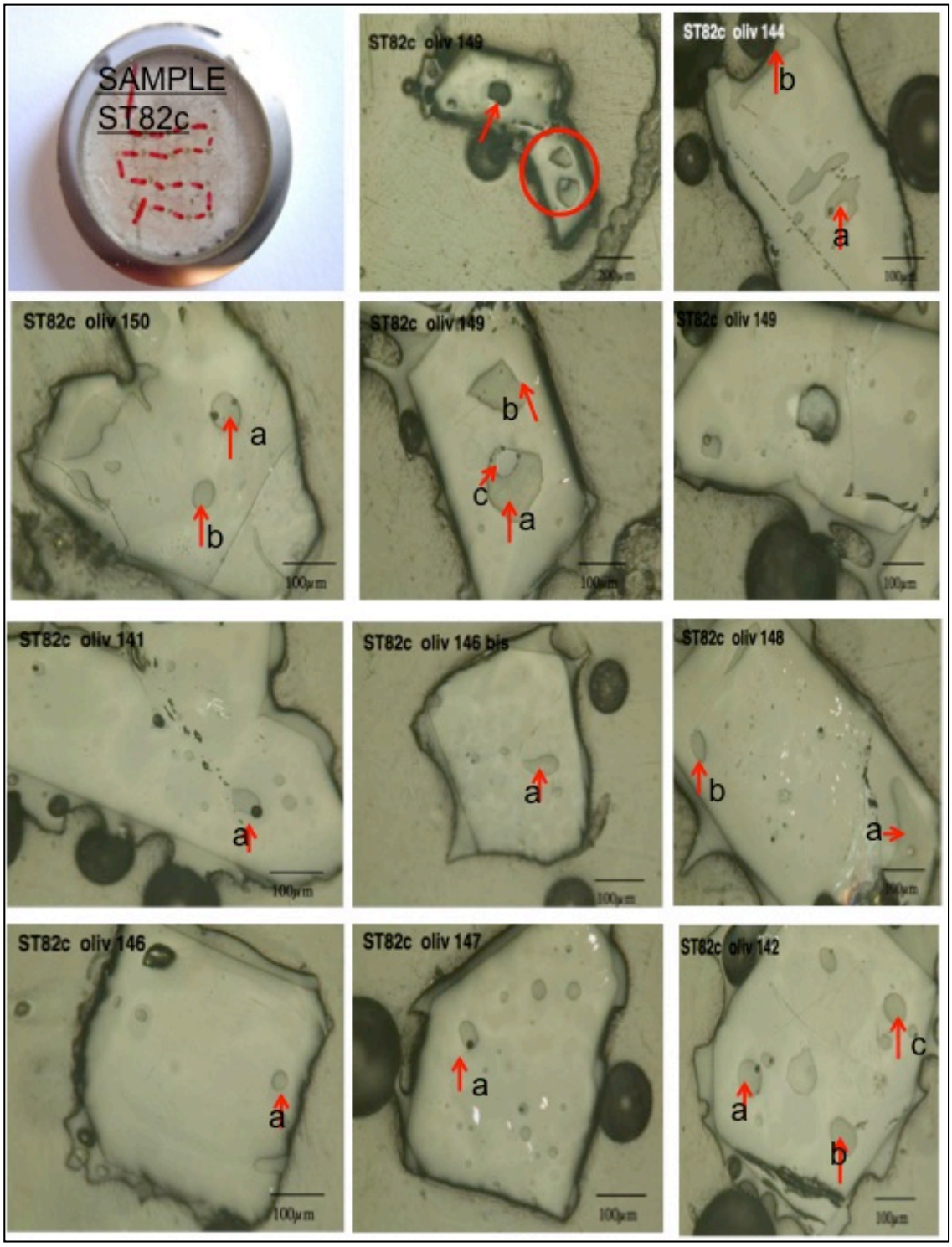

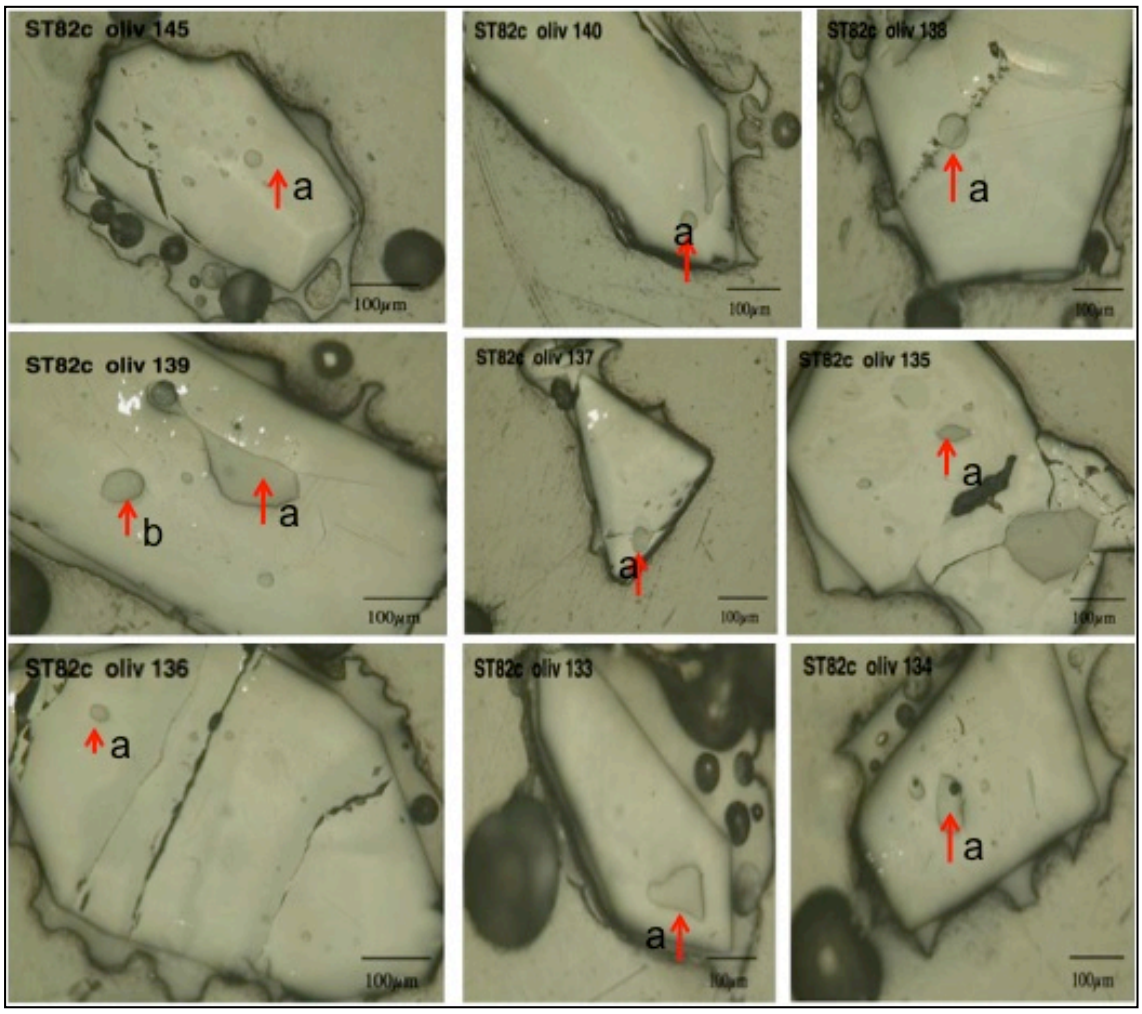
ST82c oliv 145
a
100µm
ST82c oliv 140
a
100µm
ST82c oliv 138
a
100µm
ST82c oliv 139
b
a
100µm
ST82c oliv 137
a
100µm
ST82c oliv 135
a
100µm
ST82c oliv 136
a
100µm
ST82c oliv 133
a
100µm
ST82c oliv 134
a
100µm

3.2 a

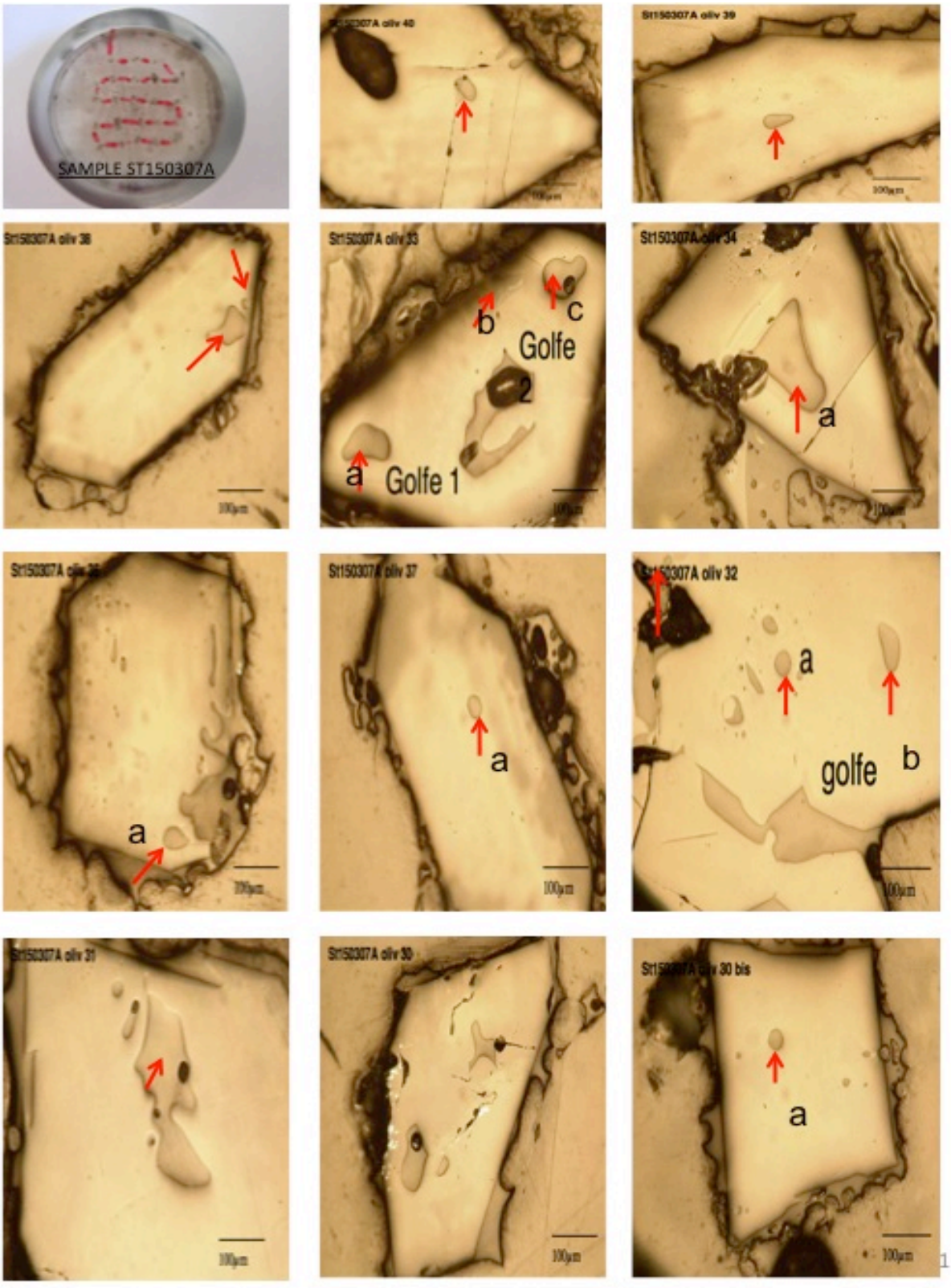
SAMPLE ST150307A
St150307A oliv 40
St150307A oliv 39
St150307A oliv 38
St150307A oliv 33
b
c
Golfe
2
a
Golfe 1
St150307A oliv 34
a
St150307A oliv 36
a
St150307A oliv 37
a
St150307A oliv 32
a
golfe
b
St150307A oliv 31
St150307A oliv 30
St150307A oliv 30 bis
a

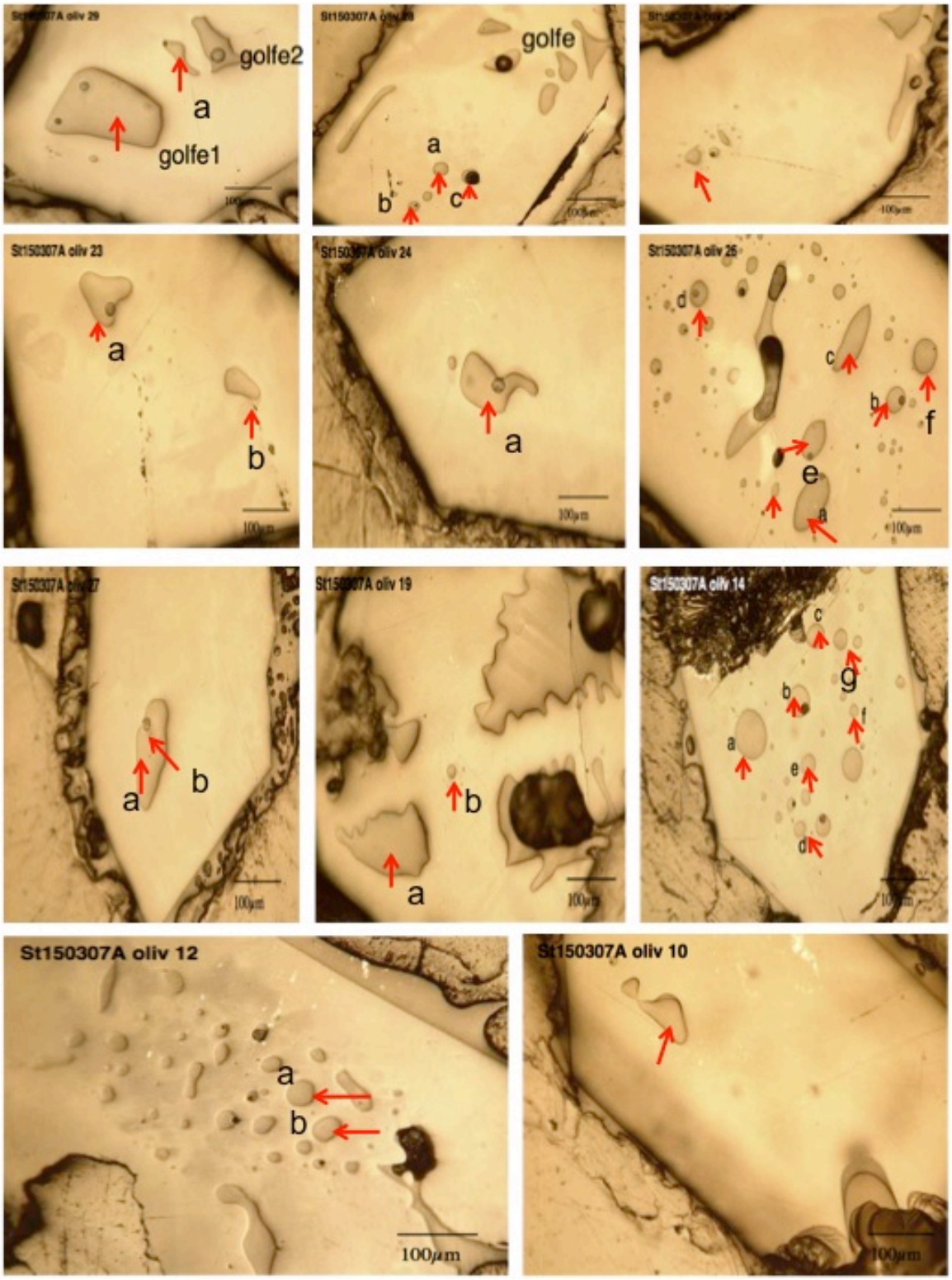

3.2 b

Figure 3.2, a-b: optical micrographs of melt inclusions and hosted-olivines in sample ST82c. (a) and ST150307 (b). Red arrows indicate melt inclusions have been analised.

3.2.2 Etna MIs set

Etna products analysed belong to two very different phase of activity of Mt. Etna: the historical eruption FS and the recent activity of 2001-2006 eruption.

FS is a fall stratified (FS) basalts ejected violently ~4 k.y. ago, classified as a sub-Plinian eruption, due to the significant heights (18–20 km) reached by its eruption column (Kamenetsky et al., 2007 and reference therein). Erupted products are highly vesiculated (30–60 vol%) scoriae containing euhedral crystals of olivine (<8%), clinopyroxene (<3%), and Cr spinel (<0.1%). High-Mg compositions of the FS olivine phenocrysts (Fo 90–91 mol% in the majority of crystals) point to the primitive unfractionated nature of their parental magmas (~13 wt% MgO, Kamenetsky et al., 2007 and reference therein).

Olivine-hosted melt inclusions in FS set were found to be very big (up to 250 um) with scalloped edges and appear as brownish glass with a spherical vapor bubble which is sometimes larger than typical shrinkage bubbles (Kamenetsky et al., 2007).

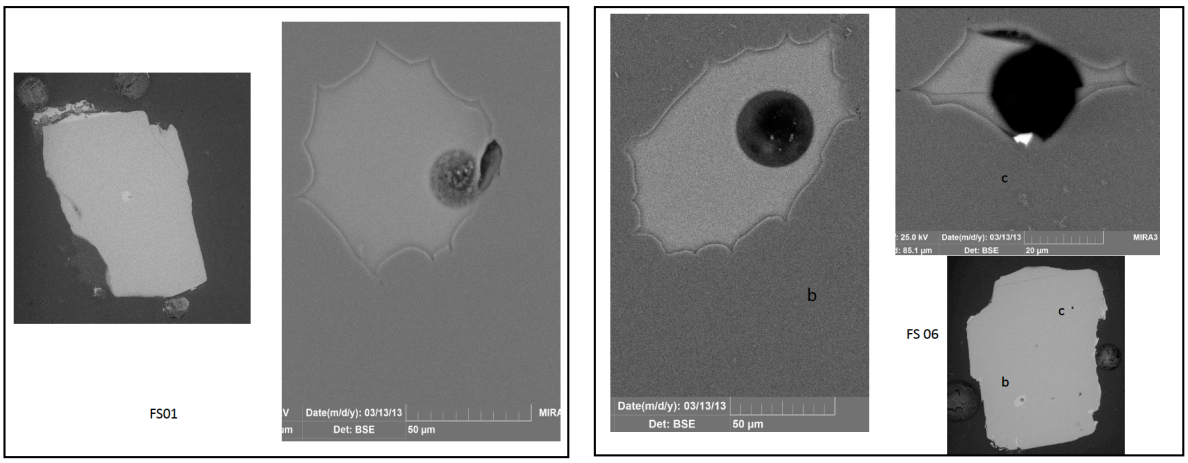

Figure 3.3: electron microscans on Fs host-olivines melt inclusions. Images are kindly provided by E. Gennaro.

MIs collected from **recent eruption** of Mt. Etna come from trachybasalts emitted during explosive activity from 2001 (LV-UV), 2002-03 south and 2006-07 flank eruptions. Here, olivine crystals selected are usually idiomorphic and varies in average sizes from 0,2 - 0,3 mm to 0,8 – 1 mm. MIs from Etna recent eruptions were found to be very small, ranging from a

few to 20-30 um in size and the most part of them seems to be partially crystallized (Fe-Ti oxides).

Some olivine crystals display reactive dissolution re-precipitation features, including irregularly embayed crystal outlines and tear-drop shaped glass inclusions. These inclusions were considered secondary and were not selected for this study.

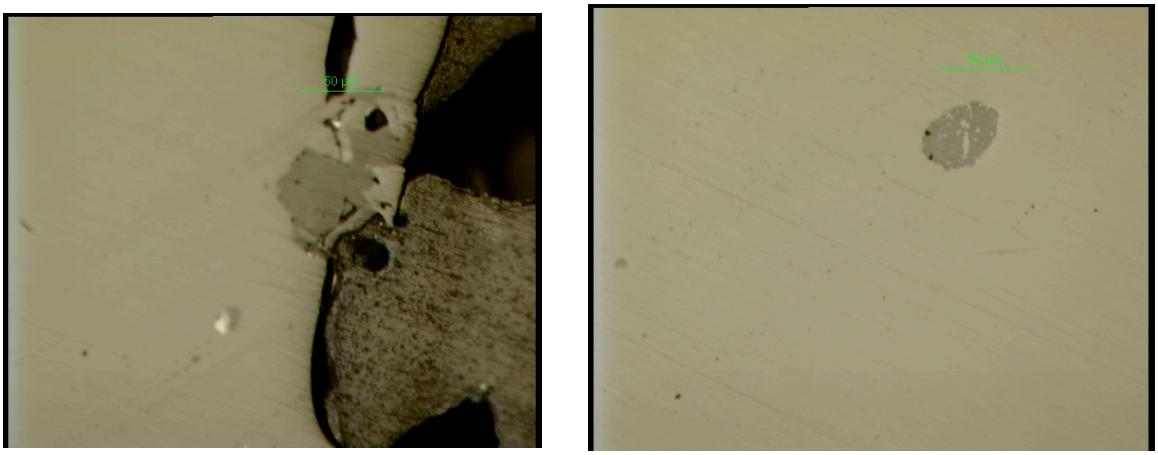

Figure 3.4: optical micrographs on Etna recent eruptions (2001 LV) host-olivines melt inclusions. Most of MIs in this set are totally or partially crystallized.

3.3 Sample preparation for analysis

Melt inclusions gas volatiles analysis are usually obtained by punctual techniques coupled with different analytical techniques such as gas or ion chromatography, atomic absorption and ICP-MS). Due to their micrometric size, analysis of MIs is a complex task and an in situ analysis technique is the best way to gain releable information from analysis of MIs (Pettke et al., 2004). Quantitative in situ spot analyses of elements in individually selected, single inclusion has been shown to be possible both by destructive (LA-ICP-MS) both by non-destructive techniques (EMPA; synchrotron X-ray fluorescence).

In this study bromine measurements on melt inclusions were performed by synchrotron-XRF at Diamond Lightsource (UK) while major elements and other volatiles were obtained by

EMPA at ISTO (FR).

Both EMPA, Synchtron XRF and LA-ICP-MS require a homogeneous sample, exposed to the sample surface.

Samples of basalts from selected eruption were crushed and sieved to the 0.5 – 1 mm size fraction. Olivine crystals were handpicked and then placed in shallow dish and viewed under a binocular microscope. In this way it is possible make a first selection among MIs, picking inclusions-bearing crystals and trying to avoid ones in which we observed cracks or fractures and so that may have lost dissolved volatiles from syn- or post-eruptive cracking of the host mineral.

After this step, olivine crystals containing MIs were placed in a cylindrical support and carefully oriented so that the maximum number of inclusions would be intersected by the polished surfaces. Then they were embedded and mounted onto an epoxy resin disk (2.54-cm Ø), and then polished one side with sandpaper of several different size and diamond paste (down to 1 um) to expose the MI.

Figure 3.5: preparation steps of melt inclusions mounts for analysis by EMP, synchtron XRF and LA-ICP-MS

Chapter 4

Experimental and analytical techniques

4.1 Gas measurements

4.1.1 Filterpacks technique

Because of their significance in many aspects of volcanic processes, as a source of invaluable information, effort has been spent in the last decades to measure halogen concentrations in volcanic gases (Aiuppa, 2009). Estimates of total volcanic Br emission to the atmosphere are typically based upon measurements of bromine concentrations in volcanic gas condensate samples (Aiuppa et al., 2005).

In-situ downwind measurements of volcanic gases and particle concentrations in a volcanic plume can provide useful tools to achieve information about volcanic processes. Often, due to logistical restrictions for measurements at volcanoes (difficult access, high temperature, dangers associated with being close to vents, safety restrictions etc.) only few data points are well constrained (Von Glasow et al., 2009). The advent of modern methods capable of remotely sensing halogens (FTIR spectroscopy) combined with the refining of classical chemical methods (filter pack) has led to the accumulation of extensive data sets, particularly at open-conduit volcanoes where degassing is sustained by halogen-rich-volcanic gas plumes (Aiuppa, 2009 and reference therein). However, the most part of data are referred almost completely to arc volcanoes, that vary widely through time for individual volcanoes, and from volcano to volcano, producing large uncertainty in computed global Br fluxes (Aiuppa et al., 2005).

Sampling of the atmospheric concentrations of acid gases HF, HCl, HBr and SO_2 in the summit crater area of Mt. Etna volcano was done using the filter-pack method (fig. 4.1) during several fieldwork carried out both by INGV and DiSTeM - Università di Palermo.

Filterpacks method is a in-situ, active technique consisting in trap volatile acid gases by pumping air in controlled conditions through two impregnated filters (Finnengan, 1989).

The filterpacks instruments consists of two plastic packs holders in parallel, each containing 4 cellulose filters assembled in series: first one is a dry filter which blocks solid and liquid particles; the latter three were impregnated with a saturated sodium bicarbonate solution (1M $NaHCO_3$), to trap acidic gaseous volatiles (e.g., SO_2, HCl, HF, HBr, and HI). Pumping was

done through a small vacuum pump which sucks the ambient gases at a constant flow rate (4 l/min; sampling time, 60 min). Filtration time was chosen so that nearly all of the acid gases were absorbed by the first two filters in the filter stack. In this manner, we avoided problems of over-saturation of the three filters that results in inaccurate measurements. From the flow rate measurements and total filtration time, we calculated the total volume of filtered air.
Two sets of filter pack samples were collected. One set was exposed for 54 min and the other for 60 min.

Figure 4.1: Filter-pack instrumentation

Br compositional data were collected from Mt. Etna's Voragine and North-East (NEC) craters, on the rims of the degassing craters, a few hundred meters from the gas sources, in the centre of the dense plumes.
In the laboratory, each filter was eluted in 20 ml bi-distillate H_2O into teflon vessel. Vessels were kept into ultrasonic bath for 2 h to homogenize solution.

A 10 ml aliquot of each extract was spiked with 50 microl H_2O_2 to oxidize any reduced S present. After about 1 h we added a very small amount of MnO_2 to avoid H_2O_2 excess. The total mass of SO_2 , Cl, F absorbed onto the filter paper were determined by ion chromatography.

The oxidation of sulfite to sulfate during the analysis was blocked by adding a few μL of formaldehyde to all samples. Total sulfur (as SO_2) was obtained by summing the concentrations of sulfite and sulfate.

The remaining 10 ml were divided into other 2 aliquots: a 5 ml aliquot is stored in fridge for F analysis by a specific electrode and the other one aliquot is acidified by addition of concentrated HNH_3 until analysis (for dissolved Br and I) by ICP-MS (Agilent 7500 ce).

4.2 Experiments by IHPV

4.2.1 Introduction

Knowledge of the physico-chemical conditions prevailing in magmas is a prerequisite for modelling igneous systems and volcanic eruptions. Possible approaches to reach this goal include: 1) geothermometry and geobarometry on phenocryst and cumulate assemblages from quenched eruption products; 2) melt inclusion studies; 3) experimental simulations of crystal-liquid equilibria (Di Carlo et al., 2006).

During the past 20 years, experimental petrology approach has increasingly been used to constrain the pre-eruptive parameters and to investigate both magma chemical properties (phase equilibria at different pressures and temperatures, melting, crystallization, gas-melt volatile saturation, element partitioning, diffusion) both physical properties (measurements of rheological parameters, deformation studies). Since they employ high-pressure and high-temperature apparatus, allowing a reliable simulation of P-T-fO_2 conditions during magma ascent or inside magma chamber, experiments are extremely useful as a valid support to volcanological/geochemical investigation.

Concerning investigation on bromine chemical and physical parameters, experiments have mainly concerned silicic to intermediate volcanic systems, almost excluding mafic compositions. Bureu et al., 2000 investigated the partitioning coefficient of chlorine, bromine and iodine between an albitic melt and an acqueous fluid at 900 °C, 200 MPa. They demonstrated a linear relationship between the logarithm of the partition coefficients and the ionic radius of the anion. After, further experiments were carried on in order to investigate bromine behaviour in melt (Bureau and Metrich, 2003; Bureau et al., 2010) but always focusing on silicic composition.

Clearly there is the need for further experiments aimed to extend the bromine investigation including mafic magmas, in particular to complement data from melt inclusions studies.

In this work we carried out two sets of experiments by Internally Heated Pressure Vessel (IHPV) at ISTO of Orléans laboratories (FR) with two different main purposes. First one was aimed to create H_2O-Br bearing synthetic glasses to be used as standards for melt inclusions measurements. In order to analyse Br in melt inclusions, in fact, a problem to be solved is the lacking of certified Br standard glasses, which have not been obtained so far. Second set of experiment was run to investigate Br partitioning coefficient ($D^{melt/fluid}$) to point out Br

behaviour in distribution between fluid and melt phase.
Here we report procedures, techniques and experimental conditions of performed run.

4.2.2 Starting material

Starting material for preparation of H_2O-Br bearing synthetic glasses was an hawaiitic, glassy alkaline basalt from 2001 Etna eruption. The basalt was crushed, grinded and melted in a platinum crucible in a 1-atm furnace at 1400 °C, for 3 hours in order to remove any H_2O and CO_2 naturally present. Two cycles of melting of 2-4 hours each (with grinding between them) were performed (Alletti et al., 2009; Di Carlo et al., 2006). The resulting glass was an homogeneous, bubble and crystal-free gas glass already used as starting glass by Alletti et al., 2007; 2009 and Iacono Marziano et al., 2010. The starting material was grinded under acetone in agate mortar in order to obtain a fine powder (50-100 um) and then dried and stored in an oven at 120°C before use.

4.2.3 Preparation of H_2O-Br solutions

We prepared H_2O-Br simple solutions by adding known quantities of NaBr salt to millipore water. We calculated NaBr required to obtain two Br concentration set of solution: a low concentrated one (from 0,5 ppm to 10 ppm) and an high concentrated one (from 50 ppm to 6000 ppm). Such a wide concentration range is suitable to analyse both Br-natural samples and high Br-doped synthetic samples.
The necessary amount of NaBr (mg) has been dissolved in about 100-200 ml (the low-concentrated set) and 50 ml (the high-concentrated set) of millipore water inside glass bottles with tight cups. Solutions were homogenized by ultrasonic bath for about 1h, so as to dissolve NaBr into the water. List of solution and related concentration are reported in table 4.1.
In order to check error in preparing solutions, we analysed samples from each solutions by ionic chromatography at INGV of Palermo and we found an uncertainty around 5% with respect to the expected value.

Solutions	M.pore water (g)	NaBr (g)	Br (g)	Br in solution (wt%)	H_2O in solution (wt%)
H1	40	25.76	20.00	30	61
H2	40	7.74	6.01	13	84
H3	40	2.58	2.00	5	94
H4	40	1.56	1.21	3	96
H5	40	0.77	0.60	1	98
H6	40	0.26	0.20	1	99
H7	40	0.13	0.10	0.3	99
L1	200	0.006	0.005	0.002	99.990
L2	100	0.007	0.005	0.005	99.990
L3	20	0.007	0.005	0.025	99.970
L4	20	0.013	0.010	0.050	99.940

Table 4.1: solutions preparing conditions.

4.2.4 Preparation of capsules

Capsules are extremely important elements in planning experiments since they are the containers of the reactants and they have to minimize the interactions with the outer system. Capsules composition depends on experiment temperature. Most used materials are Au (< 1050°C), Pt (> 1050°C) and Pd alloys (either Ag- or Au-bearing). Noble metal containers have several advantages, namely they are rather inert chemically material and easy to weld.

Au-Pd (0,5 mm outer diameter; 3 cm length) and Pt (3 mm outer diameter; 3 cm length) capsules were loaded with solution (2 wt% of the total mass of powder) in the bottom of the capsule, using a graduate microsyringe. After, about 200-300 mg and 100 mg of starting glass powder was loaded respective in Pt and in AuPd capsules.

Solution content was added according to water saturation curve for Etna basalt (Lesne et al., 2010) following two different strategies: in standard glasses we added water in order to stay in undersaturated conditions. Since experiments were run between 3-4 kb (H_2O saturation around 6 wt%) we added 2 wt% solution inside capsule so that all volatiles are dissolved in the glass and we are able to find in final standard the same amount of solution we put into the capsules. This condition is mandatory to produce a very good and reliable set of standard

glass. Differently than standard experiments, in partitioning glasses we required the formation of a fluid phase, so this time we added an excess of solution in order to stay in over-saturated conditions field. In this way we promoted Br partitioning between the silicate melt and the related fluid phase.

After loading, capsules were sealed by arc welding (during welding, capsules were kept in a liquid nitrogen bath to prevent water loss). After sealing, capsules were dipped inside hot oil to check for any possible leaks of volatiles, stored in oven for 2 hours and then reweighed. Capsules preparing conditions (both for standard and for partitioning experiments) are listed in tab. 4.2.

Sample name	Basalt powder added	Solution added	Solution added	P exp.	H_2O dissolved in melt	Sample name	Basalt powder added	Solution added	Solution added	P exp.	H_2O dissolved in melt
	(mg)	(%)	(mg)	(bar)	(wt%)		(mg)	(%)	(mg)	(bar)	(wt%) *
Year 2012						Year 2012					
Standards						Partitioning					
STD H1	295	2	6	3500	7.32 *	Caps3 a	58.07	2	1.09	250	1.54
STD H2	196	2	4	3500	7.32 *	Caps3 b	50.77	2	1.08	250	1.54
STD H3	196	2	4	3500	7.32 *	Caps3 c	51.07	2	1.07	250	1.54
STD H4	196	2	4	3500	7.32 *	Caps3 d	52.97	2	1.14	250	1.54
STD H5	195	2	4	3500	7.32 *	Caps3 e	54.57	2	0.55	250	1.54
STD H6	196	2	4	3500	7.32 *						
STD H7	196	2	4	3500	7.32 *	Caps4 a	50.85	1.5	0.48	100	0.89
						Caps4 b	49.95	1.5	0.59	100	0.89
STD L1	98	2	2	3500	7.32 *	Caps4 c	49.95	1.5	0.48	100	0.89
STD L2	98	2	2	3500	7.32 *	Caps4 d	50.45	1.5	0.75	100	0.89
STD L3	98	2	2	3500	7.32 *						
STD L4	98	2	2	3500	7.32 *						
Partitionings						Year 2013					
Caps1 a	47.30	5	2.39	1000	3.49 *	Caps d	99			1000	3.49
Caps1 b	46.70	5	2.46	1000	3.49 *						
Caps1 c	46.70	5	2.44	1000	3.49 *	Caps a	95			2000	5.26
Caps1 d	48.40	8	2.44	1000	3.49 *	Caps b	95			2000	5.26
Caps1 e	47.6	5	2.60	1000	3.49 *	Caps c	95			2000	5.26
Caps2 a	49.06	3.5	1.99	500	2.32 *						
Caps2 b	49.06	3.5	1.86	500	2.32 *						
Caps2 c	49.36	3.5	1.87	500	2.32 *						
Caps2 d	52.36	3.5	1.80	500	2.32 *						
Caps2 e	49.36	3.5	1.80	500	2.32 *						

Table 4.2: capsules preparing conditions (both for standard and for partitioning experiments)

* theoretycal value on the basis of water saturation curve for Etna basalt (Lesne et al., 2010)

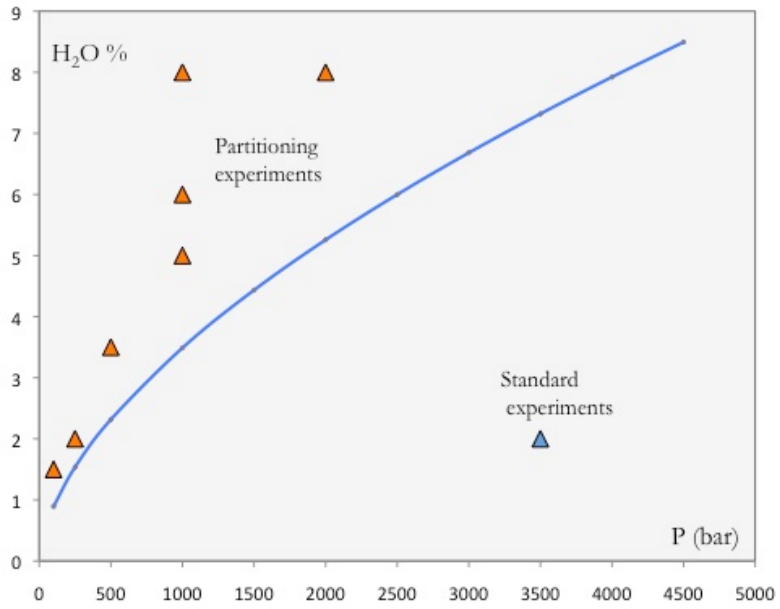

Figure 4.2: water saturation line for Etna basalt (Lesne et al., 2010). Red points represent P (bar) and H_2O contents (%) conditions of partitioning experiments; blue point is referred to conditions of standard experiments.

4.2.5 Experiments by IHPV instrument

All experiments were performed at the facilities Institut des Sciences de la Terre d'Orléans (ISTO-France) using rapid-quench Internally Heated Pressure Vessels (IHPV), operating vertically and pressurized either with Ar or with an Ar–H_2 mixture (Di Carlo et al., 2006 and references therein). The vessel is used to perform high pressure-temperature experiments at various redox conditions to investigate magmatic processes in earth's crust or upper mantle and to synthesize high pressure materials.

The instrument (figure 4.3) is equipped with a molybdenum furnace where two S-type thermocouples are used to monitor temperature gradients into the hotspot that is strongly affected by gas convection (Roux and Lefevre, 1992). This gradient was constantly controlled in order to be less than 10 °C. Run temperature is reached in ~ 1 hour. Pressure was recorded by a transducer calibrated against a Heise–Bourdon tube gauge (precision of 1.5–2.0 MPa).

Capsules were placed togeter in a alumina tube that served as a sample holder. The tube was hung in the furnace hotspot by a thin (0,2 mm) Pt wire.

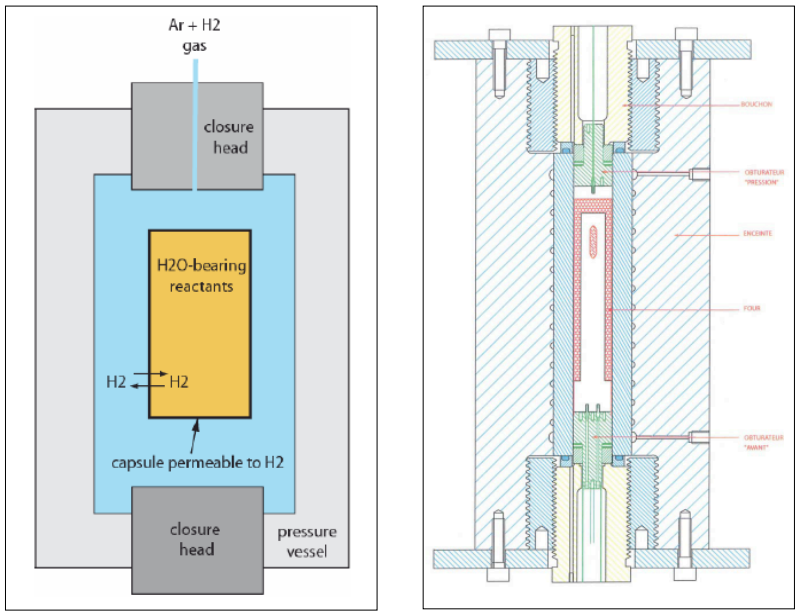

Figure 4.3 a-b: General draws of an internally heated pressure vessel in operation at ISTO, Orleans.

All experiments were conducted at a temperature of 1200 ± 10 °C, in order to ensure super-liquidus conditions. Experimental durations was set depending on the expected time to reach equilibrium. Alletti et al., 2009 pointed out that a 6-8 hours run-time was enough to reach equilibrium at same P-T conditions for chlorine. Diffusion of Br appears to be a factor of about 2-5 lower than the other halogen at magmatic temperatures, according to the larger ionic size of Br (Baker, 2008). So, to be in a safer range we run experiments for about 24 h.
At the end of the experiment, the capsules were isobarically quenched by a drop-quench device modified after Roux & Lefevre, 1992. It consists in supplying an electrical current so as to fuse the Pt wire allowing the porcelain sample holder to fall down into the cold part of the vessel. Details of the sample area are shown in figure 4.4. The thermocouple and the vertical quench wire are mechanical supported in grooves shaped along a thin ceramic tube (20 mm outer diameter (figure 4.4-a) fastened to the centre of the bottom closure head. The quench wire (fig 4.4-a) is a thick (1 mm o.d.) Pt wire. It is thinned with a small grinding-wheel at the point where the wire suspending the capsules is supported. At the end of the run the two

electrodes are connected to a variac and the voltage is rapidly (1 s) raised to about 50 V. The process is controlled using an ampere-meter connected to the circuit. The cooling time for a quenched sample down to room temperature depends obviously on the sample size (Roux & Lefevre, 1992). With this device, nearly isobaric quench rates of about 100 °C/s were achieved (Di Carlo et al., 2006). Dropping of the sample holder causes the cold bottom gas to heat and a successful quench is indicated by a peak of several tens of bars on the pressure readout. (Di Carlo et al., 2006).

4.2.6 Creation of a set of Br synthetic standard glasses

Experiments to synthesise Br-bearing glasses to be used as Br standards were run at P ~ 3.5 kb, T = 1200°C for about 24 h. Capsules were filled following the procedure described in paragraph 4.2.4. Since up to 300 mg of basalt powder were put inside each capsule, sample holder was filled with no more than 2 capsules for time. This, in order to ensure a good quench at the end of the experiment.

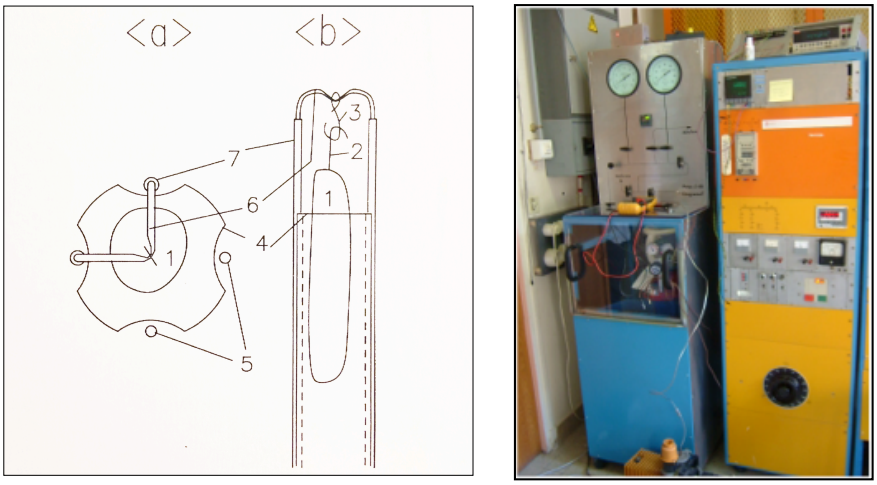

Figure 4.4: .a) Schematic sketch of sample assembly: horizontal (a) and vertical (b) sections (at different scales). 1) experimental charge in a gold or platinum capsule. 2-3) Pt wire arc welded to the capsule. 4) inconel tube with grooves supporting the quench wire and thermocouples. o.d. = 20 mm, length = 20 cm. 5) sheathed thermocouples. 6) thick Kanthal wire (1mm o.d) thinned at the top, to control the point where it will be fused electrically to drop the capsule. 7) alumina insulator (from Roux & Lefevre, 1992). b) picture of control panel of IHPV.

4.2.7 Partitioning experiments

Partitioning experiments were carried out in order to investigate the partition coefficient of Br between a melt and a fluid phase ($D^{m/f}$ Br) in a hydrous Etna basalt.
Experiments were run using the same procedure described in previous paragraph. The only difference was the addition of an Ar-H_2 mixture in the IHPV obtained by sequential loading of H_2 and Ar at room temperature, so as to vary redox conditions (fO_2) depending on the XH_2 in the mixture. The redox conditions of the partitioning experiments were estimated to lie in the range of the moderately reduced conditions of nickel-nickel oxide buffer NNO-NNO+1, in order to stay near natural conditions on the basis of experimental conditions (i.e. total pressure, H_2 pressure, and amount of H_2O loaded in the capsule).

Differently of standard experiments, partitioning experiments, being oversaturated, need to be run longer in order to permit the system to reach equilibrium. On the basis of experiments described in Alletti et al., 2009, and considering that Br diffusion coefficient is lower than Cl diffusion, we run experiments longer (more than 24 h).
Initial purpose was to investigate a pressure range from 100 bar to 1000 bar, being 250 bar and 500 bar intermediates steps, in order to reproduce typical conditions of the shallow plumbing system of Mt. Etna. Unfortunately, after several failed experiments we were forced to leave this idea and concentrate only on a couple of successful experiments, because of several problems. In fact, we had to face several difficulties occurred during experiments, related to

1) AuPd interference: some problems with interference between Au of AuPd capsules and Br occurred by INAA (see paragraph 4.3.3)
2) quench crystals: first glasses products were found to contain several crystals due to some problem occurred during quench process (maybe a quench-rate slower than the optimal one or to too much material inside the capsule.).
3) "auto-quench" events: some systematical failures of the experiments due to unknown causes.
4) low pressures experiments: some capsules were found swollen and damaged, others with dramatic loss of water.

When the quench was unsuccessful, the vessel was opened and the experiment was restarted and run for a few additional hours before quenching was attempted again.
Here we report experimental runs parameters of run performed during 2012-2013 years.

N° Run	Date	Type experiment	Capsules material	Run-time (h)	P (bar)	P H_2 (bar)	N. capsules	Tot. weight (g)	Note
Run 1	26/01/12	Standard	AuPd	8	3724	-	2	3,06	ok
Run 2	14/02/12	Standard	AuPd	7	3093	-	2	2,86	ok
Run 3	16/02/12	Partitioning	AuPd	8	1128	2	4	4,7	quench-crystals
Run 4	17/02/12	Standard	AuPd	7	3210	-	2	2,95	quench-crystals
Run 5	27/02/12	Standard	AuPd	8	3450	-	2	3,45	ok
Run 3R	22/03/12	Partitioning	AuPd	10	1110	2	2	2,13	quench-crystals
Run 4R	28/03/12	Partitioning	AuPd	24	1089	2	2	2,13	ok
Run 6	06/04/12	Partitioning	AuPd	24	1180	2	2	2,59	ok
Run 7	07/06/12	Standard	Pt	12	3657	-	2	3,21	auto-quench
Run 7R	12/06/12	Standard	Pt	13	3459	-	2	2,99	ok
Run 8	03/10/12	Partitioning	AuPd	24	567	1,5	2	2,34	H_2O lost
Run 8R	15/01/13	Partitioning	AuPd	24	513	1,5	2	2,34	ok
Run 9	22/02/13	Partitioning	AuPd	24	252	1	2	2,89	ok
Run 10	21/03/13	Partitioning	AuPd	24	112	0,5	3	3,08	Capsules explosed
Run 11	19/04/13	Partitioning	AuPd	24	1050	2	3	3,14	ok
Run 12	25/07/13	Partitioning	AuPd	24	2376	1	2,3	2,59	ok
Run 13	26/07/13	Partitioning	AuPd	24	1104	0,5	2	2,36	failed

Table 4.3: List of runs performed by IHPV at ISTO, Orleans. T was set at 1200 ± 10 °C for all experiments.

4.2.8 Opening capsules, weight and preparation of mounts

At the end of experiment, after pressure decreasing, capsules were put out from furnace and weighed to check for possible leaks, opened and weight again. Regarding standards, if experiments were successful and no any leaks were occurred, after cutting, weight of each

capsule would be the same as before the experiment. In case of partitioning glasses, a weight difference would be reported after opening of the capsule, due to the formation of an exceeding fluid phase. This is a very important element which has to be reported in mass balance calculation (see chapter 5).

Sometimes, for supersaturated capsules, we note the release of a white and smelly foam in correspondence of the cut, due to the exsolution of the fluid phase. Finally, capsules were put in oven at 120°C for 2-3 steps of 30 minutes to allow the complete exsolution of fluid phase.

In order to check for possible inhomogeneity in Br concentration within every single capsule, in case of an anomalous distribution of NaBr, each capsules was opened carefully, separating the bottom, the centre and the top of the glass.

Very small chips of synthetic glass for each capsule were embedded in epoxy, polished with sandpapers of decreasing size and lubricated through diamond paste (9 ,3, 1 um) and carbon coated for LA-ICPMS, SEM and EMP analyses. The rest of the sample was powdered to INAA bulk analyses. After EMP analysis, the samples were re-polished using 1 um sandpaper in order to assure complete removal of the carbon coat prior to other analysis.

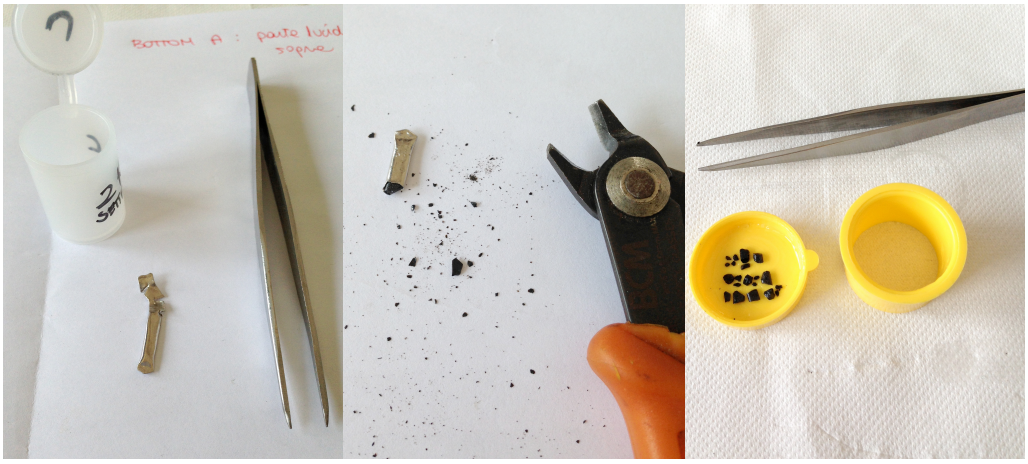

Figure 4.5: opening capsules and embedding procedures.

4.3 Analytical methods

4.3.1 Homogeneity of glasses

In order to test the quality of experiments and to verify absence of quench crystals glasses, run-products were checked by optical microscopy and by SEM, at ISTO Orléans facilities.
Some small cross-shape quench-crystals were found in some glasses, probably due to a cooling rate slower than the optimal one (100 °C/s). For this reason most of the experiments have to be run again in order to produce crystal-free glasses. We considered as good experiments where the density of quench-crystal was estimated to be less than 1 %. However, the most part of producted glasses were found to be almost clean and homogeneous, as in figure 4.6 a) and b).
Homogeneity of Br distribution in every piece of glass was checked by LA-ICP-MS. No difference was found between the top and the bottom of the same glass (where solution where concentrated during capsule preparation). A very small, negligible Br gradient was found between the central part and the sides of the capsules.

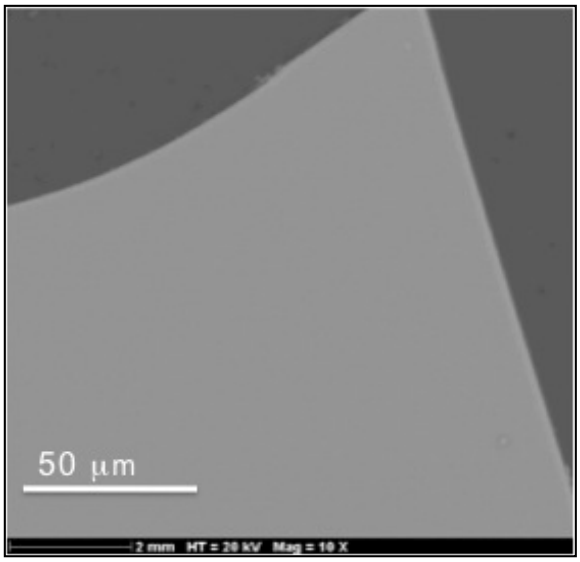

a)

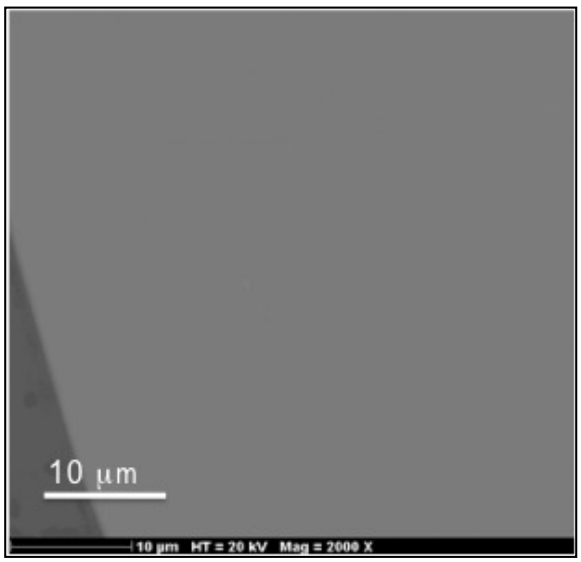

b)

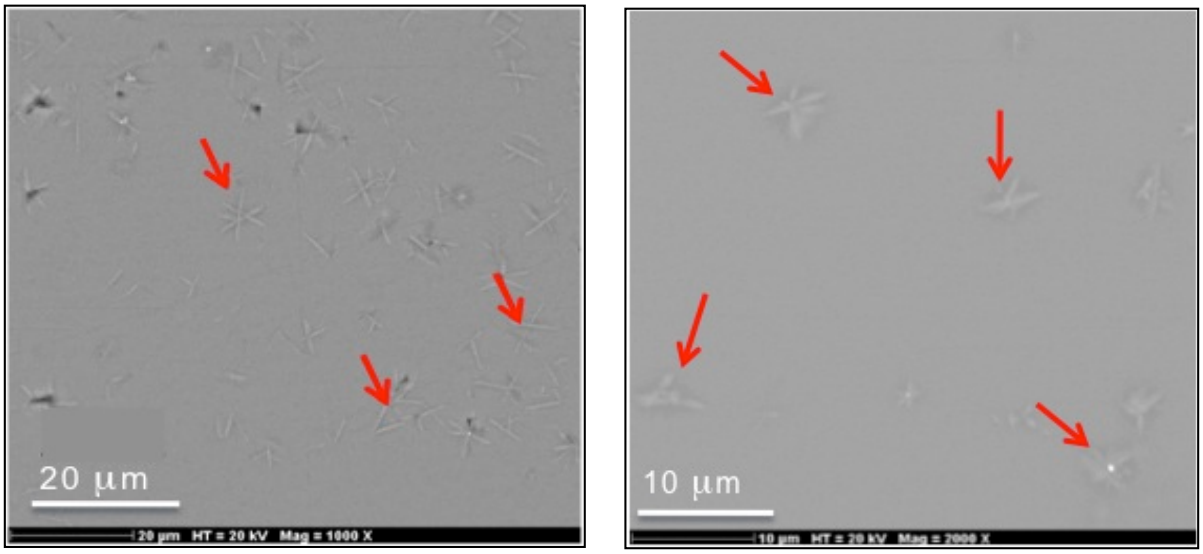

c) d)

Figure 4.6: Some different scale SEM pictures of samples glasses synthetised by IHPV. Samples appears to be crystal-free (figure a and b) while some cross-shape crystals are found in a few samples (figure c and d).

4.3.2 Major elements analysis on glasses: EMP (Electron Microprobe Analysis)

Major elements, S and Cl were analysed by Electron microprobe (EMP) at ISTO-BRGM joint analytical facilities in Orléans (FR).

EMPA is a fully qualitative and quantitative method of non-destructive elemental analysis of micron-sized volumes at the surface of materials. EMPA works by bombarding a micro-volume of a sample with a focused electron beam (typical energy = 5-30 keV) and collecting the X-ray photons thereby emitted by the various elemental species. Because the wavelengths of these X-rays characterize the emitting species, the sample composition can be easily identified by recording WDS spectra (Wavelength Dispersive Spectroscopy). WDS spectrometers are based on the Bragg's law and use various moveable, shaped monocrystals as

monochromators.

We set accelerating voltage of 12 kV, beam current of 6 nA and peak counting time of 10 s for every element. In order to verify the homogeneity of the experimental glasses we made at least 15 analyses per chip on 3-4 different chips randomly selected from each capsule. The low standard deviations of these analyses show that the experimental products were homogeneous with respect to their major elements.

We attempted to measure Br concentration introducing an higher counting time, but among the four Br peaks that we would expect to see by EMPA, two were totally outside the EMPA detection limit, one was covered by Al signal and the last one was too weak even at high concentration (about 6000 ppm).

So, while Bureau et al., 2000 pointed out that for their experiments, detection limit of EMPA for Br was around 1500 ppm, we found that EMPA is not useful at all for Br analysis in basaltic composition. This could depend on the different composition (a simply albitic composition in Bureau et al., 2000 and a natural basalt from etna in this case). This makes electron microprobe a non-suitable method to analyse Br concentrations in basaltic composition. By comparing analysis on major elements in synthetic standard glasses (this study) with analysis on major elements on starting material (Alletti et al., 2009) we conclude that run products are homogeneous and no interfering processes have occurred, since Na_2O concentrations in glasses depend on the amount of NaBr loaded in the capsule.

Major elements, SO_3 and Cl measurements are reported in table 4.4.

The redox conditions of the experiments were estimated to lie in the range of nickel–nickel oxide buffer (NNO; moderately reduced conditions, so as to stay near natural conditions) on the basis of experimental conditions (i.e. total pressure and partial pressure of the water) and intrinsic fO_2 of the autoclave.

Water contents in synthetic glasses were extrapolate by difference from analysis on major elements, assuming the all the experiments were run in the same conditions.

Elements (wt.%	STD H1	SD	STD H2	SD	STD H3	SD	STD H4	SD	STD H5	SD	STD H6	SD	STD H7	SD	STD L1	SD	STD L2	SD	STD L3	SD	STD L4	SD
SiO_2	47,87	0,57	49,31	0,42	48,32	0,28	49,18	0,45	49,49	0,52	48,44	0,33	48,57	0,24	48,16	0,41	47,72	0,54	48,34	0,45	48,52	0,42
TiO_2	1,77	0,1	1,72	0,08	1,75	0,08	1,74	0,09	1,64	0,35	1,74	0,12	1,74	0,12	1,72	0,11	1,79	0,09	1,73	0,1	1,69	0,11
Sl_2O_3	16,5	0,2	16,43	0,18	16,23	0,2	16,31	0,21	16,19	0,18	16,27	0,19	16,27	0,16	16,51	0,18	16,61	0,23	16,47	0,2	16,45	0,23
FeO	10,14	0,4	9,43	0,39	10,35	0,31	9,7	0,43	9,77	0,38	10,17	0,38	10	0,17	10,19	0,4	10,4	0,36	10,3	0,44	10,12	0,39
MgO	6,56	0,14	6,25	0,13	6,53	0,12	6,35	0,12	6,32	0,16	6,53	0,14	6,44	0,14	6,38	0,16	6,37	0,78	6,19	0,74	6,26	0,13
MnO	0,18	0,12	0,19	0,1	0,14	0,12	0,18	0,13	0,21	0,1	0,18	0,12	0,18	0,09	0,18	0,11	0,17	0,1	0,2	0,1	0,17	0,12
CaO	10,52	0,16	10,38	0,24	10,56	0,17	10,41	0,18	10,51	0,19	10,52	0,19	10,64	0,19	10,77	0,35	10,9	0,25	10,83	0,22	10,73	0,22
Na_2O	3,63	0,12	3,38	0,11	3,32	0,11	3,21	0,11	3,17	0,1	3,24	0,12	3,28	0,09	3,21	0,11	3,24	0,13	3,17	0,11	3,26	0,11
K_2O	1,98	0,08	2,03	0,09	1,94	0,09	1,99	0,08	1,86	0,39	1,96	0,08	1,98	0,07	1,99	0,1	1,95	0,26	1,96	0,1	2,01	0,1
P_2O_5	0,76	0,08	0,77	0,08	0,78	0,09	0,76	0,09	0,72	0,06	0,76	0,07	0,79	0,1	0,73	0,07	0,76	0,13	0,73	0,1	0,69	0,13
Cl	0,05	0,03	0,07	0,04	0,06	0,02	0,07	0,04	0,08	0,04	0,05	0,03	0,05	0,04	0,07	0,09	0,06	0,03	0,06	0,03	0,06	0,03
SO_3	0,04	0,05	0,05	0,06	0,02	0,03	0,09	0,1	0,03	0,05	0,14	0,14	0,04	0,05	0,09	0,39	0,03	0,04	0,03	0,04	0,03	0,04
Tot	94,36	0,62	95,33	0,63	94,42	0,86	94,53	1,17	94,53	0,86	92,25	2,21	94,42	0,5	95,21	6,66	95,7	1,27	96,25	0,94	96,07	0,87

Tab. 4.4: Major elements, SO_3 and Cl measurements on synthetic glasses. Values are the average on 15 measurements points on 4 different chips for the same sample. SD: Standard deviation on measurements.

4.3.3 Br measurements on high-concentrated synthetic glasses: bulk analyses by INAA (Instrument Neutron Activation Analysis).

Br quantification on experimental high Br-bearing glasses (from H1 to H7) were performed by Instrumental Neutron Activation Analysis, a bulk independent analytical technique. Analyses were run by Actalabs laboratory (Toronto).

Very briefly, INAA is one of the most accurate analytical techniques, used for quantitative multi-element analysis of major, minor, and trace elements in samples from almost every kind of scientific field or technical interest. The procedure consists in irradiating sample with an intensive neutron flux and, then, measuring gamma rays energy emitted by decay of

radioactive isotopes produced. The primary source of neutrons for irradiation is usually a nuclear reactor. Each element which is activated emits a "fingerprint" of gamma radiation which can be measured and quantified by comparison with those emitted by certified standards. INAA quantifies the total amount of an element present in sample matrices with very high sensitivities for most of the elements: most detection limits range from ~0.05 to ~50 ppm (≤ 1 ppb for some high-purity materials).

In this study, first analyses by INAA were affected by a sort of interference occurring between Br to be analysed and Au from capsules. This interference was negligible for high concentration (from H1 to H7 glasses) but significant for low concentration (from L1 to L4). So we had to repeat experiments for low-concentrated set of glasses, using Pt capsules. Procedure was exactly the same we had already described above (paragraph 4.2.4). The main difficult we found in this point is linked to the amount of material we were able to produce. In fact, INAA permits the analysis of samples ranging in mass from ~0.001 grams to 10 grams depending on sample density. This was a very important point in our study because of the great difficulty in producing large amount of synthetic material by IHPV. In fact, due to the extreme sensitivity of quenching process from the total mass of the run, we were able to produce only a little amount of final glass for each experiment (up to 300 mg). Since INAA detection limit for Br is 0,5 ppm for sample amount around 1 g, Actalabs had to stretch irradiation time in order to obtain the same detection limit in a much lower amount of sample. Results are reported in tab 4.5. As shown, assuming that Au-Br interference has been avoided, other problems occurred in Br-low concentrated glasses since INAA reported values much higher (40-180 ppm) than the expected ones. This is probably due to a sort of contamination during preparation of low concentrated standards. For this reason, we only considered INAA analysis of high-Br synthetic glasses (ranging from 82 to 6930 ppm), which were used as reference materials to analyse run-products of partitioning experiments. Low-concentrated glasses (to be used as reference materials for natural sample) were re-prepared and analysed by Synchrotron X-Ray Fluorescence (SXRF), to avoid any further problems (i.e. detection limit of INAA not so good as expected for our samples).

Sample	Br expected (ppm)	Br measured INAA (ppm)	Mass of powder (g)
STD H1	5969	6930	0,158
STD H2	3683	3240	0,110
STD H3	967	1280	0,105
STD H4	593	634	0,120
STD H5	294	305	0,151
STD H6	100	118	0,106
STD H7	52	83	0,101
STD L1	0,5	54 *	0,286
STD L2	1	105 *	0,285
STD L3	5	182 *	0,280
STD L4	10	40 *	0,280

Tab 4.5: Expected Br concentration compared to Br concentration analyse by INAA. For each standard is reported the mass (g) of each samples. *The unexpected high Br concentrations found in sample from L1 to L$ is probably due to a kind of contamination during preparation of capsules. INAA analysis in this set of samples have not been taken into account.

4.3.4 Measurements on low Br concentrated standard glasses and melt inclusions: Synchrotron X-Ray Fluorescence (SXRF)

4.3.4.1: Introduction

Br quantification on experimental low Br-bearing glasses (from 0,5 up to 10 ppm Br) and melt inclusions were performed by Synchrotron X-Ray Fluorescence (SXRF). Analyses were run at the UK national synchrotron facility, Diamond Light Source (Oxfordshire).

A synchrotron produces very intense beams of x-rays, infrared and ultraviolet light, called synchrotron light. The potential of Synchrotron X-Ray Fluorescence (SXRF) microprobe for conducting quantitative analysis of single melt inclusions has recently been recognised. The advantages of this technique remains mainly its highly sensitive (sub-ppm detection limit), its non destructive character, a high spatial resolution, and the in-situ multi element analytical capability (Menez et al, 2001). This technique has undergone a rapid development and is still subject of continuous improvement; nevertheless, it has advanced to a powerful tool in trace element and volatile analysis of geologic samples during the past two decades (Lechtenberg et al. 1996).

The UK national synchrotron facility, Diamond Light Source (Diamond), has been operating with circulating 3 GeV electron beam in the storage ring since September 2006. It generates synchrotron radiation from infra-red to X-rays for a wide range of applications. Synchrotron light can be as much as 100 billion times brighter than the sun. This allows scientists to study samples in incredible detail.

The electrons that power Diamond are first fired from an electron 'gun', and then they are accelerated up to very high speeds (nearly the speed of light) through a series of three particle accelerators. These are called the linear accelerator (linac), the booster synchrotron and the large storage ring. When the path of the electron beam is bent by Diamond's powerful magnets, the electrons produce very intense X-rays, ultra-violet and infra-red light. Diamond accelerate theses electrons to 3 GeV, which is the same as moving them between the terminals of a giant 3,000 million volt battery.

Diamond's 3 GeV electron storage ring is the main part of the accelerator and it is long 561 m

in circumference. The storage ring is not a true circle, but a polygon, made of 24 cells with 24 identical achromat (arc) sections each 17.35 m long and 24 straight sections angled together with bending magnets. These magnets (also called dipole magnets) are used to steer the electrons around the ring.

As the electron passes through each magnet it loses energy in the form of light. This light can then be channelled out of the storage ring wall and into the experimental stations, called beamlines where the experiments are carried out. Each beamline is optimised for a different kind of experiment, but they have some key components in common. First the optics hutch, where the light is filtered and focused. Next there is an experimental hutch, where the experiments are carried out. Because both of these hutches will contain X-rays when the machine is operating, there is a third hutch called a control cabin, where scientists control the experiments and collect and analyse data.

Third generation synchrotrons like Diamond also use special arrays of magnets called insertion devices which placed in the straight sections of the ring. These cause the electrons to follow a wiggling path, which produces more intense and tuneable light.

According to the design objective, the operating pressure is critical parameter for the lifetime of the stored beam and it should be 10^{-9} mbar or lower (Malyshev and Cox, 2012).

4.3.4.2: Operating conditions and detection limit

Differently to ion probe and electron microprobe, where only the uppermost volume of the sample at the surface is analysed, in Synchrotron analysis the primary X-ray beam penetrates deep into the sample, so that the spatial resolution of element to investigate is controlled by beam size and geometry of the sample. Mounts were prepared following procedure discussed in paragraph 4.2.8. Thickness of every chips range from 30-100 um.

Analyses were run at ID22 beamline (figure 4.7). The high brilliance of the insertion device source on ID22 allows structural investigation with reliable access to millisecond and shorter time scales.

The sample holder was inserted into the synchrotron beam in a 45 degree geometry. The beam diameter measured 12 um, counting times were set to 1000 s. This setup allows spatially high-resolution measurements and reduces detection limits to 0.5 ppm. The X-ray spot was

focused to values between typically 10 to 40 um.

About five-six points measurements were performed on standard synthetic glasses used as reference samples and at least two points measurements were made per each inclusion. Here, in natural samples, points were chosen taking into account the geometry of the melt inclusions (i.e. presence of a shrinkage bubble).

The analytical error of the synchrotron Diamond Lightsource is very small (<5% in glasses; <10 % in melt inclusions) for elements with an atomic number (Z) > 35 (Kutterolf et al., 2013). We made a total of 252 on melt inclusion and about 36 on synthetic glasses.

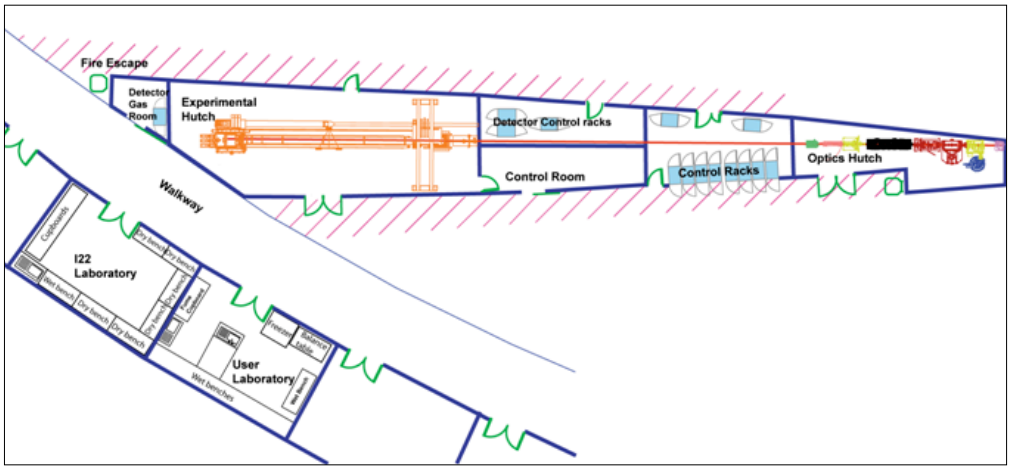

a)

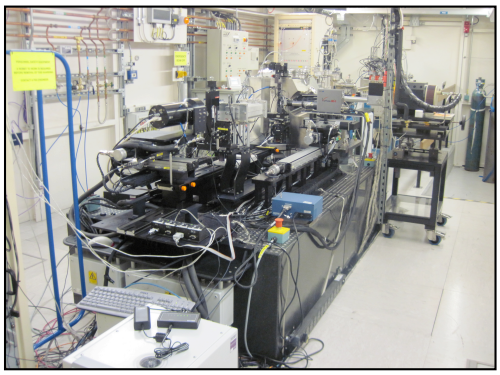

b)

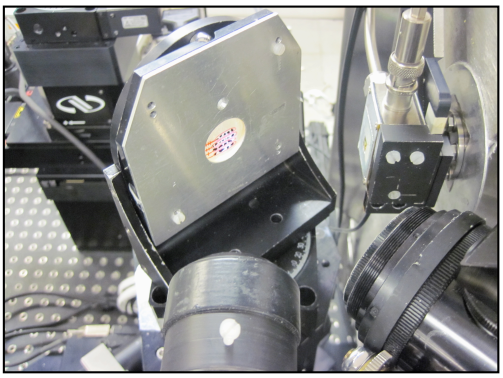

c)

Figure 4.7: a) ID22 beamline layout at Diamond Light Sourse Synchrotron facility; b) Experimental hutch; c) detail of the sample-holder.

4.3.4.3: Data reduction software: Pymca

Data were processed by PyMca, an X-ray Fluorescence Toolkit developed by the Software Group of the European Synchrotron Radiation Facility (ESRF). PyMca provides a powerful collection of tools for the visualization and analysis of fluorescence spectra collected using synchrotron radiation. The PyMca program is open source software with a number of options for use. PyMca can be used to identify individual elemental contributions to complicated spectra, and can yield trace element concentrations with surprisingly good accuracy. It offers the user the possibility to quantify XRF data using iterative simulations that takes into account secondary and higher order excitations in the sample which will lead to a more reliable quantification. The quantification procedure (based on the Levenberg-Marquardt algorithm) is explained in the schematic: the net-line elemental areas obtained by fitting the experimental spectrum with PyMCA, are compared with the elemental areas produced by a Monte-Carlo simulation determined by a number of input parameters. If the sum of the squares of the area deviations is smaller than a certain threshold, then the procedure is stopped. If not, then the sample composition is adjusted and the simulation will be performed again after which the results will be compared with the experimental elemental areas. The iteration will continue until convergence is achieved. This method also has the extra advantage that it produces a spectrum allowing direct comparison with the experimental data. Control over the simulations is possible through the existing PyMCA Advanced Fitting interface, by adjusting the different parameters such as beam characteristics, attenuator and matrix composition etc. The Monte-Carlo simulations themselves will be performed by an executable, spawned by PyMCA.

PyMCA is using two different types of concentration, "Mass Fractions" (MF) and "Molar". The MF approach is much more flexible and for this reason it is set by default. To do quantification of Br in melt inclusions sample with Pymca we first analysed spectrum from the reference material. Pymca requires some additional information about reference material in terms of main composition, density and thickness. It is also necessary to describe parts of the experimental setup. Analysing a spectrum from the unknown sample, Pymca describes if it is different from the reference material, reporting any changes to the setup. At the end of the fitting process PyMCA gives a calculated concentration in terms of **peak area**. Once we obtained peak area values, normalized for the number of pixels, we calculated the effective Br

concentration on samples. Bromine concentrations on melt inclusions are based on external calibration to measurements of reference samples performed within the same experimental session. References samples contain glasses with Br contents between 0,5 and 118 ppm). Peak area/pixel resulted for standards are listed in tab. 4.6. Diagram in figure 4.8 show the calibration line obtained by fitting area/pixels measured by synchrotron and nominal Br concentration (ppm). On the basis of the equation expressed by this curve, we have calculated the effective Br concentrations in natural samples of melt inclusions. The resulting equation is ($y=1.7\ E^{-07}x^{1.43}$) where y is the normalized peak area. The observed accuracy for Br contents in reference sample was better than 15 % at concentration levels between 0,5 and 10 ppm.

Sample	nominal Br concentration (ppm)	Peak area/pixel
blank	0	4,20E+04
STD L1	0,5	2,30E+04
STD L2	1	4,00E+04
STD L3	5	1,04E+05
STD L4	10	3,51E+05
STD H7	83	9,08E+05
STD H8	118	1,61E+06

Tab. 4.6: Peak area normalised to pixels for each sample (average on 3 measurements on each melt inclusion).

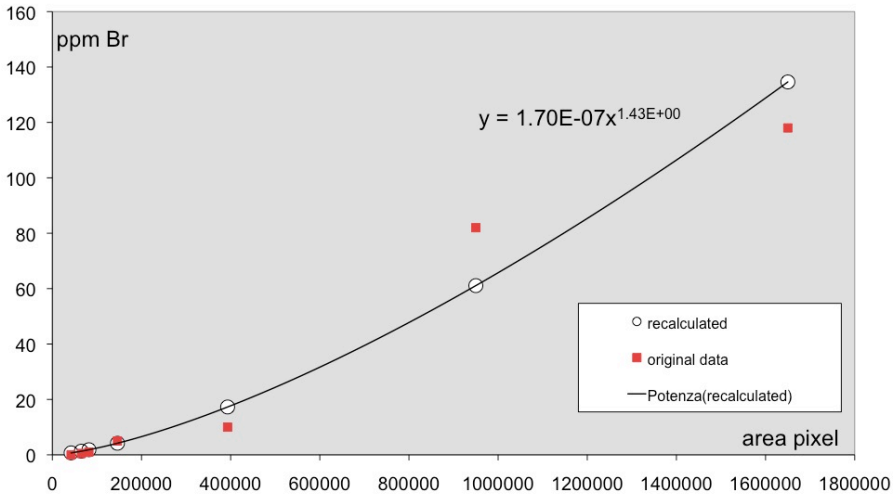

Figure 4.8: Br concentration vs. averages peak area of reference samples. The calibration line which has been used to calculate the Br concentration is: ($y=1.7$ E-07 $x^{1.43}$) where y is the normalized peak area.

4.3.5 Laser Ablation-Inductively Coupled Plasma – Mass Spectrometry (LA-ICP-MS) method for Br measurements

4.3.5.1 Introduction, principle and instrumentation

Among in-situ spot microanalytical techniques context, Laser Ablation Inductively Coupled Plasma Mass Spectrometry **(LA-ICP-MS)** is a rapidly evolving as a cheap, fast, sensitive and suitable method for multi-element analysis. It consists in the assembly of a laser and a ICP-MS (Perkins et al., 1995; Fryer et al., 1995; Chen, 1997).

A laser produces a spatially narrow and extremely intense beams of UV radiation having identical frequency, phase, direction and polarisation properties. In excimer laser light is emitted by a short-lived molecule made up of one rare gas atom (Gunther et al., 1996; 1998; Arrowsmith et al., 1997; Becker et al., 2000) and is used to ablate a small quantity of sample material which is transported into the Ar plasma of the ICP-MS instrument by a stream of Ar or He carrier gas (Arrowsmith, 1987).

The ablation process occurs into the **ablation chamber** where the sample to be analysed is placed. Chamber has a quartz glass lid transparent to UV light emitted by laser and it is mounted on a stage that allows the sample to be moved relative to the laser beam in the forward-backward, left-right and up-down (i.e. focus) directions.

Beam bombarding sample generates a minute ablation crater (in the order of tens of um in diameter and depth). The result is a very fine solid particles vaporisation of most of the exposed solid surface.

The material ablated mixes together with a stream of He-Ar carrier gas injected inside the sample chamber through a silicon tube with an in-put and an out-put hole. During its flowing inside the chamber, carrier gas picks up fine sample particles produced by the ablation process and transporting them into the Ar plasma of Inductively Coupled Plasma Mass Spectrometer (ICP-MS) instrument. Here atoms are ionized and separated according to their mass to charge ratios and therefore they can be identified and measured. The transport efficiency to the ICP is typically low for small diameter particle <5 nm, which tend to be lost by diffusion, and is also low for large particles > 3 mm, which will settle out owing to gravity (Becker et al., 2000). Particles with diameters between these extremes are carried with an efficiency of >80% (Perkins et al., 1993). Briefly, the **ICP-MS** standard instrument configuration consists of a

plasma (luminous volume of partially ionised gas) as ion source (ICP), generated from radio frequency magnetic fields induced by a copper coil, wounded around the top of a partly demountable glass torch, with removable alumina injector. Nickel cones (sampler and skimmer), in vacuum environment represent the interface for extracting ions from the plasma and transferring them in the region of the mass spectrometer (D'Oriano et al., 2008).

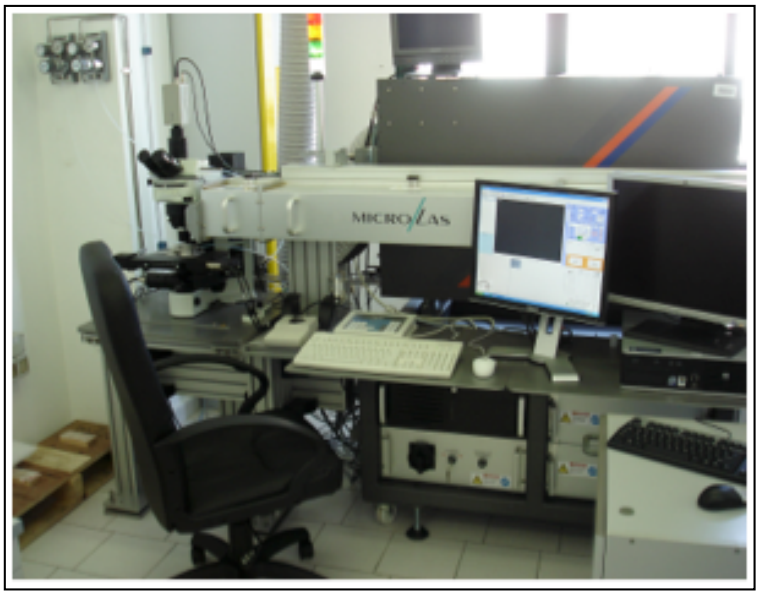

Figure 4.9: detail of Laser ablation instrumentation

4.3.5.2: Laser setting parameters for Br analysis, detection limit and reproducibility

Laser used in our instrument setup is a Compex pro 102, 193 nm ArF excimer laser ablation system (GeoLas Pro), of Istituto Nazionale di Geofisica e Vulcanologia (INGV) – Palermo. It is connected to a Agilent 7500 ce Inductively Coupled Plasma Mass Spectrometer (fig. 4.9).
This set-up is routinely used for major and trace elements measurement in melt inclusions. During this study, we developed a technique for Br routine measurements by LA-ICP-MS at INGV of Palermo in high concentrated sample, that was not obtained since so far. Here we present instrumentation, setting parameters, calibration procedure and data reduction software

we carried out.

Analysis by laser ablation requires a small amount of sample, with polished and clean surface to get reasonable detection limits and reliable quantification. Sample preparation is described in section 4.2.8.

The biggest challenge for LA-ICP-MS analysis of Br, as an anion, lies in its high ionization potential, that results in its absorption during the line-path to ICP. Using the standard setting configuration, analyses produced very high background signal referred to Br (both in 79 and in 81 mass) and we were not able to investigate concentration < 1000 ppm Br. This was probably due to the presence of Br from contamination of ablation chamber, ambient air, and formation of minor ^{40}Ar - ArH. However, analysis seemed to be quite repeatable and this was an evidence that standard are homogeneous.

We changed several parameters configuration, following procedure of Seo et al., 2011 at ETH, in order to reach the best setting to avoid interference with other elements and to obtain a good Br signal. Finally, we obtained the best configuration for ablation (laser power, carrier flux, pulse frequency) in term of signal/blank ratio where for "signal" we mean ablation of a Br-doped sample, and for "blank" we mean ablation of a sample without Br. Here we report the best setting configuration we obtained during this study. In high concentrated synthetic glasses used standard was NIST 610 (33 ppm Br). We used also Scapolite17, an in-house characterized crystal (Br = 438 ppm) which have been calibrated through synthetic glasses analysed by Rutherford Backscattered Spectroscopy (RBS), kindly provided by Dr. Markus Walle (ETH Zurich laboratory). Setting parameters are summarised in table 4.8

Laser wavelenght is probably the most important parameter which influences ablation mechanisms. Shorter wavelengths offer higher photon energies for bond breaking and ionisation processes. This parameter is a characteristic propriety of every laser instrument (Cromwell et al., 1995; Ducreux-Zappa et al., 1996; Durrant, 1999; Kinsley, 1997).

Fluence Energy is another one of the most important parameter to set. The quality of signal depend in the most part on it. We set fluence energy at 15 J/cm2 after several measurements tests. For values higher than 15, we obtain a better Br signal but the peak value during ablation was not constant and there was much spattering of material around the ablation hole. In fact, comparing spot area obtained from different set of fluence energy it is evident as for high values, the area around the crater is damaged and interested by the deposition of a quantity of ablated material (figure 4.10).

Helium gas was used as carrier inside the ablation cell and mixed with Argon, the makeup gas, before entering the ICP. In this way, reduction of the observed fractionation magnitude, both at the ablation site and during the transport toward the ICP-MS, was obtained, enhancing the transport efficiency of ablated material (Longerich et al., 1993; Gunther et al., 1998) (Concerning the dwell time we pointed out that values over 80ms have an effect on increase cps but not in improving signal/noise ratio.

Parameters	**Setted value**
Fluence energy (J/cm2)	15
Pulse energy (mJ)	100
Laser pulse duration (ns)	15
Laser wavelenght (nm)	193
Gas carrier flux (ml/minute)	800
Dwell time (ms)	60-80
Laser power (mj)	<0,5 to ~5
Pulse repetition rate (Hz)	20
Aperture (um)	90

Tab. 4.7: Setting parameters configuration for Br analyses by LA-ICP-MS at INGV of Palermo.

The selection of the spot size used during ablation is a critical parameter and depends on the sensitivity of the ICP-MS instrument to the elements of interest so that the smaller is the ablation crater, the smaller is the amount of sample material introduced into the plasma and the lower is the analysed signal intensities. Also, it depends on the size of what we have to analyse, so that if samples to be analysed are melt-inclusions, it is opportune to choose an appropriate spot size (in the range of melt-inclusions size). Various spatial resolutions can be achieved and, in spite of a small spot size could be the best solution for analysis in little chips of sample, it causes a dramatic increase of the detection limit (Schroeder et l., 1998). The best Br signal was obtained for diameter of the laser beam (and so the diameter of the ablation crater generated) of 90 μm. However, we changed several diameters and we observed a large spattering of material occurred during ablation with too small diameter aperture (e.g. 20 μm where a small diameter of ablation is required. It has to be taken in account that detection

limit is inversely proportional to the square of the ablated area (Sheppherd et al., 1995; Taylor et al., 1997).

Focusing on sample is another critical factor responsible both of the stability of the signal through time, both of the behaviour of elements during ablation-volatilisation. During a normal analysis the depth for a single ablation is about 20-40 μm (Mank et al., 1999). It depends on the duration of ablation and on the laser energy (Gunther et al., 2000; Craig et al., 2000). The ablation efficiency drops off as the depth of ablation in the sample increase depending on the focal length of the objective (Yoon et al., 1997).

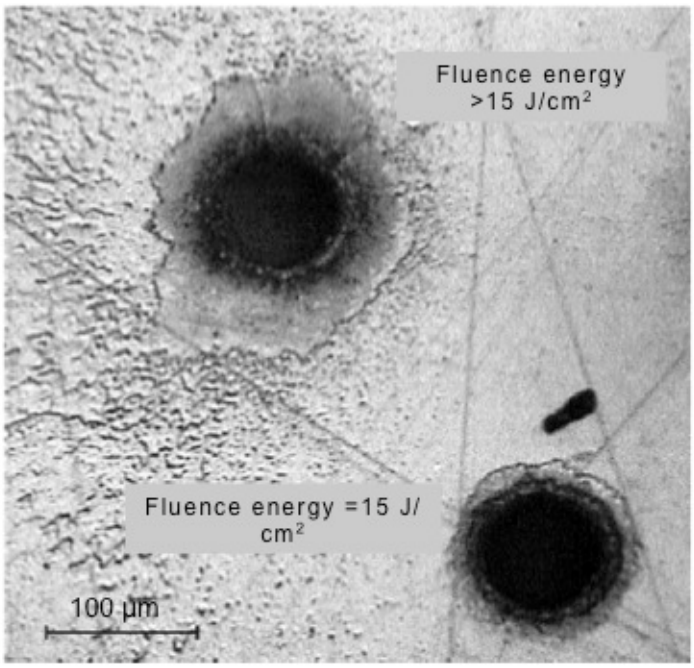

Figure 4..10: Comparing spot area using difference fluence energy. In the crater above we can notice that the crater ablation is affected by spattering phenomena and the area nearby is damaged and interested by deposition of ablated material. This effect is avoided in spot below. The black bar corrispond to 100 μm.

In order to test Br detection limit of LA-ICP-MS and to approach a comparison to others analytical techniques we conducted some experiments on the capacity of laser ablation to measure the concentrations of Br in melt inclusions. To evaluate the accuracy and reproducibility of LA ICP MS measurements, several run have been performed on single

different days. Results are shown in figure 4.12a.

During every measurement session, samples were analysed according to a specific sequence. Usually it starts with the analyses of two or more standards, then ten-twelve samples and then again with two standards, and so on.

In figure 4.11 are reported diagrams showing Br concentration in synthetic glass samples, measured by LA-ICP-MS vs Br concentration verified by INAA technique.

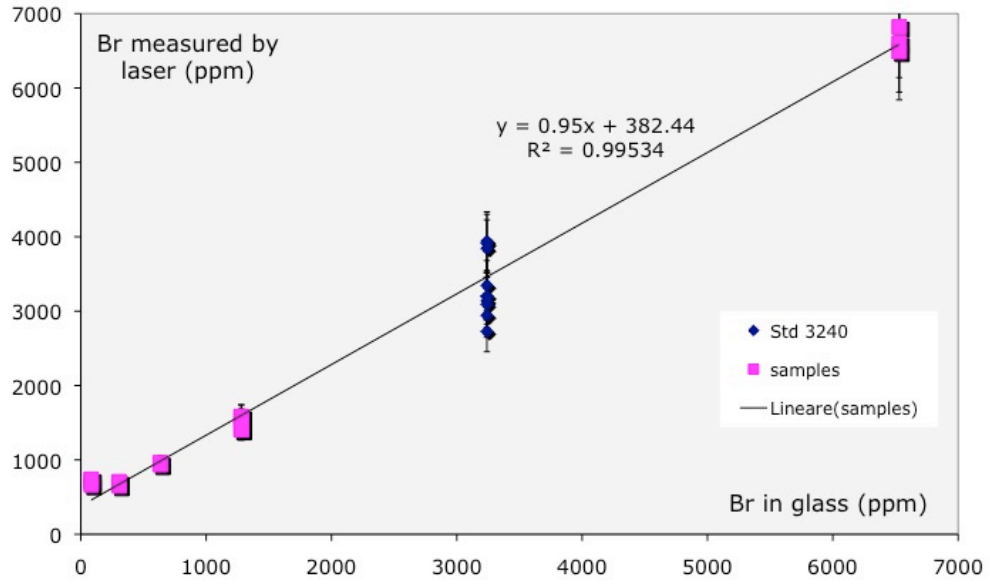

a)

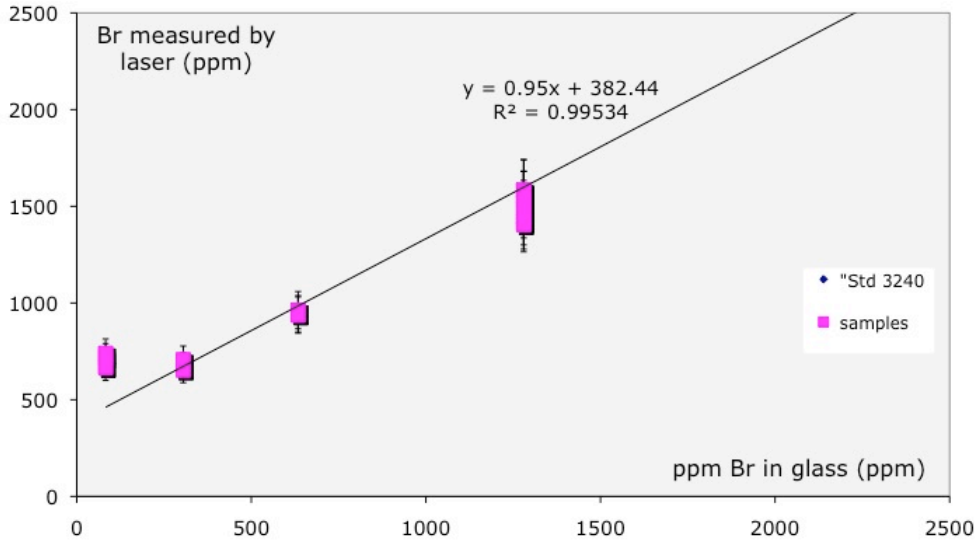

b)

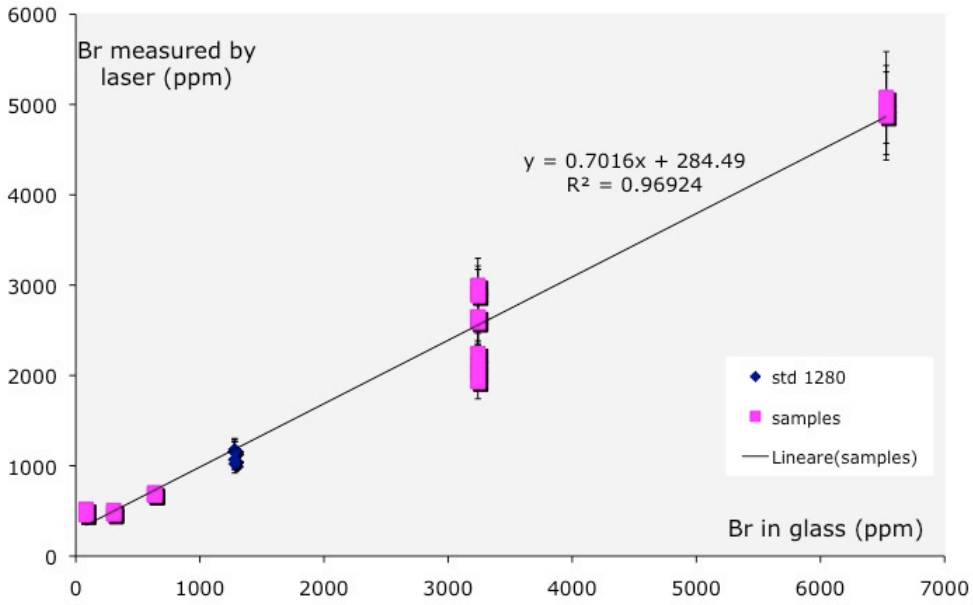

c)

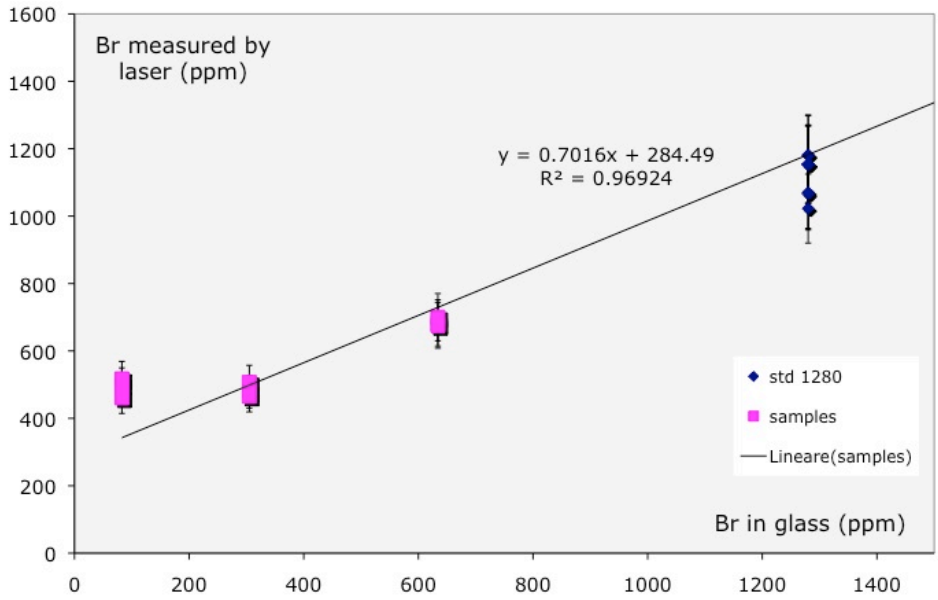

d)

Figure 4.11: Br measured by laser vs Br measured by INAA. Error has been estimated to be less than 10%; a) samples measured using STD 3240 ppm Br as a standard; b) zoom of diagram in a for low concentrations only; c) samples measured using STD 2180 ppm Br as a standard; d) zoom on diagram b for low concentrations.

To test the best sample to use as standard and verify the detection limit of the instrument on Br measurements, we run analysis on the entire set of glasses, setting separately different samples as standards. Here we report as example tests on two samples (3240 ppm and 1280 ppm of Br). With setting configuration shown in tab. 4.8, we obtained a detection limit for Br around 500-600 ppm.

In figure 4.11, diagram a) and c) shows samples from 100 ppm to 6930 ppm, lying in a calibration line obtained by setting respectively sample with Br concentration of 3240 ppm and 1280 ppm as standards. Setting a 10% error bar and zooming (diagrams b and d) for the low concentration only (<1000 ppm) we found a detection limit of ~ 300 ppm.

These considerations highlight that, in spite of setting the best parameters configuration in order to maintain a detection limit as low as possible, this was not enough to analyse melt inclusion where expected Br concentration is a few ppm.

So, due to the extremely low Br concentration in melt inclusions, it was not possible to asset an analytical method to measure Br in natural samples by LA-ICP-MS. It was used, in this study, only for analysis in high-doped Br glasses (synthetic glasses for partitioning study on $D^{melt/fluid}$).

Results on synthetic glasses of the partitioning experiments are shown in figure 4.12b. Partitioning samples measured during every analytical session are recalculated on the basis of the calibration line resulted from every session-day (Figure 4.12 a). Diagram shows calibration lines resulted for two consecutive measurements days in a Br measured by laser vs Br measured by INAA plot. Red line is the line resulted from the average values from different measurment on the same sample. Diagrams shows that measurements run in two different days are quite well repeteable.

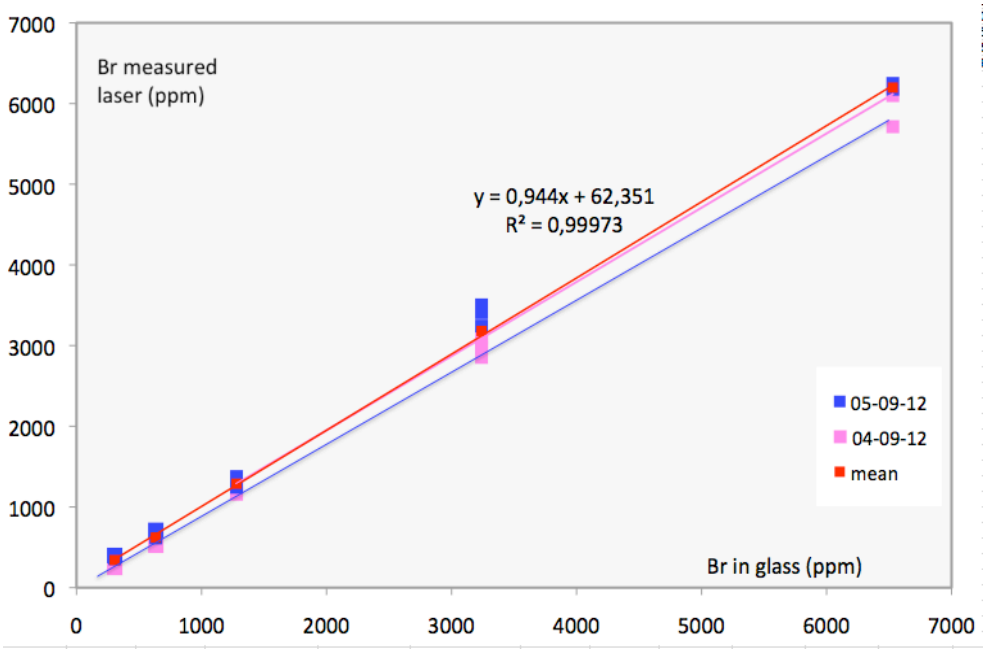

a)

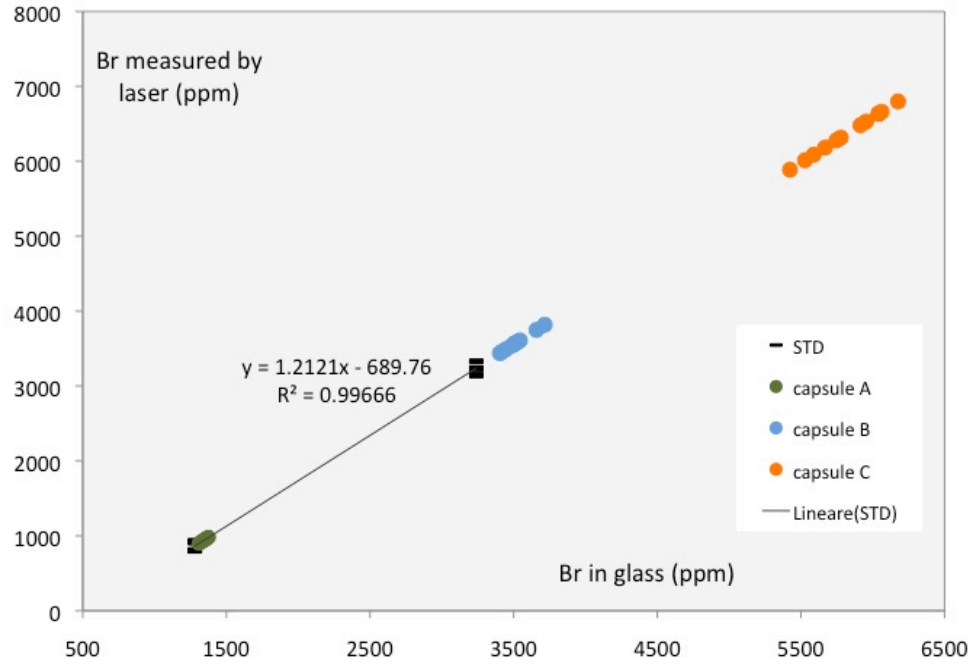

b

Figure 4.12: a) Different days measurements on standards confirm the good reproducibility of analysis. b) Estimation of the Br contents of 3 samples of the partitioning experiments, by using the calibration curve defined by the standards.

4.3.5.3: Data reduction software : Glitter

Once microparticulate material has been transported by the stream of argon to the plasma, the number of ions which reach the detector depends on (a) the atomic proportions of the element in the source mineral, (b) the amount of material removed during ablation, (c) the ionisation potential of the element in the plasma, and (d) isotopic abundance. Assuming no fractionation during ablation between volatile and other more refractory elements, it is possible to overcome these problems using an internal standard (known concentration of one element in the unknown using another analytical technique). Electron microprobe analysis is usually used to measure the concentration of the element chosen as the internal standard in the unknown. Calibration can then be achieved by comparing the response for the internal standard element in a reference material and the unknown. This element response for the internal standard allows the analyst to apply a correction for other elements included in the selected menu (assuming that the element response in the unknown is similar to that of the reference material).

We used silicate glasses produced by the US National Institute of Standards and Technology (e.g. NIST-610). This procedure is aimed to correct raw counts-per-second data for differences in the ablation characteristics between standards and samples so as to construct the calibration curve (Cps vs concentration).

Data were processed by GLITTER TM reduction software package, a data reduction software for the laser ablation microprobe, developed by the ARC National Key Centre for Geochemical Evolution and Metallogeny of Continents Exploration and Mining, to provide simpler, more consistent and real-time interactive analysis of LA-ICP-MS data. Elements measured by LA-ICP-MS with the external standardizations by NIST610 were converted to absolute concentrations by using internal standards (element in which we know concentration). As internal standard we used ^{44}Ca which concentration was previous determinated by EMPA.

Chapter 5
Results and discussion

5.1 Gas data set

In this work, a small database was populated with availables data-sets of halogens compositions of volcanic gases from a number of volcanoes of the world. The data-set is not intended to be exhaustive, but is an attempt to reproduce at the best of current knowledge - the compositional diversiry of Br contents in volcanic gases in different geodynamic settings.
The database was populated from published data (e.g., Kilauea, Mather et al., 2012; Masaya+Telica, Witt et al., 2008; Yasur, Métrich et al., 2011) and from unpublished results of measurements conducted over the last few years by personnel of INGV and DiSTeM (University of Palermo). The largest mass of information is from better-studied arc volcanoes, but the data set also includes measurements from hot-spot (Kilauea, Erebus) and continental-rift (Nyiragongo) volcanism. During this study we extended gas data set including new measurement from Etna, Kamchatka and Japan. The whole sampling data set is listed in table 5.1 and locations of volcanoes is shown in figure 5.1.

Sample	SO_2	F	Cl	Br	I	Br/S	Br/Cl	Sample	SO_2	F	Cl	Br	I	Br/S	Br/Cl
	ppm	ppm	ppm	ppm	ppm				ppm	ppm	ppm	ppm	ppm		
ETNA															
BN 1 A-C	21.9	1.2	7.0	7E-003	3E-004	0.0003	0.0010	**MASAYA**							
BN 1 B	6.1	0.1	1.5	2E-003	5E-005	0.0003	0.0011	25-Q01AA	10.3	-	3.4	4E-003	2E-004	0.0006	0.0011
BN 1 C	52.2	14.5	16.2	1E-002	4E-004	0.0002	0.0007	25-Q01BC	14.0	-	2.8	3E-003	1E-004	0.0003	0.0010
BN 2 A	51.9	12.2	18.0	2E-002	5E-004	0.0003	0.0009	25-Q01CC-	11.0	-	3.1	3E-003	2E-004	0.0005	0.0011
BN 1 A n	11.2	2.3	4.3	5E-003	1E-004	0.0004	0.0011	26-Q02AC	5.2	-	1.5	1E-003	8E-005	0.0004	0.0009
BN 2 A n						0.0010	0.0015	26-Q02BB	4.6	-	1.4	1E-003	8E-005	0.0004	0.0009
BN A	14.8	1.0	6.2	5E-003	2E-004	0.0004	0.0009	1-Q03AA-	6.0	-	1.8	2E-003	6E-005	0.0004	0.0009
NEC 1 A	16.8	2.5	5.5	5E-003	2E-004	0.0003	0.0008	1-Q03BC	4.0	-	1.2	1E-003	8E-005	0.0005	0.0012
BN 1 A	10.9	0.6	4.9	4E-003	9E-005	0.0004	0.0008	3-Q04C	2.1	-	1.7	1E-003	9E-005	0.0010	0.0008
BN 2 A	35.5	1.6	14.2	1E-002	2E-004	0.0003	0.0007	4-Q05AC	3.9	-	1.2	8E-004	7E-005	0.0003	0.0006
BN 1 A g						0.0003	0.0004	4-Q05BC	6.0	-	1.9	2E-003	1E-004	0.0004	0.0008
BN 1 A n	77.8	3.6	18.1	3E-002	3E-004		0.0016	4-Q05CC	6.2	-	1.7	1E-003	9E-005	0.0003	0.0007
Fumarole VOR	123.1	3.2	28.9	5E-002	9E-004		0.0017	6-Q07AC	5.0	-	1.7	9E-004	1E-004	0.0003	0.0005
VOR ac	45.3	0.4	11.3	8E-003	2E-004		0.0007	6-Q07BC	6.1	-	1.7	1E-003	9E-005	0.0003	0.0007
VOR df	54.3	0.9	17.0	1E-002	3E-004		0.0008	**TELICA**							
VOR gh	36.7	1.9	11.6	1E-002	5E-004		0.0009	27-T-03C	3.9	-	1.8	9E-004	2E-004	0.0004	0.0005
VOR (1 stage)	42.4	2.1	21.0	2E-002	3E-004		0.0011	27-T-04C	4.1	-	1.8	1E-003	2E-004	0.0005	0.0007
VOR df	47.7	2.6	23.8	3E-002	4E-004		0.0013	**KILAUEA**							
VOR df	9.4	0.8	5.8	2E-003	5E-005		0.0004	21-HIFP-14	4.2	0.11	0.1	1E-004	4E-006		0.0009
VOR	20.6	2.3	8.5	4E-003	1E-004		0.0005	24-HIFP-18	5.8	0.27	0.2	6E-005	7E-006		0.0003
VOR	20.2	1.6	6.6	5E-003	9E-005		0.0007	21-HIFP-08	5.5	0.12	0.2	5E-005	6E-006		0.0003
VOR ac	15.6	2.0	5.7	4E-003	1E-004		0.0008	21-HIFP-12	5.5	0.07	0.1	2E-004	7E-006		0.0024
VOR df	12.9	1.2	2.6	2E-003	7E-005		0.0006	24-HIFP-21	3.1	0.14	0.1	3E-004	6E-006		0.0027
VOR	11.9	0.8	3.0	2E-003	4E-005		0.0006	25-HIFP-39	5.1	0.26	0.2	8E-005	1E-005		0.0003
VOR	21.5	4.2	11.8	2E-002	1E-004		0.0015	25-HIFP-28	3.8	0.07	0.1	2E-004	8E-006		0.0019
VOR	15.7	4.5	11.8	2E-002	1E-004		0.0018	21-HIFP-05	5.5	0.09	0.1	1E-004	6E-006		0.0014
NEC	14.8	4.0	10.5	2E-002	2E-004		0.0021	25-HIFP-30	14.0	0.22	0.3	4E-004	1E-005		0.0012

NEC	5.5	1.0	3.8	2E-003	5E-005		0.0005	25-HIFP-33	9.3	0.19	0.3	4E-005	3E-006		0.0002
NEC	4.9	0.9	3.4	2E-003	6E-005		0.0006	24-HIFP-25	5.9	0.63	0.7	1E-004	2E-005		0.0002
NEC	11.4	2.3	5.3	7E-003	6E-005		0.0013	**MYAKEJIMA**							
NEC	11.2	2.6	6.7	7E-003	9E-005		0.0011	MYK 1 (A-C)	0.7	0.12	1.3	2E-003	3E-005		0.0018
NEC	2.4	0.9	1.6	3E-003	5E-006		0.0016	MYK 2 (A-C)	2.4	0.24	1.9	3E-003	1E-005		0.0015
NEC	1.6	0.8	1.7	2E-003	2E-005		0.0010	MYK 3 (A-C)	1.0	0.06	0.7	2E-003	6E-005		0.0025
nec ICPMS	1.6	0.6	1.7	2E-003	1E-005		0.0012	MYK 4 A	2.8	0.04	0.7	1E-003	5E-005		0.0016
nec HPLC	31.7	19.0	30.9	3E-002	2E-004		0.0011	MYK5 (A-C)	0.7	0.04	0.7	1E-003	2E-005		0.0016
nec HPLC	32.9	16.4	31.4	3E-002	2E-004		0.0010	MYK 6 A	2.3	0.04	0.8	2E-003	2E-005		0.0023
NEC	14.3	10.9	21.1	1E-002	2E-005		0.0007	MYK 7 (A-C)	0.7	0.10	1.1	2E-003	9E-005		0.0022
NEC	17.0	10.3	21.6	2E-002	2E-005		0.0008	MKY 8 (A-B)	3.5	0.07	0.9	2E-003	4E-005		0.0019
NEC	4.4	1.3	2.7	3E-003	1E-005		0.0012	MYK 9 (A-C)	3.5	0.09	1.1	2E-003	6E-005		0.0016
NEC	3.5	1.0	2.4	3E-003	1E-005		0.0011	MYK 10 (A-B)	2.3	0.06	0.6	1E-003	7E-005		0.0021
nec HPLC	17.8	5.1	15.0	1E-002	4E-005		0.0010	MYK 11(A-C)	0.3	0.07	0.7	1E-003	3E-005		0.0014
nec HPLC	2.1	4.5	8.6	1E-002	1E-004		0.0017	MYK12 (A-C)	0.5	0.04	0.7	1E-003	6E-005		0.0016
nec HPLC	10.1	3.5	10.0	1E-002	3E-004		0.0014	MYK13A	0.3	0.03	0.3	4E-004	8E-006		0.0016
nec HPLC	11.4	4.3	10.7	2E-002	5E-004		0.0015	MYK14 (A-C)	0.2	0.03	0.4	1E-003	2E-006		0.0029
nec HPLC	16.9	5.9	17.3	3E-002	6E-004		0.0015	MYK 15 (A-B)	0.1	0.04	0.4	9E-004	4E-005		0.0023
nec HPLC	15.0	6.0	15.0	3E-002	5E-004		0.0018	MYK 16 (A-C)	0.2	0.03	0.6	9E-004	3E-006		0.0015
nec HPLC	2.8	1.1	4.7	6E-003	1E-005		0.0014	MYK 17 (A-C)	0.1	0.04	0.6	9E-004	8E-006		0.0015
nec HPLC	5.6	2.5	4.6	8E-003	2E-005		0.0018	MYK 18 (A-C)	1.7	0.08	0.7	2E-003	1E-004		0.0033
nec HPLC	7.0	3.5	6.3	9E-003	1E-004		0.0014	1-Myake	0.5	0.02	0.5	2E-003	5E-007		0.0047
nec HPLC	11.1	2.7	7.3	3E-003	4E-005		0.0004	2-Myake	0.5	0.02	0.5	1E-003	6E-007		0.0026
nec HPLC	12.2	1.9	7.2	3E-003	1E-005		0.0004	3-Myake	0.2	0.01	0.1	1E-003	1E-007		0.0082
nec HPLC								**JAPAN**							
nec HPLC								MYAKE 1A	5.0		1.1	4E-004	1E-004	0.0001	0.0004
BN 1A	4.2	0.0	0.5	2E-002	1E-003	0.0057	0.0463	MYAKE 2A	3.8	0.40	1.6	1E-003	5E-004	0.0004	0.0009
BN 2A	3.9	0.1	0.4	2E-002	1E-003	0.0061	0.0648	MYAKE 3A	3.6	0.01	0.6	8E-004	2E-004	0.0002	0.0013
NEC 1A	5.2	4.0	11.1	2E-001	5E-003	0.0395	0.0185	MYAKE 4A	3.6	0.06	0.7	2E-003	2E-004	0.0005	0.0024
NEC 2A	6.7	4.5	12.1	2E-001	6E-003	0.0309	0.0172	4-ASAMA(1)	6.1	0.02	0.4	1E-003	2E-004		0.0031
NEC 1A	31.2	8.6	30.1	5E-001	1E-002	0.0173	0.0179	4-ASAMA(2)	5.8	0.02	0.4	1E-003	2E-004		0.0026
NEC 2A	27.4	9.4	30.0	6E-001	1E-002	0.0233	0.0212	5-ASAMA(1)	3.3	0.00	0.2	5E-004	9E-005		0.0021
TDF A	4.4	0.1	1.2	2E-002	1E-003	0.0056	0.0206	5-ASAMA(2)	3.1	0.01	0.2	1E-003	9E-005		0.0059
BN1A	1.5	0.0	0.5	9E-004	3E-005	0.0006	0.0019	ASAMA 1A	3.4	0.18	1.1	1E-003	3E-004	0.0003	0.0009
BN2A	0.5	0.1	0.2	1E-003	4E-005	0.0023	0.0074	ASAMA 2A	3.5	0.06	1.3	1E-003	3E-004	0.0003	0.0008
BNC 1a	5.4	0.1	4.2	4E-003	1E-004	0.0008	0.0010	ASAMA 3A	4.5	0.10	1.8	2E-003	4E-004	0.0003	0.0009
BNC 2a	4.3	0.2	3.9	4E-003	1E-004	0.0009	0.0010	ASAMA 4A	4.9	0.12	5.5	3E-003	3E-004	0.0007	0.0006
NEC 1a	5.2	0.9	2.6	4E-003	9E-005	0.0009	0.0017	ASO 1A	16.1	0.08	2.0	9E-004	1E-002	0.0001	0.0004
NEC 2a	5.2	0.8	2.9	4E-003	1E-004	0.0007	0.0012	ASO 2A	15.0	0.06	1.8	8E-004	1E-002	0.0001	0.0004
NEC 1a	4.8	1.2	5.0	7E-003	2E-004	0.0014	0.0014	ASO 3A	0.0	0.01	0.1	2E-005	4E-005	0.0005	0.0004
NEC 2a	3.1	1.5	5.0	7E-003	1E-004	0.0023	0.0014	ASO 4A	0.1	0.01	1.5	7E-004	1E-004	0.0046	0.0004
REUNION								**STROMBOLI**							
Reu1	21.8	1.2	1.4	2E-003	2E-004	0.0001	0.0015	STR 1	4.2	0.26	0.6	2E-003	3E-005		0.0027
Reu4	33.5	2.5	2.4	2E-003	2E-004	0.0001	0.0009	STR 1	0.9	0.17	0.7	1E-003			0.0015
Reu7	23.6	1.5	1.7	1E-003	1E-004	0.0001	0.0009	STR 2	4.7	0.63	2.2	3E-003	6E-005		0.0016
Reu10	10.9	0.5	0.7	9E-004	1E-004	0.0001	0.0013	**EREBUS**							
Reu13	21.0	1.2	1.5	1E-003	1E-004	0.0001	0.0010	ERE18(c+d)	0.8	0.51	0.1	3E-004	2E-006	0.0004	0.0044
Reu16	16.8	1.0	1.5	2E-003	1E-004	0.0001	0.0011	ERE16(c+d)	1.6	1.58	0.1	4E-004	3E-006	0.0003	0.0034
Reu19	14.6	0.7	1.0	1E-003	2E-004	0.0001	0.0012	**KAMCHATKA**							
NYIRAG.								Mtsky A1	22.2		6.3	4E-003	2E-003	0.0002	0.0006
NYIRA 1	0.7	0.1	0.1	6E-005	2E-005	0.0001	0.0006	Mtsky B1	21.4		5.7	3E-003	2E-003	0.0002	0.0006
NYIRA 2	0.5	0.0	0.1	6E-005	8E-005	0.0001	0.0011	Mtsky C1	23.5		7.0	3E-003	2E-003	0.0001	0.0004
NYIRA 1	7.2	0.7	0.4	8E-005	2E-004	0.0000	0.0002	Mtsky D1	21.3		6.8	2E-003	2E-003	0.0001	0.0004
NYIRA 2	8.1	0.7	0.5	9E-005	6E-005	0.0000	0.0002	Gorely A1	0.5		0.3	3E-004	5E-005	0.0006	0.0010
NYIRA 1	2.5	0.2	0.2	7E-005	3E-005	0.0000	0.0005	Gorely B1	0.5		0.3	3E-004	5E-005	0.0005	0.0010
NYIRA 2	2.7	0.3	0.2	7E-005	4E-005	0.0000	0.0004	**REDOUBT**							
NYIRA 1	1.5	0.1	0.1	8E-005	1E-005	0.0000	0.0006	1A	0.1	-	0.1	7E-004	3E-005	0.0059	0.0089
NYIRA 2	1.5	0.2	0.1	7E-005	6E-005	0.0000	0.0005	2A	0.2	-	0.1	8E-004	2E-005	0.0048	0.0070
NYIRA 1	0.5	0.0	0.0	6E-005	1E-005	0.0001	0.0011	3A	0.2	-	0.1	6E-004	2E-005	0.0037	0.0069
NYIRA 2	0.6	0.1	0.0	3E-005	2E-005	0.0001	0.0009	4A	0.2	-	0.2	8E-004	2E-005	0.0032	0.0049
NYIRA 1	2.1	0.1	0.1	4E-005	8E-005	0.0000	0.0003	MBWELE2	3.6	0.3	0.6	3E-003	2E-005	0.0009	0.0056
NYIRA 2	1.9	0.1	0.1	6E-005	4E-005	0.0000	0.0006	MBWELE 3	2.8	0.2	0.4	2E-003	2E-005	0.0008	0.0048
VANUATU								MBWELE4	1.3	0.2	0.4	3E-003	2E-005	0.0019	0.0062
YASUR 3	0.8	0.1	0.4	3E-003	3E-005	0.0040	0.0089	MBWELE 5	1.6	0.2	0.5	2E-003	2E-005	0.0014	0.0048

YASUR 5	3.0	0.3	0.7	3E-003	2E-005	0.0010	0.0046	BEMBOW 3	4.8	0.3	0.9	4E-003	3E-005	0.0008	0.0041
YASUR 6	5.0	0.5	1.4	3E-003	4E-005	0.0006	0.0022	BEMBOW 4	3.3	0.4	0.7	2E-003	2E-005	0.0007	0.0034
YASUR 8	2.1	0.3	0.7	4E-003	2E-005	0.0017	0.0052	BEMBOW 5	2.6	0.3	0.6	3E-003	2E-005	0.0011	0.0046
YASUR 9	0.8	0.1	0.4	2E-003	2E-005	0.0030	0.0063	BEMBOW 2	5.9	0.8	1.9	6E-003	4E-005	0.0011	0.0033
NIRITATIN	0.8	0.1	0.3	3E-003	2E-005	0.0037	0.0086								

Tab. 5.1: List of whole gas measurements performed through filterpacks method, both by INGV and DiSTeM Palermo). The data set comprends halogens and SO_2 data and collects measurements both on arc-volcanos and on non-arc volcanoes.

According to our dataset, Br concentrations in volcanic gas plume span several orders of magnitude, from 0.64 ppm (for one Etna sample) to as low as 2.2 x 10^{-5} ppm (for Aso volcano, Japan).

The hystograms of Figure 5.2 have been obtained from the log-populations of S/Cl, S/Br and Br/Cl (molar) ratios in the gas dataset.

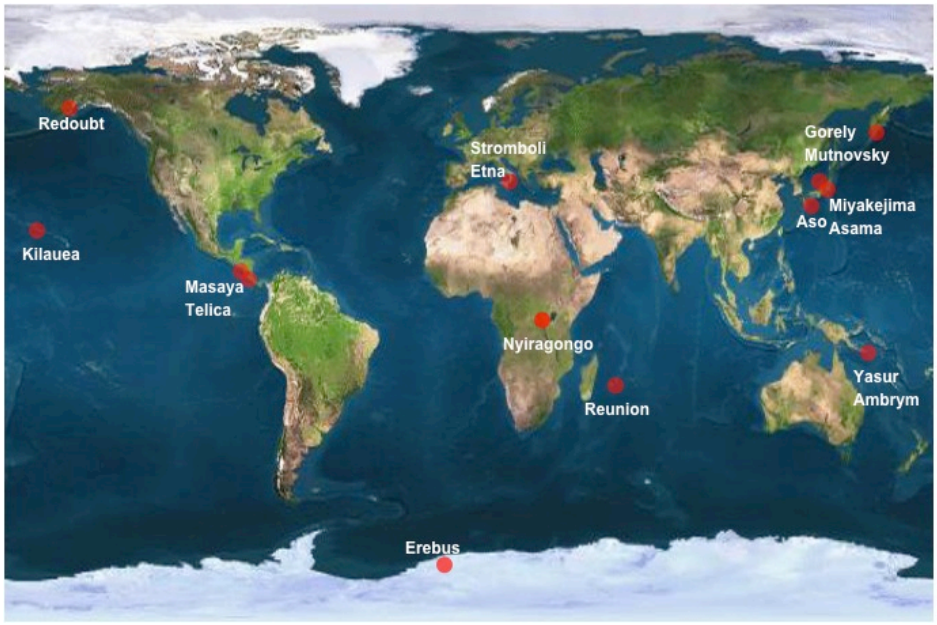

Figure 5.1: Map with location of volcanos listed in the dta set. Samplings were have been performed both by INGV and by DiSTeM of Palermo. In this study we extended measurements on Etna.

The hystograms reinforce previous ideas (e.g., Aiuppa, 2009; Aiuppa et al., 2009) of a large contrast in sulphur/halogen compositions of arc and non-arc volcanic gases. Broadly speaking, non arc-volcanoes are typically characterised by higher sulphur/halogen ratios than arc volcanoes (Figs. 5.2a, b). It should be noted, however, that while the arc-gas population appears to approximate a log-normal frequency distribution, a far less-defined distribution is obtained for non-arc gases, implying that the available dataset is far too incomplete to be representative of the natural variability of compositions. Fluxes of halogens to the atmosphere from non-arc volcanoes, infact, are far less well-constrained than those for arc-volcanoes, since there are fewer available measurements (Pyle and Mather, 2009). The distributions of Br/Cl ratios appear overalling for arc and non-arc volcanic gases, instead (Fig. 5.2c).

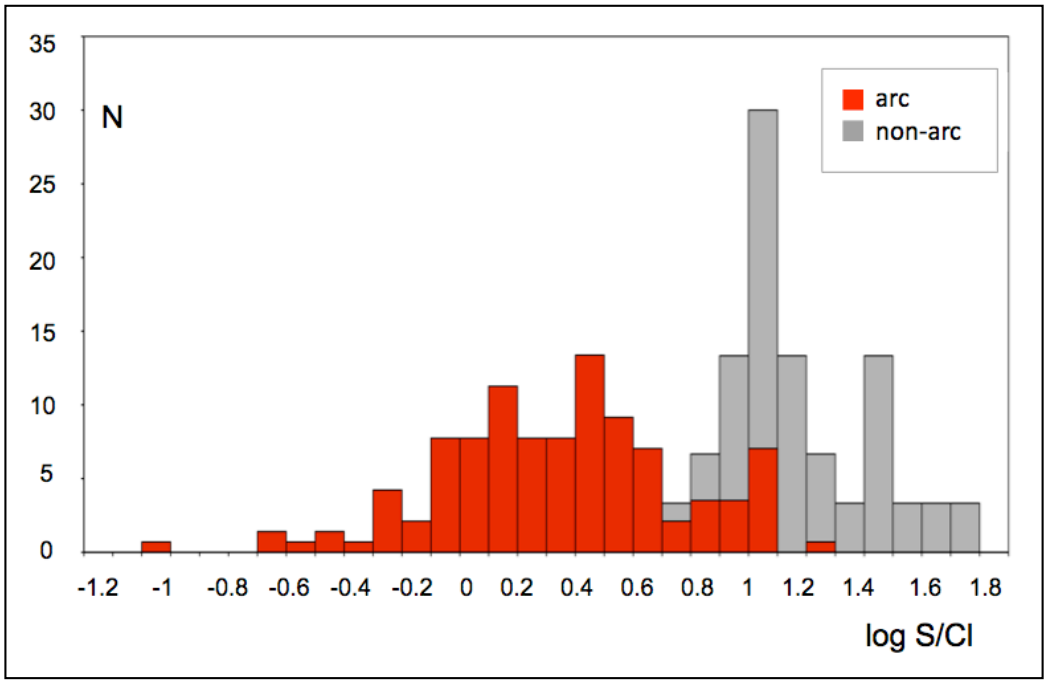

a)

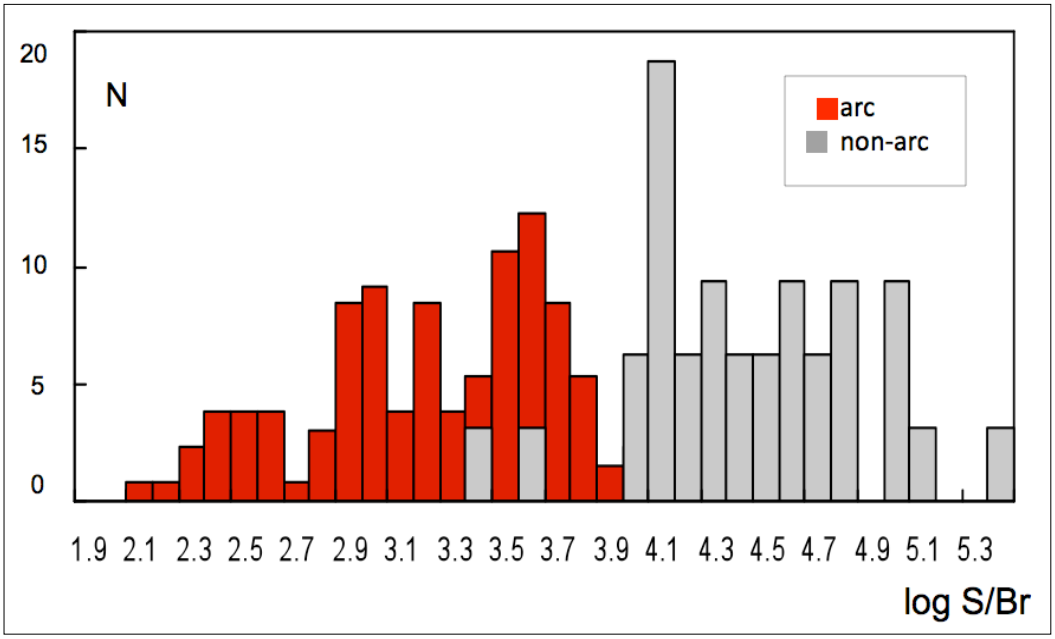

b)

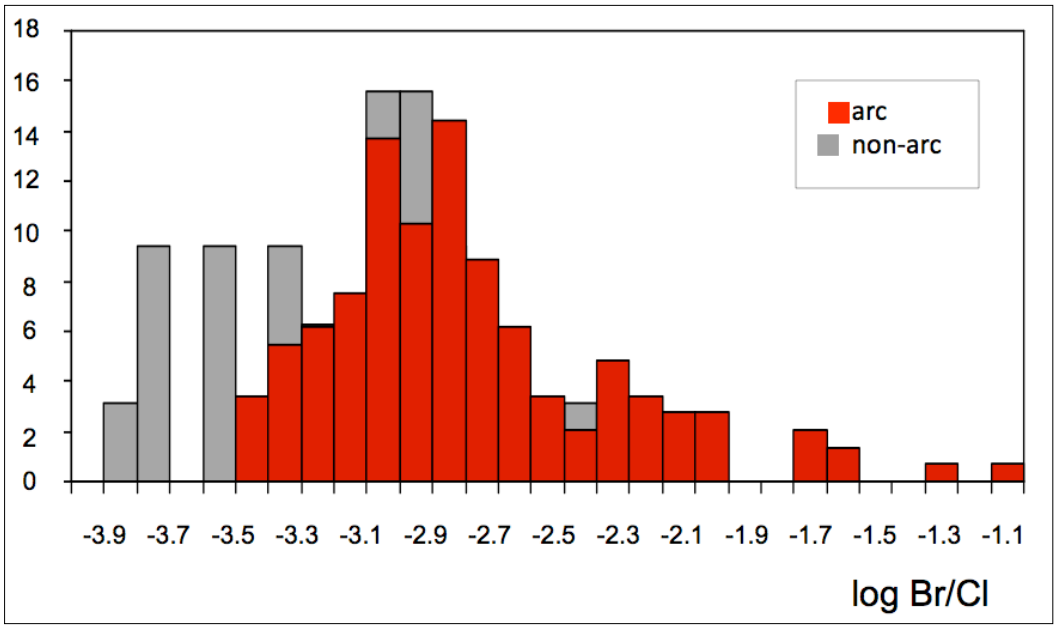

c)

Figure 5.2: Histogram diagrams of S/Cl, S/Br and Br/Cl for the whole gas data-set. Red bars represents arc-volcanoes; grey bars represents non-arc volcanoes.

Figure 5.3a is a plot of S/F versus S/Cl molar ratios in volcanic gas samples listed in Table 5.1. In such a sort of diagram, volcanic gas data split into two different clusters, both trending from SO_2-poor to SO_2-rich compositions. These linear arrays are visible both for any single volcano, and in the general arc vs non-arc data-sets.

These presence of two separate clusters of data in Figure 5.3a reflects the diversity of Cl to F proportions in arc and non-arc gases: for any given S/F ratio, non-arc volcanic gases have S/Cl ratios 1 to 2 orders of magnitude higher than arc volcanoes, e.g., they have lower Cl/F ratios. This element is in line with earlier finding of Aiuppa (2009), who had already recognised similar separated concentration trends (fig 5.3b) in a dataset of volcanic gas compositions from 28 different volcanoes located in arc, divergent-plate, hot-spot and continental-rift settings. The low S/Cl ratios of volcanic arc gases in Figure 5.3 is consistent with the Cl-rich nature of volcanic gases and melt inclusions from the corresponding magmas (Aiuppa 2009 and references therein). This general pattern predominantly reflects the addition of a Cl-rich component in subduction zones, likely due to a contribution from recycled fluids (Pyle and Mather, 2009).

Focus on arc gas datasets, identified by red markers in all the diagrams reported in fig. 5.3, shows that compositional variations of volcanic gases from arc volcanoes is impressive, in line with previous compilations (Symonds et al., 1994).

Bromine systematics in volcanic gas samples, considered in Figs 5.3c and 5.3d, allow identifying similar distribution in the data sets. In fact, diagram in fig. 5.3 c confirms the existence of two different clusters of data, one for arc volcanoes (lower S/Br and S/Cl ratios) and one for non-arc volcanoes (higher S/Br and S/Cl ratios). The existence of these two trends again support the general halogen-enrichment of arc volcanoes compared to non-arc volcanoes. A coherent behaviour of Br and Cl during magma generation and evolution is suggested by 5.3 d which highlights similar enrichment of Cl and Br shows in arc volcanism and relatively costant Br/Cl ratios in volcanic gases (arc and non-arc gases are aligned along the same almost-linear compositional trend in Figure 5.3 d.

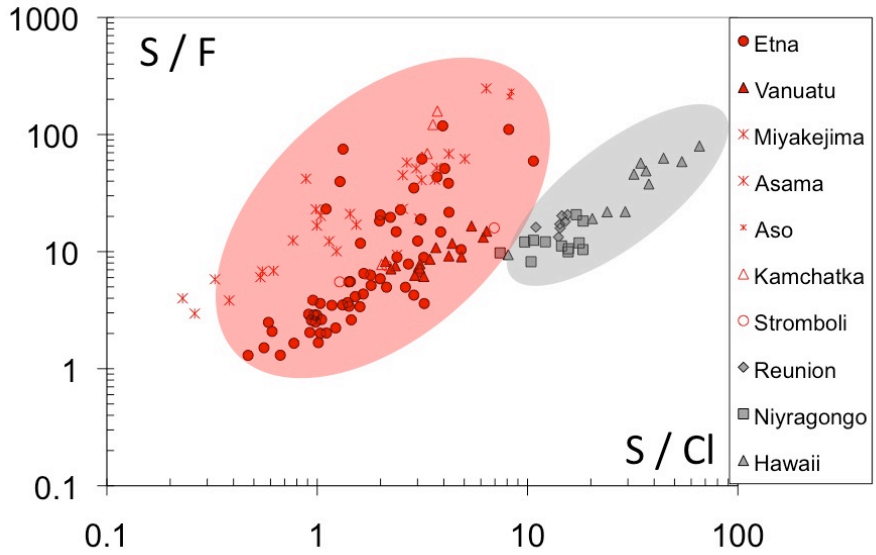
S / F
S / Cl
1000
100
10
1
0.1
0.1
1
10
100
Etna
Vanuatu
Miyakejima
Asama
Aso
Kamchatka
Stromboli
Reunion
Niyragongo
Hawaii

a)

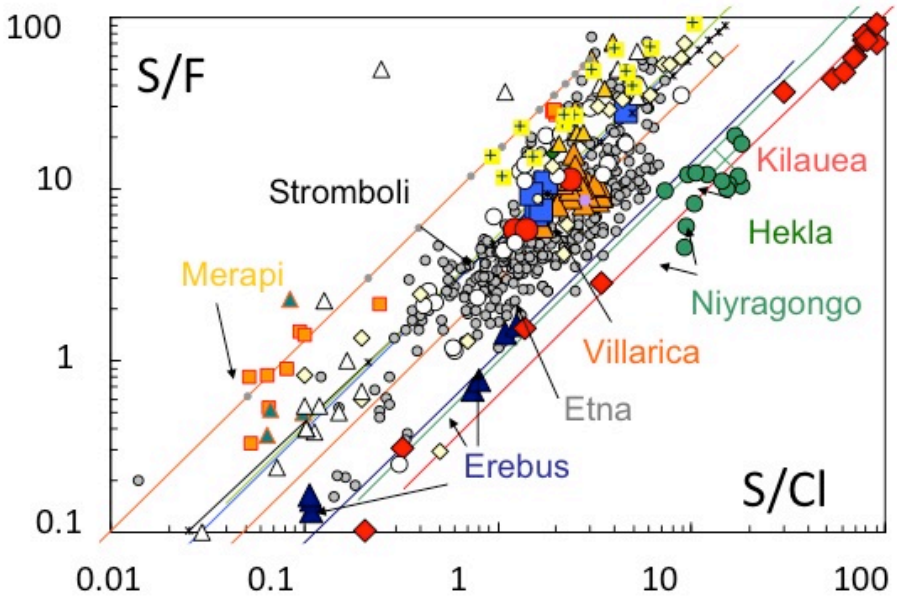
S/F
S/Cl
100
10
1
0.1
0.01
0.1
1
10
100
Stromboli
Merapi
Kilauea
Hekla
Niyragongo
Villarica
Etna
Erebus

b)

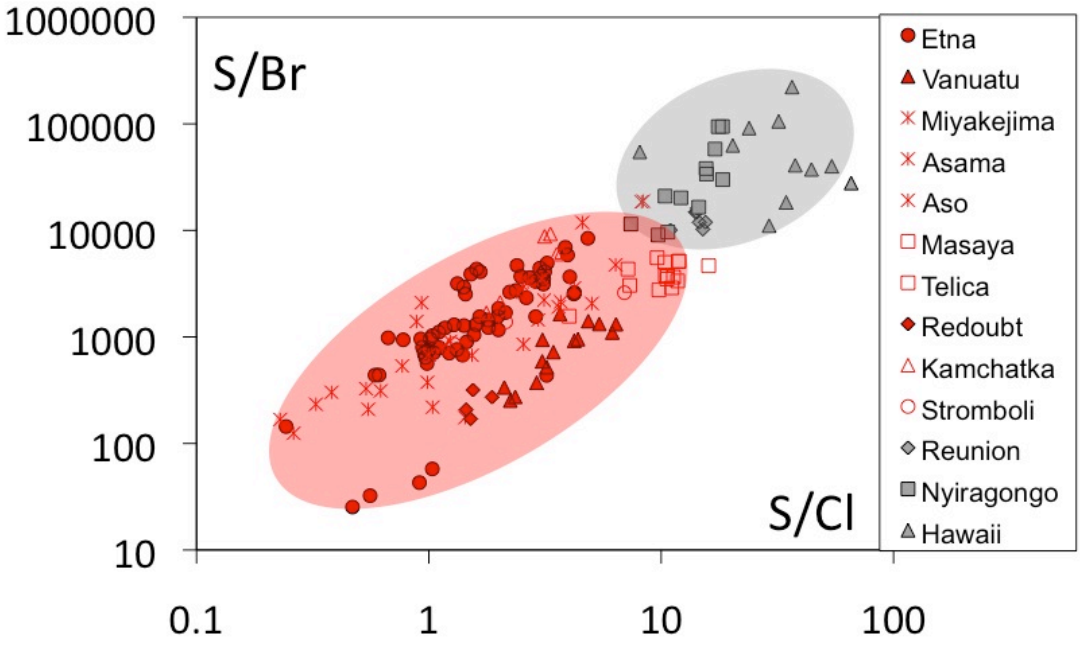

c)

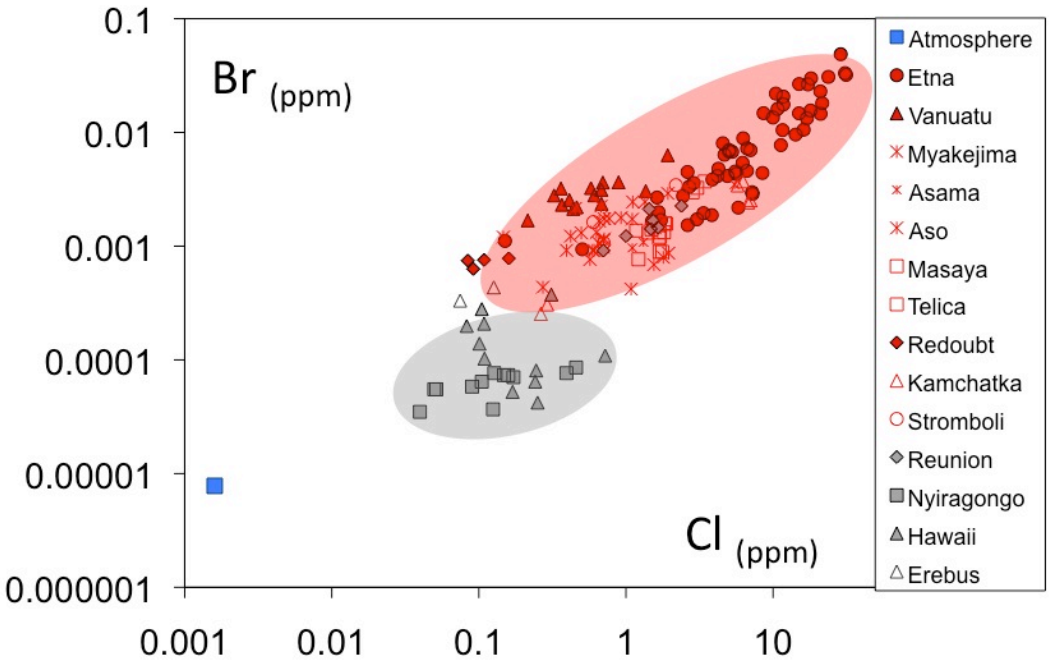

d)

Figure 5.3: a) S/F vs S/Cl plot of gas data set, molar ratio, in this study; b) S/F vs S/Cl plot from Aiuppa, 2009; c) S/Br vs S/Cl (c) and ppm Br vs ppm Cl (d) in the volcanic gas samples.

In this context, data from Etna are the best constrained in the whole data set, due to the huge amount of volcanic gas data accumulated at Etna over the years. S/halogen ratios in Etna's volcanic gases are particularly variable, while F/Cl and Br/Cl ratios are relatively more homogeneous. This confirms earlier findings that volcanic gas data from Etna cluster along a continuous trend from sulphur-rich to halogen-rich compositions (Aiuppa, 2009 and references therein).
Due to the unsafe access to the summit area of the volcano, where persistent strombolian activity takes place, determinations of halogen abundance in Stromboli's volcanic gas plume are relatively fewer if compared to Etna. The range of measured compositions at Stromboli overlaps the Etna's compositional field and, as noted above for Etna, F/Cl and Br/Cl ratios are relatively less variable than S/halogen ratios.

Figure 5.4 is a Cl-S-Br ternary plot drawn for the entire dataset. In line with indications from binary plots, the ternary diagram shows a typical halogen enrichment in gas samples from arc volcanoes, compared to samples from divergent plates and hot spot volcanoes. While the majority of gas measurements from non-arc volcanoes plots at the top part of the diagram, suggesting S-dominated composition, volcanic arc gases are more widely distributed, and shifted to more halogen-rich compositions.
The different concentrations of halogen species in different volcanic gas sources reservoirs leads to contrasting behaviour during generation of magmas. Likely, fluids in subduction zones should play a major role in recycling halogens into the mantle. In fact, according to several assumptions from various authors (Wallace, 2005; Aiuppa 2009; Pyle & Mather, 2009 and references therein), the most likely explanation for this Cl - Br enrichments in convergent-plate gases is that their magmas are enriched in Cl and Br, compared to divergent-plate volcanoes and hot-spot. This explanation is consistent with the H_2O enrichments of subduction zone magmas, and it fits the modern conceptual tectonic framework (Symond et al., 1994). In fact, the chemical composition of volcanic volatiles obviously depends strongly on magma composition, is intimately linked to geodynamic setting, and ultimately the expression of a different gas contribution to the mantle and dissimilar composition of parental magmas. Naer convergent plate boundaries, the transfer of solutes and heat between the ocean and the altaered oceanic crust, and then to the mantle wedge, are likely to play a key role

(Martin et al., 1993). Halides can be carried in significant amounts by volcanic gases, due to a variety of potential halogen sources: (a) the hydrated subducted crust and mantle, (b) the subducted marine sediments, (c) the mantle wedge, (d) assimilated crust, and (e) recycling by hydrothermal fluids (Wehrmann, 2005; Schilling et al., 1980). Subduction of hydrothermally altered Cl-Br-rich oceanic slabs and sediments beneath convergent plate volcanoes is implicit in plate tectonic theory, and the subducted materials provide an important source for volatiles associated with arc magmatism. Prohgrade metamorphic reaction in the oceanic crust and de-watering of marine sediments drive H_2O, Cl, Br and other volatiles from the subducted slab into the overlying mantle wedge, and these recycled volatiles enrich subduction zone magmas and their gas discharges (Symond et al., 1994).

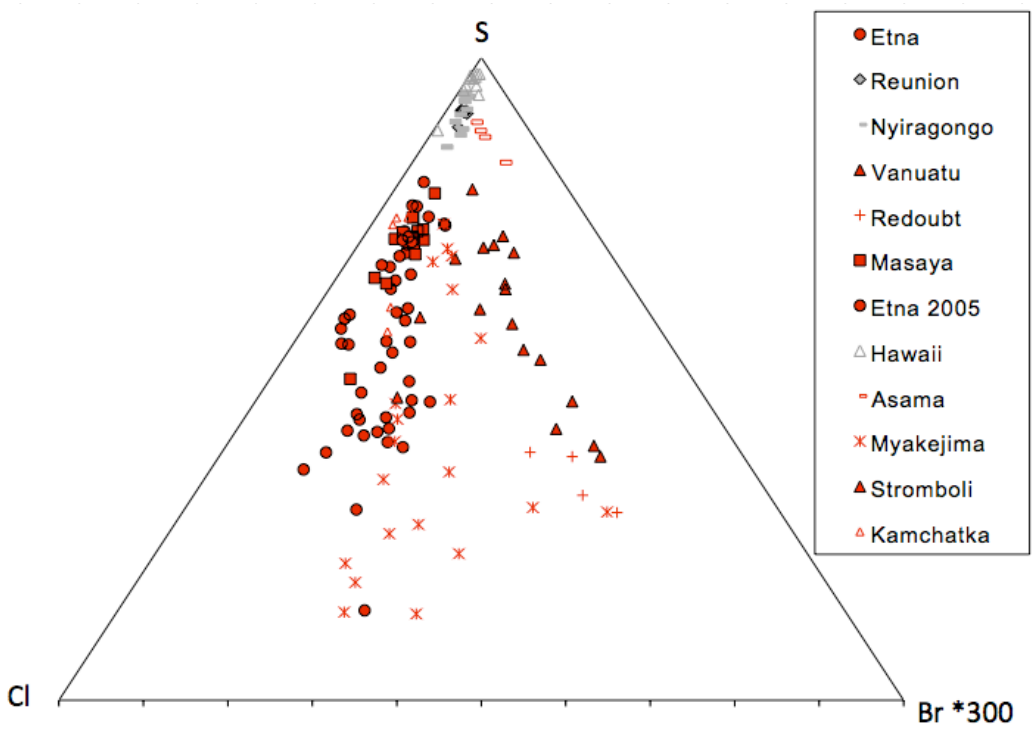

Figure 5.4: S-Cl-Br triangular diagram for the whole gas data set.

5.2: Results on partitioning experiments: mass balance and a preliminary D estimation

The aim of partitioning experiments we performed in this study, as already mentioned, it is to promote the partition of Br between a fluid phase and a melt phase, in order to calculate the Br distribution coefficient ($D^{melt/fluid}_{Br}$) and to investigate its affinity for the melt phase (D>1) or for the fluid phase (D<1). For this reason, partitioning experiments were planned with an excess of solution inside the capsule, in order to reproduce oversaturated condition, according to the saturation line for etna basalt composition (Lesne et al., 2010). With these conditions, once capsules were opened, the excess of gas trapped into the capsule escapes, and the effect is an appreciable weight loss respect to the initial weight.

The partition coefficient can be defined as :

(1) $$D^{\frac{m}{f}} = \frac{CBr_m}{CBr_f}$$

where CBr_m is the Br concentration in the melt phase and CBr_f is the Br concentration in the fluid phase. In order to use the above equation to calculate D from a partition experiment, we measure CBrm, that is the Br concentration measured in the quenched glass as discussed above. On the other hand, due to the complexity of extracting and analyzing the extremely small quantities of quenched fluid from each experiment capsule, we were not able to measure CBr_f. The latter can instead be estimated by a mass balance approach given that the total amount of Br loaded in the capsule is a known datum.

In doing this, we followed the approach of Signorelli and Carroll, 2000 and Paonita, 2005 applying the relation

(2) $$MBr_L = M_m \times CBr_m + M_f \times CBr_f$$

where MBr_L is the mass of bromine loaded in the capsule through the solution, M_m is the

mass of melt t and M_f is the mass of fluid. CBr_m and CBr_f are respectively the Br concentration in the melt and in the fluid phases. Equation (2) can be developed by expliciting loaded amounts:

(3) $$\frac{Br_L}{tot} = \frac{bas + (H_2O)_m}{tot} \cdot CBr_m + \frac{(H_2O)_f + MBr_f}{tot} \cdot CBr_f$$

where

$$\frac{bas + (H_2O)_m}{tot}$$

is the contribute of the melt phase (basalt + H_2O dissolved in the glass) normalised to total mass (we have neglected MBrm in the summation being Br always a fraction of percentage in the capsule) and

$$\frac{(H_2O)_f + MBr_f}{tot}$$

is the contribute of the fluid phase (mass of Br in the fluid + H_2O dissolved in the fluid) normalised to total mass.

Basing on the results of experiments reported by Bureau et al, 2000 for albitic composition, where they found a $D^{m/f} \sim 0{,}003$ (strongly supporting an affinity of Br for the fluid phase) we assumed a similar behaviour also for basaltic composition. From this assumption it derives that the most part of the bromine loaded into the capsule should be dissolved in the fluid phase while the amount of Br dissolved in the melt being negligible. On this basis, we can assume MBrf ≅ MBrtot (namely the total amount of Br loaded in the capsule) and solve the mass balance calculation to obtain CBr_f . Once we measured CBr_m by analysis of glasses by LA-ICP-MS, we are able to calculate the partition coefficient through equation (1).

Mass balance, in experiments from RP1 to RP8 (tab. 5.2), was complicated by an unexpected anomalous partition of Br in the melt phase so that the Br mass in fluid phase resulted less

abundant than mass in melt phase at the point that in many cases $D^{m/f}$ assumed negative values. This implies that above assumption MBrf ≅ MBr tot is not more suitable to calculate $D^{m/f}$.

In contrast, the term M Br_f in $\frac{(H_2O)_f + MBr_f}{tot}$

could be neglected since the mass of Br in the fluid phase was negligible. So, equation can be written as

(4) $$\frac{Br_L}{tot} = \frac{bas + (H_2O)_m}{tot} \cdot CBr_m + \frac{(H_2O)_f}{tot} \cdot CBr_f$$

This equation and eq.(1) have been used to calcolate $D^{m/f}$ once C Br_m has been measured.
List of the total partitioning experiments, reporting amount of basalt and solution added into the capsules, amount of H_2O dissolved in the melt (%), pressure of the experiment (bar), volatile loss for each capsule (mg) and resulting $D^{m/f}$ values is shown in tab. 5.2.

Cutting off $D^{m/f}$ negative values, we obtained a few results with a wide range of variability that suggest that the mass balance is extremely sensitive to Br concentration in melt, obtained by LA-ICP-MS measurements. In fact, even an error < 10% in C Br_m is able to strongly modify the ratio between Br concentration in the melt and Br concentration in the fluid (and then D). The occurrence of negative $D^{m/f}$ values and the high sensitivity to the mass balance is explained by the fact that almost all Br is in the melt. To reduce this problem, further experiments were planned, adding more solution inside the capsule in order to increase the amount of partitioned fluid phase and then the Br mass in the fluid phase with respect to that in the melt, even if D is unchanged. This set of experiments (RP9-RP10c) showed a $D^{m/f} > 1$ and this would probably mean that Br seems to be much more compatible with melt phase than our expectations, relative to basaltic melt composition. In any case, mass balance was still very sensitive to measured CBrm, because most of Br was in the melt.

Before assuming this range of values ($D^{m/f} > 1$) as a reliable Br partition coefficient, we tried to understand why our results on D were so different from the expected ones. One possible reason that could justify this problem is the formation of a Br-rich brine coexisting with the two other phases, as found for chlorine by Signorelli and Carrol, 2000.

In spite of we cannot exclude the occurrence of a brine within our system, the homogeneity of the samples we tested by LA-ICPMS makes poorly probable that high-Br concentration are due to ablation of vesicles of brines.

Experiment	Sample	P	Basalt loaded	Solution loaded	Br loaded	H_2O dissolved in melt	Br measured by laser	H_2O in fluid phase	Volatile loss	Br in fluid phase	$D^{m/f}$
		(bar)	(mg)	(mg)	(mg)	(mg)	(ppm)	(mg)	(mg)	(%wt)	
Year 2012											
RP1	Caps1 a	1000	47.30	2.39	0.0029	3,49	173	0.65	0,90	-	-
RP1	Caps1 b	1000	46.70	2.46	0.0301	3,49	710	0.72	1,30	-	-
RP2	Caps1 c	1000	46.70	2.44	0.1950	3,49	4328	0.70	1,00	-	-
RP2	Caps1 d	1000	48.40	2.44	0.4333	3,49	11120	0.70	0,70	-	-
RP2	Caps1 e	1000	47.6	2.60	1.0096	3,49	20653	0.86	1,40	-	-
RP3	Caps2 a	500	49.06	1.99	0.0028	2,32	447	0.84	1,20	-	-
RP3	Caps2 b	500	49.06	1.86	0.0267	2,32	1346	0.71	1,20	-	-
RP4	Caps2 c	500	49.36	1.87	0.1771	2,32	6728	0.71	1,00	-	-
RP4	Caps2 d	500	52.36	1.80	0.3881	2,32	13509	0.64	0,70	-	-
RP4	Caps2 e	500	49.36	1.80	0.8542	2,32	19607	0.64	1,00	-	-
RP5	Caps3 a	250	58.07	1.09	0.0041	1,54	553	0.32	1,60	-	-
RP5	Caps3 b	250	50.77	1.08	0.0083	1,54	697	0.32	0,80	-	-
RP6	Caps3 c	250	51.07	1.07	0.0222	1,54	1249	0.30	0,50	-	-
RP6	Caps3 d	250	52.97	1.14	0.0455	1,54	1784	0.37	0,60	-	-
RP6	Caps3 e	250	54.57	0.55	0.0364	1,54	2438	-	0,40	-	-
RP7	Caps4 a	100	50.85	0.48	0.0100	0,89	614	0.04	0,90	-	-
RP7	Caps4 b	100	49.95	0.59	0.0847	0,89	1610	0.15	0,60	0.02	0,08
RP8	Caps4 c	100	49.95	0.48	0.1695	0,89	2592	0.04	0,60	0.19	0,01
RP8	Caps4 d	100	50.45	0.75	0.2329	0,89	11790	0.26	1,10	-	-
Year 2013											
RP9	CapsX d	1000	100.61	8.35	1.19	3,49	11000	4.55	0,0052	0.007	1,48
RP10	Caps5 a	2000	95.22	8.38	0.103	5,26	1343	2.93	0,0037	-	-
RP10	Caps5 b	2000	94.42	8.56	0.309	5,26	3522	3.11	0,0031	-	-
RP10	Caps5 c	2000	94.56	8.88	0.606	5,26	5827	3.43	0,0033	0.006	1

Tab 5.2: List of all partitioning experiment run. LA-ICP-MS are the average measurements on 5 points. $D^{m/f}$ has been calculated on the basis of concentration of Br measured by laser and of the Br mass in fluid phase

Unfortunately, we cannot use Na as a tracer of the presence of NaBr bearing brine because the related Na anomalies (as computed by the measured Br contents) would be too small with respect to the content of Na_2O of the basalt.

From a more theoretical point of view, a solubility model for Br in basaltic composition is lacking in scientific community, thus there is a gap in understanding NaBr behaviour inside

capsule, at any concentration. In their experiments on Cl solubility in melts, Signorelli and Carrol, 2000 predicted the formation of a Cl-rich brine by using the well-known immiscibility gap in the system NaCl-H_2O at high pressure-temperature (Fig.5.5). According to this idea, the authors, for high concentrated samples, found a subcritical region where the presence of a brine occurred. In this region there is the coexistence of three phases (melt + fluid + brine) and thus only an apparent fluid/melt distribution coefficient could be obtained.

On the basis of these consideration we could hazard a comparison with NaCl solubility model described. If we assume a similar miscibility gap also for NaBr-H_2O system (even if with a different shape compared with the NaCl system), we can suppose the presence of conditions where a Br-rich brine could be exist. The presence of a brine could be a possible answer to explain the high melt/fluid partition coefficient we found in our experiments.

We prepared a set of experiments at two different pressures (1 and 2 kb) with three different NaBr concentrations on the basis of two hypothetic $D^{m/f}$ resulting ($DBr^{m/f}$ <1 and $DBr^{m/f}$ >1). Assuming a similar size and shape for the immiscibility region between Br and Cl, our consideration predict two different possibilities. In the first one, melt phase is in equilibrium with a fluid phase only ($DBr^{m/f}$ <1; low Br amount in the glasses; green points). In the second case, the melt is in equilibrium both with a fluid phase and with a Br-riched brine (subcritical region; $DBr^{m/f}$ >1; red points). List of these partitioning experiments run is reported in tab 5.2.

On the basis of all consideration we made above and since analysis on Br-doped partitioning glass are quite repeatable, it seems that no significant error occurs during each experiments. In spite we obtained a set of experiments (RP7-RP8) where $D^{m/f}$ was <1, we prefer to use last experiments set only (RP9-RP10) since, on the basis of previous considerations, they could be near a more reliable condition. This last results support an unexpected high partitioning of Br in the melt phase showing a $D^{melt/fluid}$ range ≈1,48. This is in contrast with the common idea of a increasing affinity for the fluid phase for volatile elements with strong incompatible feature and large ionic radius as Br.

We cannot completely exclude that in our compositional conditions Br would behave differently than expected, showing a deviation from what is observable in other system with different melt composition.

Obviously this is just an approximate estimation since these results have to be verified by further experiments. However, this study confirms the complexity of interaction between a

basaltic melt and its coexisting fluid phase and highlights the extreme

The most important challenge is to understand where the two-phases system (a system composed of a silicate melt and an vapor fluid) is complicated by the occurrence of a separate Br-rich brine, resulting in the forming of (a three phases system). The conditions at which this could occur are variable and they could depend on the initial composition of melt, temperature, pressure and total amount of both basalt and solution added into the capsules.

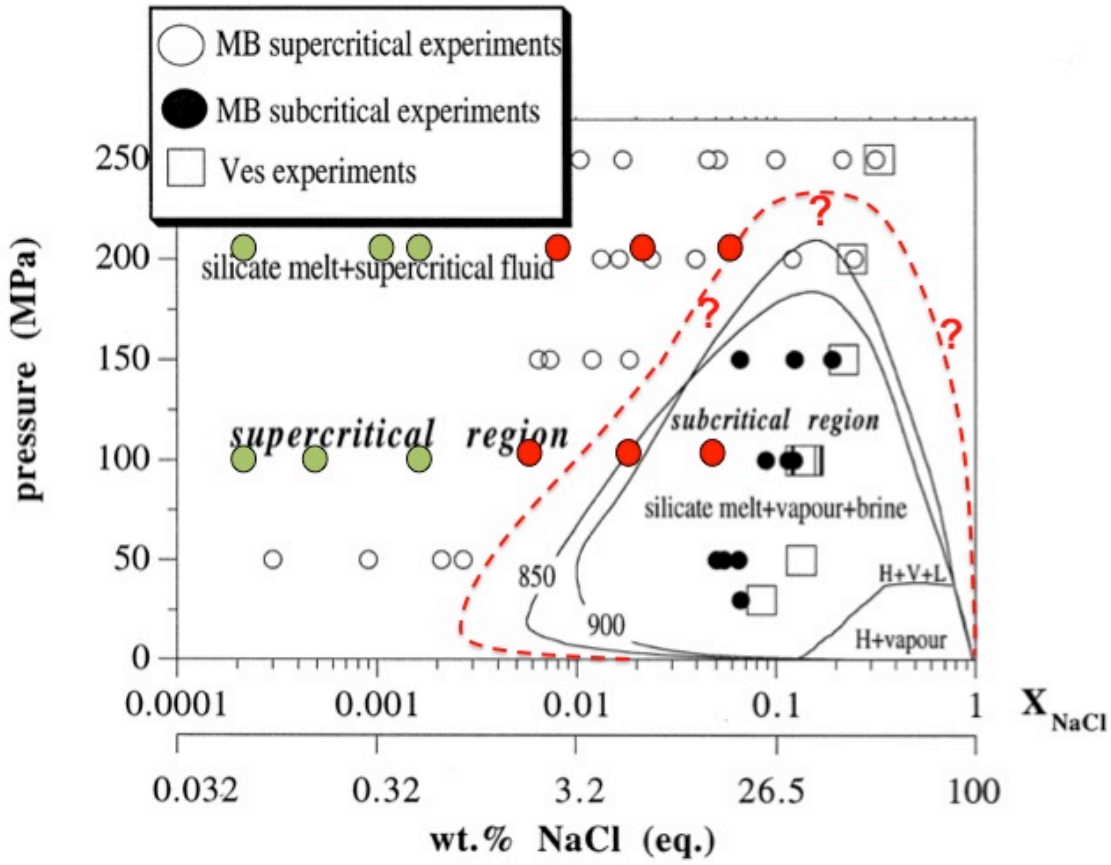

Fig. 5.5 Pressure–XNaCl diagram of the system NaCl–H2O with 850°C and 900°C isotherm (modified by Signorelli and Carrol, 2000).

5.3 Melt-inclusion

5.3.1 Br abundance in MIs

The concentrations of Bromine in melt inclusions from Etna and Stromboli, determined using the technique detailed in chapter 4, are reported in Table 5.1. The same table also lists the concentrations of other volatiles (S, Cl, H_2O) and some selected major elements (K_2O, CaO, Al_2O3) determined on the same inclusions by EMPA (Stromboli: data from Métrich et al., 2001, 2010; Etna: EMPA measurements made at ISTO-Orleans, courtesy of E. Gennaro and G. Iacono-Marziano). The Forsteritic content of the olivines (Fo-host olivine) hosting the inclusions is available for the Stromboli samples (Métrich et al., 2001, 2010).

sample	Ol.	MI	Br	Cl	S	H_2O	CO_2	K_2O	CaO/Al_2O_3	Fo ol.	sample	Ol.	MI	Br	Cl	S	H_2O	CO_2	K_2O	CaO/Al_2O_3	Fo ol.
			ppm	wt %	wt %	wt %	wt%	wt %		mol %				ppm	wt %	wt %	wt %	wt %	wt %		mol %
ST150307	40	a	0.50								ST82c	139	b	1.66	0.177	0.195	2.56	1548	1.53	0.94	86.5
ST150307	39	a	0.64								ST82c	138	a	1.27							
ST150307	38	a	6.16								ST82c	137	a	4.81	0.170	0.200	2.90	2264		0.93	89.8
ST150307	33	a	1.09	0.151	0.160	2.70	1636	1.58	0.7	85.9	ST82c	132	a	3.12	0.181	0.204	2.81	1420	1.53	0.99	87.6
ST150307	33	b	1.42								ST82c	133	a	2.51	0.168	0.180	2.90	1294	1.16	0.89	89.3
ST150307	33	c	1.99								ST82c	134	a	1.35							
ST150307	34	a	0.52	0.156	0.159	1.90	1231	1.79	0.69	86.2	ST82c	135	a	2.11							
ST150307	36	a	1.50								ST82c	135	b	0.50							
ST150307	37	a	0.50																		
ST150307	32	a	0.50								Etna FS	10	b	0.50	0.14	0.17			0.92	1.34	
ST150307	32	b	0.50	0.156	0.125			1.75		84.9	Etna FS	10	c	0.50	0.13	0.15			0.76	1.34	
ST150307	31	a	0.74	0.161	0.160	2.50	1065	1.68	0.69	85.6	Etna FS	11		0.50	0.09	0.12			1.31	1.22	
ST150307	30a	a	3.16	0.160	0.156	2.60	1236	1.44	0.7	85.6	Etna FS	13	c	1.09	0.21	0.26			0.77	1.49	
ST150307	30b	a	5.67								Etna FS	13	b	0.50	0.20	0.26			0.89	1.46	
ST150307	29	g1	0.50	0.152	0.167	2.70	1266	1.6	0.69	85.9	Etna FS	14		0.50	0.17	0.23			1.21	1.41	
ST150307	28	a	1.18								Etna FS	5		0.50	0.16	0.12			1.46	1.41	
ST150307	28	b	1.08								Etna FS	6	b	0.63	0.14	0.17			0.99	1.37	
ST150307	28	c	1.90								Etna FS	6	c	0.76	0.16	0.28			0.90	1.49	
ST150307	23	a	0.71	0.155	0.165	3.00	1152	1.48	0.74	83.9	Etna FS	7		0.50	0.17	0.23			1.05	1.47	
ST150307	23	b	0.64								Etna FS	8	b	0.50	0.13	0.18			1.21	1.24	
ST150307	24	a	1.27	0.149	0.157	2.80	1498	1.62	0.69	85.3	Etna FS	8	c	0.50	0.11	0.18			1.25	1.39	
ST150307	26	a	5.00								Etna FS	9		0.50	0.20	0.28			1.09	1.42	
ST150307	26	b	0.50								Etna FS	00		0.50	0.17	0.11			0.88	1.29	
ST150307	26	c	0.50								Etna FS	1		0.50	0.19	0.23			1.09	1.33	
ST150307	26	d	0.50								Etna FS	3		0.50	0.11	0.18			0.86	1.49	
ST150307	26	e	0.76																		
ST150307	26	f	0.68								2001 UV	C10		0.50					3.11	0.54	
ST150307	27	a	0.50	0.152	0.167	2.80	1586	1.5	0.71	84.4	2001 UV	C7		0.50					3.28	0.45	
ST150307	19	a	0.50	0.152	0.116	1.70	926	1.69	0.7	84.9	2001 UV	D2		0.50	5.25	0.05			3.80	0.47	
ST150307	19	b	0.79	0.154	0.156	3.10	1372		0.7	84.9	2001 UV	F10a		0.50					3.95	0.47	
ST150307	14	a	0.94								2001 UV	F10b		1.40					4.01	0.46	
ST150307	14	b	0.50								2001 UV	H3		0.50	5.73	0.07			4.04	0.43	
ST150307	14	c	0.50								2001 UV	L7		0.50					4.40	0.39	
ST150307	14	d	0.50								2001 UV	B10		0.88					3.52	0.45	
ST150307	14	e	1.13								2001 UV	E8		0.50					4.00	0.34	
ST150307	14	f	1.19								2001 UV	F9a		0.59					3.84	0.38	
ST150307	14	g	0.50								2001 UV	M9		0.50					2.84	0.54	

ST150307	12	a	1.03															
ST150307	12	b	1.27								2006	B5	0.50				3.70	0.46
ST150307	10	a	1.71								2006	C1 1	3.33				3.40	0.47
ST150307	8	a	1.63	0.153	0.164	2.90		1.62	0.69	85.3	2006	C7	5.30				3.33	0.38
ST150307	8	b	0.91								2006	F5	0.77				2.99	0.44
ST82c	150	a	0.50								2006	I6	0.50				4.18	0.38
ST82c	150	b	0.50								2006	B3	0.74				3.90	0.42
ST82c	149	a	1.39			2.48		1.43	0.63	88	2006	B8	1.57				3.66	0.39
ST82c	149	b	0.56			2.29		1.98	0.65	81.4	2006	D9	4.47				3.40	0.46
ST82c	149	c	0.86								2006	H2	2.36				3.20	0.42
ST82c	148	a	3.66								2006	H4	1.86				2.60	0.54
ST82c	148	b	2.19								2006	C8	1.97				3.46	0.37
ST82c	147	a	1.86								2006	B6	1.14				3.46	0.41
ST82c	146	a	2.66								2006	E2	2.10				3.30	0.48
ST82c	146	b	2.72								2006	H7	3.98				3.44	0.49
ST82c	141	a	1.47															
ST82c	142	a	2.72								2002 S	E8 a	0.50				3.33	0.55
ST82c	142	b	2.09								2002 S	E8 b	0.50				2.95	0.53
ST82c	142	c	0.95								2002 S	M3	4.15				2.58	0.58
ST82c	144	a	1.06			1.23		1.43	0.89	88								
ST82c	144	b	1.43			1.27		1.48	0.88	88	2001 Lv	A3	0.94				2.95	0.53
ST82c	145	a	0.50								2001 Lv	B1	2.70	0.381	0.078		3.06	0.47
ST82c	140	a	0.50								2001 Lv	C1	5.30	0.300	0.068		3.17	0.47
ST82c	139	a	1.27	0.173	0.197	3.50		1.57		87.3	2001 Lv	E2 a	5.12				3.12	0.51

Tab. 5.3: List of the whole data set of melt inclusions sample s. Bromine measurement (by synchrotron) perferomed in this work are reported together with Cl, S, H_2O, major elements and Fo olivine). These latter analysis were kindly performed by E. Gennaro and G. Iacono Marziano (for Etna samples) and kindly provided by N. Metrich (for Stromboli samples).

The Br compositional range of all melt-inclusions set is illustrated in the histograms of figure 5.6. Histograms in a) and c) show the whole Stromboli and Etna data-sets. The diagram b) shows separate distributions for the suites of Stromboli MIs.

The concentrations of Br in the Stromboli melt inclusions range from <0,5 to 6,2 ppm, with the highest Br value being observed in MI 38a (sample ST150307) (Fig. 5.6a). There is no obvious difference between historical (ST82) and recent (ST150307) paroxysms in terms of their bromine contents (Fig. 5.1b). In both cases, the majority of the MIs analyses have less than 0.5 ppm Br (18% and 38% for ST82 and ST150307, respectively). If measurements where Br is above detection limit are only considered, the two samples have similar distribution, with modes in the 1-1.5 ppm range, and similar mean values (average Br concentrations are 1,8 ppm for sample ST82c and 1,3 ppm for sample ST150307). The peak Br concentrations are also similar for both samples (4.8 and 6.2 ppm for ST82 and ST150307, respectively).

Concerning the Etna samples, we find comparable values in melt inclusions for recent (2001, 2002 2006) eruptions (mean+1σ = 2.2±1.6). These samples display a range of Br concentrations (<0.5-5.7 ppm) perfectly overlapping the range of Stromboli MIs. Conversely, Etna MIs from the FS eruption are characterised by much lower Br concentration, ranging from around detection limit (0,5 ppm) to a maximum value of 1.5 ppm (note only a couple of MIs have Br contents higher than 1 ppm). The histogram of fig. 5.1c shows a dominance of MIs with low (<1 ppm) Br contents. If measurements where Br is above detection limit are only considered, the Etna dataset has a mean (+ 1σ) mean Br concentration of 1.9±1.6).

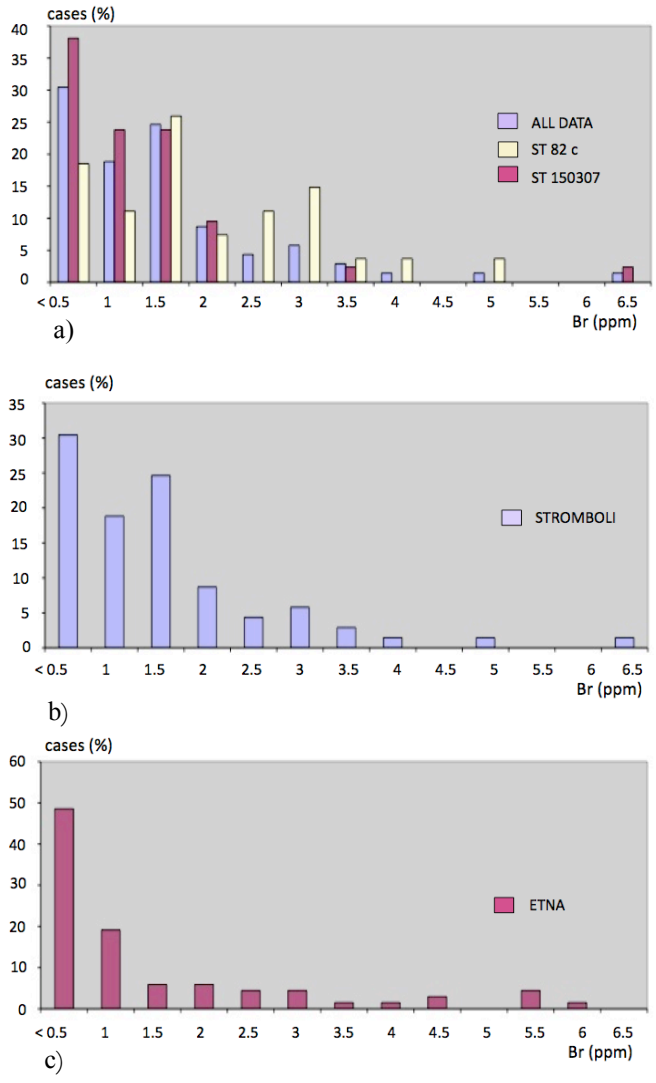

Figure 5.6: Histograms of melt inclusions data set showing: a) both the sets of data; b) and c) the separate abundances respectively for Etna anf for Stromboli.

5.3.2 Br vs. MI differentiation indexes

Figure 5.7 is a plot of the CaO/Al_2O_3 ratio of the MIs versus their corresponding K_2O content. These two variables are commonly used (Kamenetsky et al., 1996; Metrich et al., 2004; Spilliaert et al., 2006;) as proxies of magma differentiation, e.g., as indexes taken to illustrate the crystallization and magma differentiation history of the melts entrapped as inclusions in the crystals. CaO/Al_2O_3, is a parameter that clearly identifies the variations in composition of MI. Due to pyroxene crystallization, in fact, CaO/Al_2O_3 is expected to decrease in the melt together with differentiation processes (Rosciglione PhD thesis).

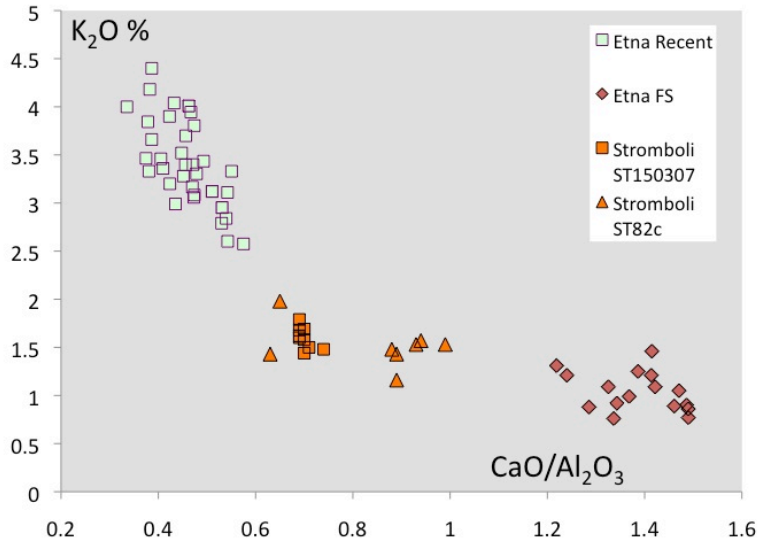

Figure 5.7: K2O vs. CaO/Al2O3 for the whole data set of MIs (Etna recent eruptions; Stromboli; Etna FS).

The diagram illustrates the different extents of differentiation of the studies inclusions, from primitive (poorly differentiated) Ca-rich and K-poor FS basaltic inclusions, to more evolved (Ca-poor and K-rich) Etna-recent inclusions. The Stromboli MIs lie in a intermediate positions (e.g., are intermediately evolved) in between the two above end-members.

In order to illustrate the behaviour of bromine during magma crystallization and differentiation, plots of Br contents in MIs against the corresponding K_2O and CaO/Al_2O_3 contents have been created, and are presented in Figures 5.8. Note that different panels have

been constructed for the three suits of differently evolved inclusions, discussed above.

Figure 5.8b and 5.8e are plots of Br vs K_2O and Br vs. CaO/Al_2O_3 for Stromboli MIs. The plots demonstrate a general, although manifestly weak, trend of decreasing Br contents with melt evolutions. There is an apparent tendency of more primitive (K-poor, Ca-rich) samples to be more Br-rich than more evolved (K_2O>1.5 %; CaO/Al_2O_3 <0.8) MIs, a trend that sems not to be at fit with the hypothesised (Kendrick et al., 2012) concentration of bromine in melt during the differentiation process: a totally opposite trend (e.g., a positive Br vs. K relation) would have to be expected if Br was to be associated with an incompatible behaviour (such as potassium) during magmatic differentiation.

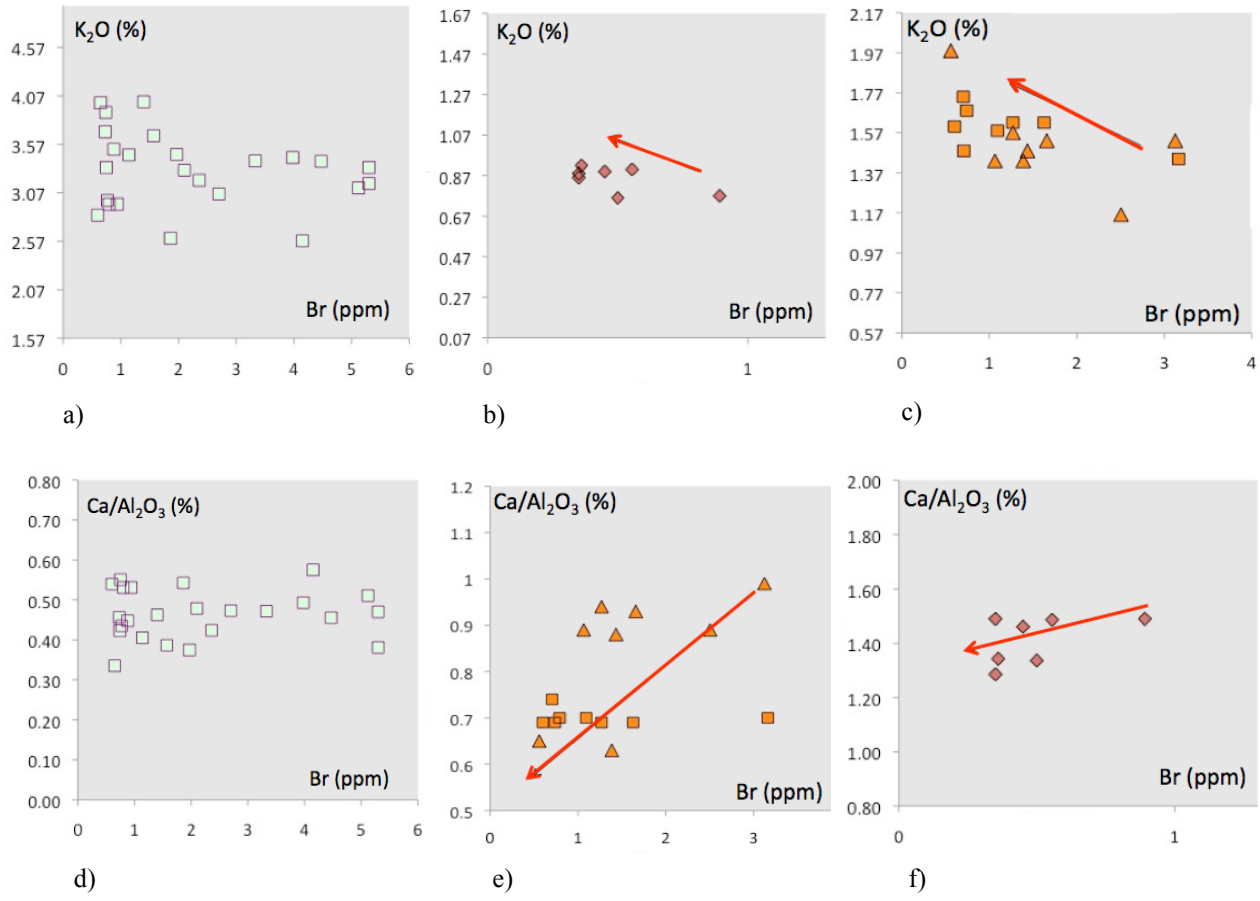

Figure 5.8: Diagrams showing Br variation with differentiation index: a), b) c) K_2O – Br ; d), e), f) CaO/Al_2O_3 Br

A further element corroborating the considerations above is the significant positive relation

between the Br content in the melt inclusions and the Forsteritic content of the corresponding host-olivine (Métrich et al., 2001, 2009) (Fig. 5.9). The figure demonstrates a trend in which more-primitive (deeply formed) Mg-rich (Fo 89-90) olivines typically host inclusions with far higher Br content than inclusions hosted in Mg-poorer (Fo 88-81) more evolved (shallow-formed?) olivines. Again, this relation seems to support the idea of magma evolution (differentiation) melt inclusions (being also characterised by the highest K_2O content) being associated by Br depletion. Since Br is though to behave as an incompatible element relative to most-common rock-forming minerals, similarly to chlorine (Saal et al., 2002; Kendrick et al., 2012), the above line of evidences seems to support a volatile-loving nature bromine, in which magmatic degassing deplete the melt in Br progressively as the melt evolves during ascent and de-compression. Whatever the case, it remains, however, that the weak correlations observed in Figs 5.8b and 5.8e (particularly for sample ST 150307) seem to suggest a more complex Br evolution scenario than crystallization alone may be able to account for. Similar indications are offered by the similar correlations plots for primitive (FS) and evolved (2001-2006) Etna MIs. The low-Br MIs from FS eruption display some weak but systematic negative dependence of Br contents on both differentiation indexes (Figs. 5.8c and 5.8f). The CaO/Al_2O_3 vs Br and K_2O vs Br correlation plots for Etna recent eruptions (Figs. 5.8a and 5.8d), however, indicate less significant relations between the highly variable Br contents and the differentiation indexes.

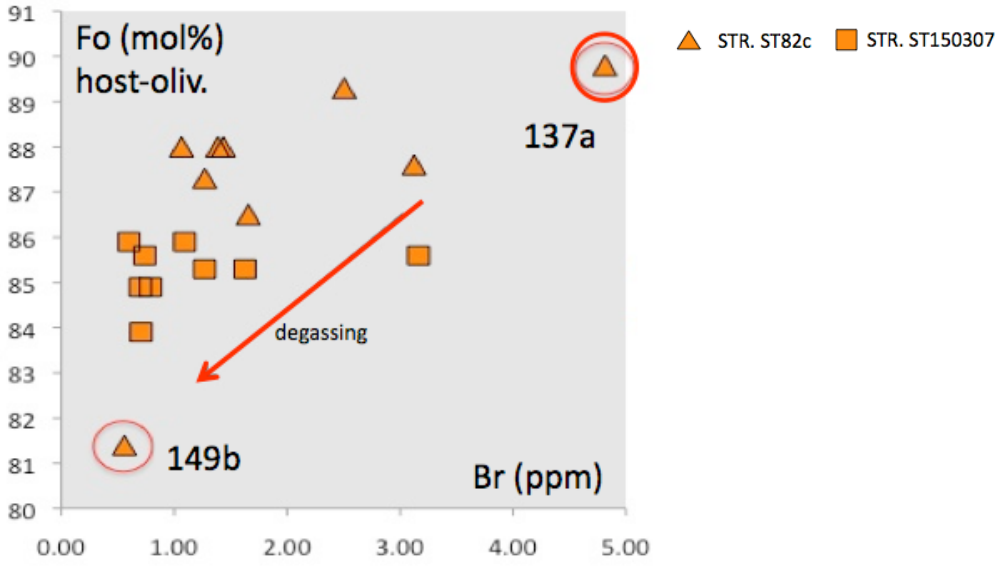

Figure 5.9: Fo-hosted-olivine as differentiation index vs Br content in the corresponding melt inclusion.

5.3.3 Br vs. other volatiles in MIs

An high-affinity of bromine for the vapour phase appears to be strongly supported by the relations with other volatiles in MIs, that are explored in Figs. 5.10 to 5.11.

Figure 5.10 shows that dissolved H_2O contents (Métrich et al., 2001, 2009) are largely variable for the suite of Stromboli MIs in which Br was consistently measured. As a whole, H_2O concentrations range from 1,2 to 3,5 %, supporting the presence of different MI generations, likely trapped at different storage levels along the volcano's plumbing system (Métrich et al., 2001, 2009).

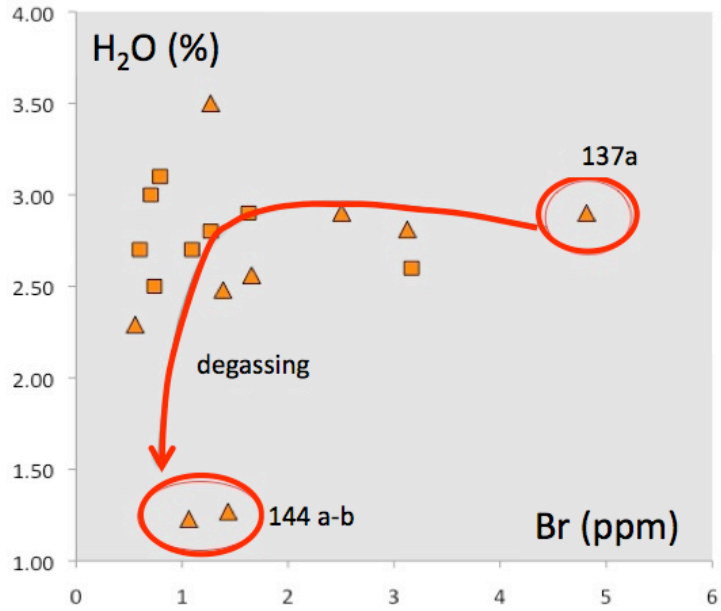

Figure 5.10: dissolved H_2O contents in melt inclusions from Stromboli data set.

When the relation between Br and H_2O is considered (Fig. 5.10), three main sets of significant information can be extracted:

(i) Br is far more variable than H_2O in the dataset; in particular, one notes that the majority of samples in the Stromboli MI population describe, in Fig. 5.10, a nearly

horizontal trend of variable Br contents (from ~5 ppm to<1) at nearly constant (~2.75±0.2 wt %) H_2O contents;

(ii) Along this compositional trend, the Br-richest sample (sample 137a in ST82c MIs; Br=4.8 ppm) stands out for also being the most CO_2-rich (2264 ppm; Table 5.3) and for being hosted in the most primitive (Fo-89.8) olivine (see Fig. 5.9);

(iii) Two samples (ST 144a, b; Table 5.1) depart from the general trend, for being characterised by far lower (1.23-1.27 wt%) H_2O contents; interestingly, these MIs are also among the Br-poorest (1.1-1.4 ppm); the next most water-poor (ST 149b; H_2O= 2.29 wt %) sample is also characterised by very low Br (0.56 ppm), and is trapped in the most evolved (Fo = 81.4) olivine (Fig. 5.9).

The indications above are qualitatively consistent with a degassing scenario in which MI 137a (sample in ST82c) is the pole representative of the most-primitive (un-degassed) magmas at Stromboli. Ascent of this primitive Br-rich (4.8 ppm) magma would then be associated by degassing path (arrow in figure 5.10), consisting of an earlier pulse of Br degassing (at nearly constant H_2O contents), followed by later (more shallow) H_2O degassing from the resulting Br-depleted melts. This interpretation requires that Br is strongly partitioned toward the magmatic gas phase upon decompression of magmas, a fact which is already proved from felsic compositions (Bureau et al. 2010), but that finds instead no supporting evidences from our vapour-melt experiments for mafic compositions (Chapter 4), pointing instead to a poorly volatile nature of Br. We also admit that, given the limited number of MIs analysed here for both Br and H_2O (fig. 5.10), this interpretation remains somewhat speculative, and requiring corroboration from additional measurements.

Still, an early-step degassing of Br is also consistent with analysis of co-variations between bromine and other volatiles (Cl, S), which are summarised, for Stromboli and Etna (FS) MIs, in figure 5.11. Extensive research, recently conducted on MORB (Kendrich et al., 2012a), has clearly emphasised a coherent behaviour of Cl and Br upon generation (mantle-melting) and evolution (e.g., crystallization) of basaltic magmas. The fact that the two elements maintain constant proportions (constant Br/Cl ratios) in MORB magmas under different evolution stage (see figs. 5.12 and 5.13a, b) has been taken as evidence for the lack of significant fractionations during mantle partial melting and/or fractional crystallization (e.g., that the two elements have similar mineral-melt incompatibilities). Similar results have also been obtained

for OIB and BABB rocks (Kendrick et al., 2012b) (fig. 5.12), which again exhibit remarkably constant Br/Cl ratios in spite of their (occasionally wide) range of differentiation degrees (given by the range of Br or Cl concentrations in figures 5.12).

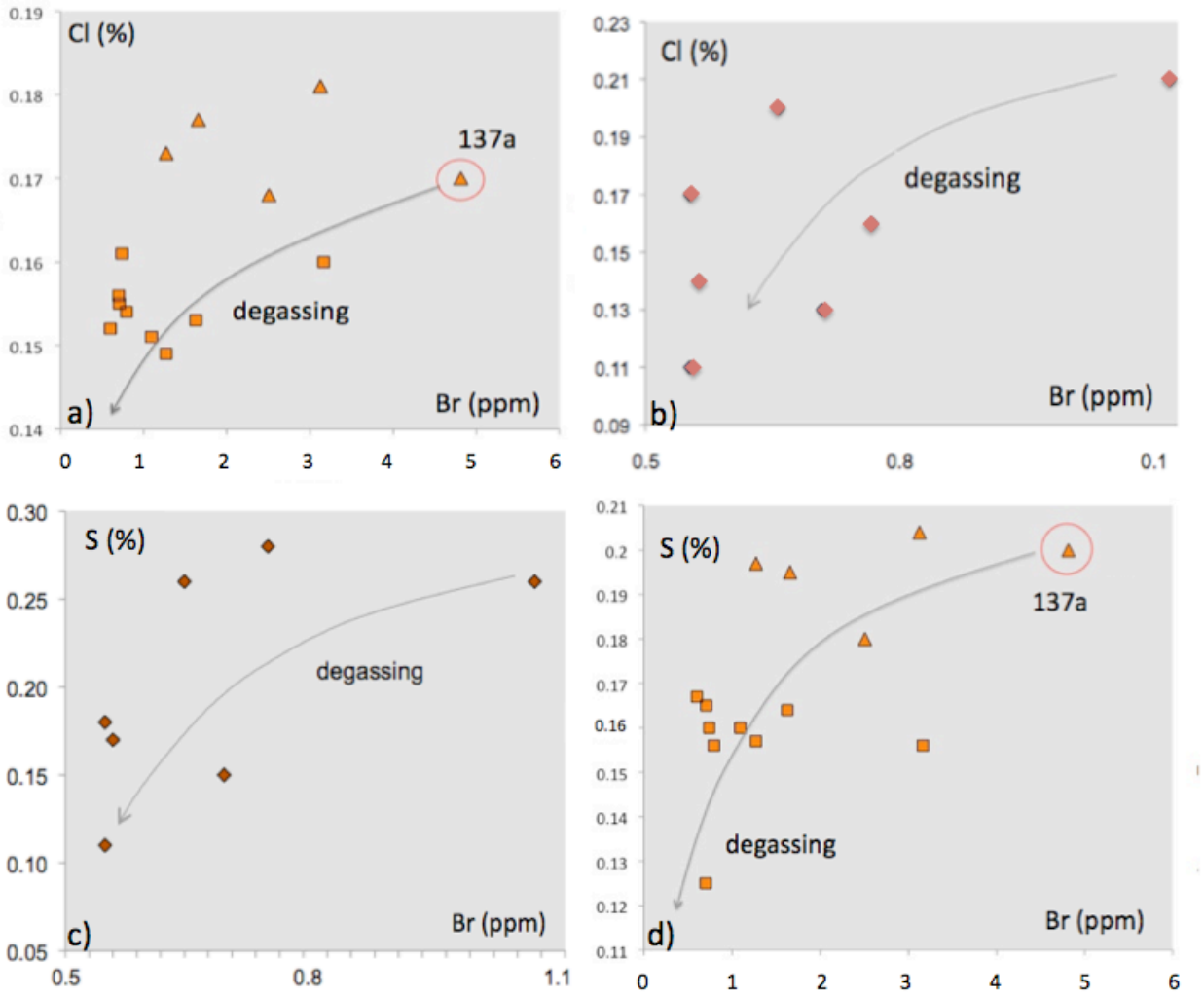

Figure 5.11: Cl-Br; S-Br plots for Stromboli and FS melt inclusions

STR. ST82c STR. ST150307 Etna FS Etna recenterupt.

Our Stromboli (Fig. 5.11a) and Etna (5.11b) MIs also exhibit positive correlations in Br vs. Cl scatter plots. For both suites of MIs, however, the dependences between the two elements are far from being linear (as seen in oceanic basalts; Kendrich et al., 2012a, b) (fig. 5.12), while

they assume instead the form of hyperbolic functions. This implies that, along the degassing path captured by the MI record, Br and Cl would have undergone substantial relative fractionations. A simple back-of-the-envelope calculation expresses the extent of such fractionation: if sample ST137 is again taken as the compositional pole for the primitive (un-degassed) melt in fig. 5.11a, then it is implied that while >90% of the original Br (~5 ppm in ST137, to <0.5 ppm in the most-degassed samples) is lost during the degassing path, only a far smaller fraction (30-40%) of the original Cl burden (~0.17-0.18 wt %) is released to gas over the same ascent interval (consistent with previous assessments of Métrich et al., 2001, 2004, 2009 and Spilliaert et al., 2006a, b). Figures 5.11c and 5.11d additionally demonstrate that similar arguments hold for S, which is apparently fractionated, relative to Br, during the degassing (ascent) path of mafic sub-aerial magmas (fig. 5.13). The extents of these Cl-Br-S fractionations are further explored in the section below.

5.3.4 Br in Etna and Stromboli MIs in a broader context

In the attempt to evaluate the origin and degassing behaviour of bromine over the subduction cycle, and along the different steps of magma generation, ascent and degassing, it is mandatory to understand how basaltic magmas in general, and the Etna and Stromboli magmas in our specific case, are linked to the general earth halogen cycle. In this section, we take advantage of the mass of information derived from our analysed melt inclusions (discussed above), in the attempt to contextualize our data in the framework of the currently known terrestrial bromine abundance scenario. At this aim, a comparison is made in the following plots between the volatile abundances (Br, Cl, S) in the melt inclusions analysed in this study (Etna and Stromboli volcanoes) and the corresponding set of information available in the literature for magmas and MIs taken in different contexts and geodynamic settings.

Figure 5.12 is a plot of Br vs Cl contents in bulk rocks and MIs of different nature and provenance. The largest mass of information in the diagrams comes from middle Oceanic Ridge Basalts (MORB). Kendrick et al., 2012a determined the abundances of Cl and Br in enriched Mid-Ocean Ridge Basalt (E-MORB) glasses from Macquarie Island in the southwest Pacific. These data, combined with earlier determinations on MORBs for different

provenance (Schilling et al., 1980; Jambon et al., 1995), form in figure 5.12 a cluster of diagonally oriented data at nearly constant Br/Cl ratios. Kendrick et al. (2012a) concluded that Cl and Br have coherent behaviour in these magmas, e.g., they are not fractionated during melting of the far more Cl-Br-poor mantle source (Palme and O'Neill, 2003; Arevalo and McDonough, 2010; fig. 5.12) and during subsequent magma crystallization.

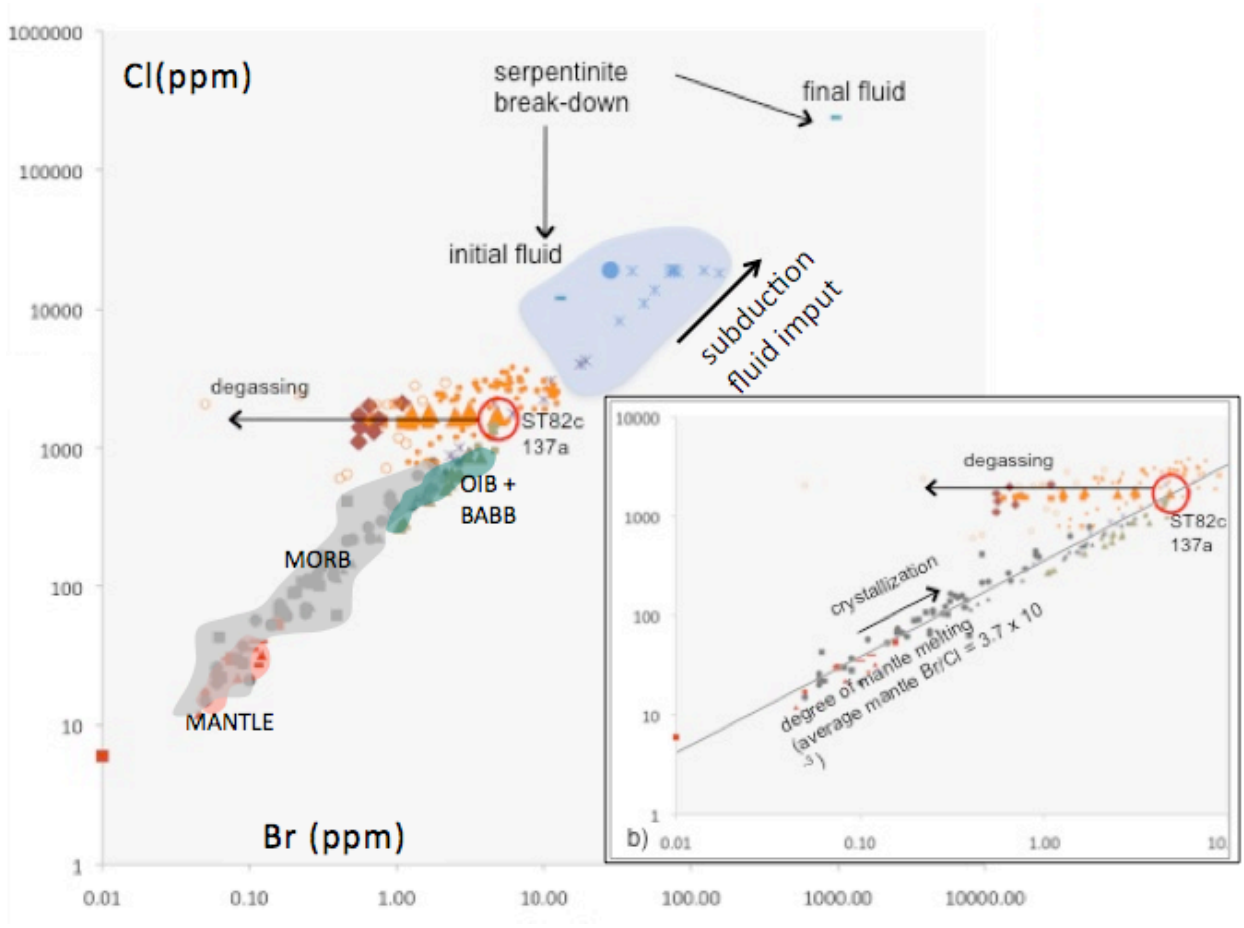

Figure 5.12: Cl-Br plot contents in bulk rocks and MIs of different nature and provenance.

▲ ST82c; ■ ST150307; ♦ FS; ▲ Mantle (Kendrick, 2012); ● Mantle (revalo&McDonough, 2010); ■ Mantle (Palme & O'Neill, 2003); ■ Mantle (Burgess et al., 2002); — Mantle (Deruelle et al., 1992; Jambon et al., 1995); ▲ Macquarie Island Basalt (E-MORB; Kendrick et al., 2012); ● MORB (Schilling et al., 1980); ■ MORB (Jambon et al., 1995) ; ▲ OIB (Pitcairn; Kendrick et al., 2012); OIB (Society; Kendrick et al., 2012; ✳ BABB (Manus Basin; Kendrick et al., 2012); ● Seawater (Kendrick et al., 2012); — Fluids from deydratation of subducted serpentinites (Kendrick et al., 2012); ○ Matrix glasses (Nicaragua; Kutterolf et al., 2013; ● Melt inclusions (Nicaragua; Kutterolf et al., 2013); ✳ Pore fluids (Muramatsu et al., 2001)

They therefore argue that mean Br/Cl ratio of MORBs can be taken as representative of the average Earth mantle Br/Cl ratio ($3.7\pm0.5 \cdot 10^{-3}$; fig. 5.12, 5.13). Kendrick et al., 2012b reported the first high-precision measurements of chlorine, bromine, for pristine glasses from the Manus back-arc basin basalt (BABB; Papua New Guinea) and ocean island basalt (OIB) glasses from Pitcairn and Society seamounts (Polynesia) that were erupted in water depths of >400 m and were formed from enriched mantle (EM) reservoirs. These data are also shown in figures 5.12 and 5.13. Overall, BABB and OIB fall in figure 5.12 at the upper end of the same MORB trend; they partially overlap with the Macquarie Island E-MORB (Kendrick et al. 2012a), though the they extend the MORB population to even more Cl-Br-rich compositions. Kendrick et al., 2012b, using K/Cl and I/Cl systematics, argued that the halogen enrichments of BABB, relative to MORB, possibly reflect addition of initial fluids derived from initial breakdown of subducted serpentines, these fluids being typically I-Cl-rich (relative to Br; see figs. 5.12, 5.13). If such, arguments of Kendrick et al., 2012b would demonstrate that halogens can be subducted past magmatic arcs to moderate depths in the Earth's mantle; so that subduction of serpentinized peridotites and oceanic crust ac enable transport of strongly incompatible, fluid-mobile, volatile elements, beyond zones of arc-magma generation. However, the similar Br/Cl (Fig. 5.12 and 5.13) and I/Cl (Kendrick et al. 2012b) ratios of OIB and MORB indicate that these serpentine-related fluids are unlikely to reach the deeper mantle where OIB are generated, suggesting lower subduction efficiency of halogens, relative to lithophile elements (e.g., K; Kendrick et al. 2012b). Halogen abundance ratios therefore provide a useful tool for evaluating the extent to which crustal recycling influences the distribution of fluid-mobile volatile elements in the mantle. The similarity of Br/Cl and I/Cl in the MORB and EM-type OIB glasses suggests that volatile components are gradually lost from subducting slabs and may have been well mixed throughout the entire mantle.

Now, if the Etna and Stromboli MI dataset is considered, a clear diversity emerges. In figure 5.12, our MI samples plot on nearly horizontal trend, that clearly diverge from submarine basalt (MORB+OIB+BABB) alignment, toward Cl-enriched compositions. This implies that, during the magmatic path recorded by the MIs, Br and Cl undergo substantial fractionation, as clearly indicated by the large spread of Br/Cl ratios (fig. 5.13a, b). More in the specific, while our best-guess estimate for the primitive (un-degassed) Stromboli magma composition (MI 137a; see above), has a Br/Cl ratio ($2.8 \cdot 10^{-3}$) within the MORB+OIB+BABB range, virtually

all the remaining MI samples have Br/Cl ratios far below the above submarine basalt range, pointing to substantial Br depletion at virtually constant Cl (see fig. 5.13b).

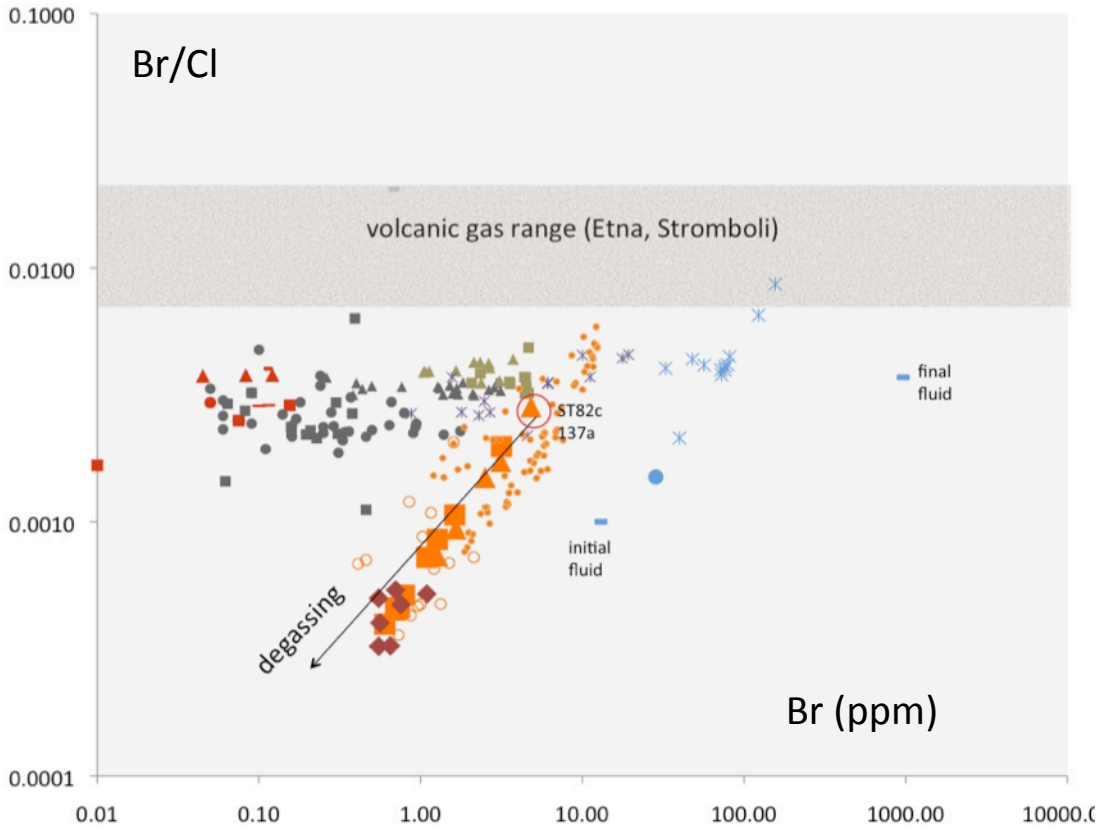

Figure 5.13a: Br/Cl vs CBr contents in bulk rocks and MIs of different nature and provenance.

ST82c; ST150307; FS; Mantle (Kendrick, 2012); Mantle (revalo&McDonough, 2010); Mantle (Palme & O'Neill, 2003); Mantle (Burgess et al., 2002); Mantle (Deruelle et al., 1992; Jambon et al., 1995); Macquarie Island Basalt (E-MORB; Kendrick et al., 2012); MORB (Schilling et al., 1980); MORB (Jambon et al., 1995) ; OIB (Pitcairn; Kendrick et al., 2012); OIB (Society; Kendrick et al., 2012; BABB (Manus Basin; Kendrick et al., 2012); Seawater (Kendrick et al., 2012); Fluids from deydratation of subducted serpentinites (Kendrick et al., 2012); Matrix glasses (Nicaragua; Kutterolf et al., 2013; Melt inclusions (Nicaragua; Kutterolf et al., 2013); Pore fluids (Muramatsu et al., 2001)

Interestingly, the suite of melt inclusion and matrix glass compositions analysed by Kutterolf et al., (2013), which represent the only available analog to our Etna-Stromboli dataset, shows a very similar behaviour. Kutterolf et al. (2013) investigated the Br-Cl compositions of MIs and

matrix glasses from 14 basaltic to rhyodacitic tephra deposits (less than 70 ka old) emplaced during large Plinian eruptions at 5 volcanic centers along the Nicaraguan subduction zone segment. They similarly obtained large fractionations of Br/Cl ratios (fig. 5.13), which they ascribed to earlier (pre-eruptive), more extensive Br degassing relative to more soluble Cl.

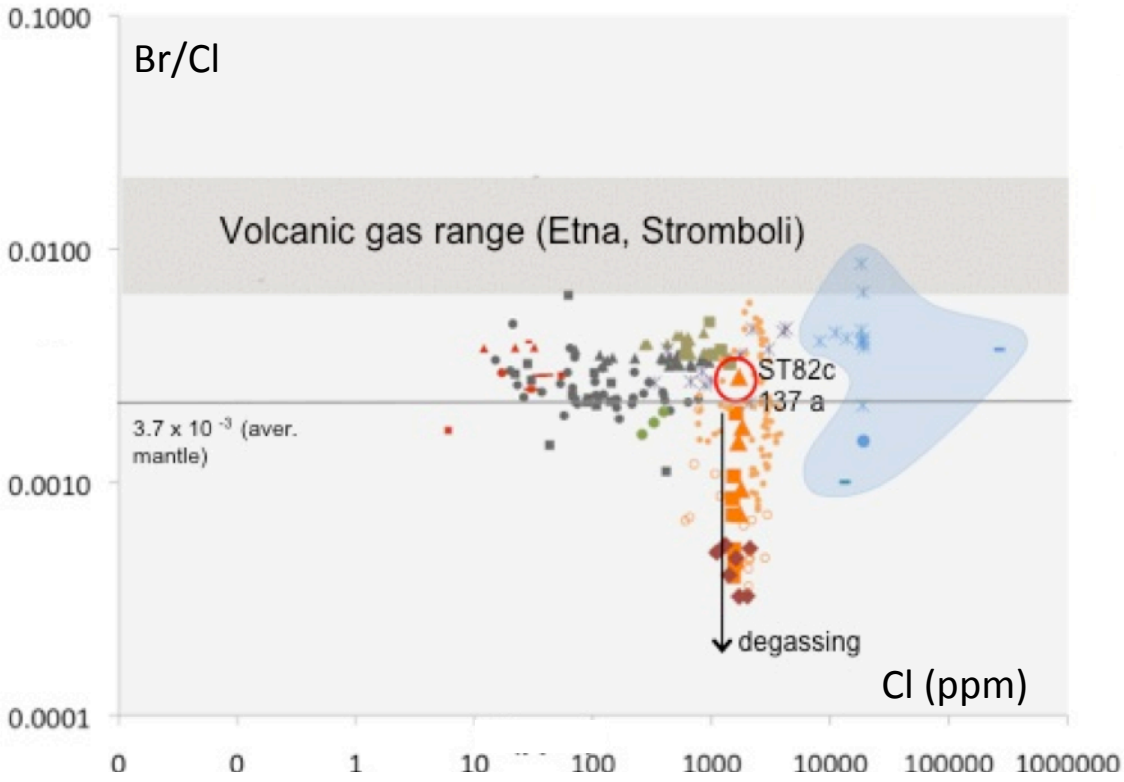

Figure 5.13b: Br/Cl vs Cl contents in bulk rocks and MIs of different nature and provenance.

▲ ST82c; ■ ST150307; ♦ FS; ▲ Mantle (Kendrick, 2012); ● Mantle (revalo&McDonough, 2010); ■ Mantle (Palme & O'Neill, 2003); ▬ Mantle (Burgess et al., 2002); ─ Mantle (Deruelle et al., 1992; Jambon et al., 1995); ▲ Macquarie Island Basalt (E-MORB; Kendrick et al., 2012); ● MORB (Schilling et al., 1980); ■ MORB (Jambon et al., 1995) ; ▲ OIB (Pitcairn; Kendrick et al., 2012); OIB (Society; Kendrick et al., 2012; ✳ BABB (Manus Basin; Kendrick et al., 2012); ● Seawater (Kendrick et al., 2012); ─ Fluids from deydratation of subducted serpentinites (Kendrick et al., 2012); ○ Matrix glasses (Nicaragua; Kutterolf et al., 2013; ▮ Melt inclusions (Nicaragua; Kutterolf et al., 2013); ✳ Pore fluids (Muramatsu et al., 2001)

This interpretation is strongly corroborated by matrix glasses (the end-up residual products of volatile degassing) being typically Br-depleted relative to MIs (e.g., at the low-Br, low Br/Cl ratio lower limit of the MI populations; figs. 5.12 to 5.13).

In summary, the antithetic behaviour observed in figure 5.7 and 5.8 between submarine magmas, which have escaped substantial halogen degassing, since erupted at depth in the sea-floor (Kendrick et al., 2012), and subaerial magmas appears to reflect the result of extensive bromine degassing (at the expenses of more melt-affine Cl) in the latter circumstances. This higher Bromine volatile (relative to chlorine) seems to further be confirmed by compositions of volcanic gases, which at both Etna and Stromboli have Br/Cl ratios far above the magma (MI) range (fig. 5.13).

One final remarks goes to S-Br systematics (fig. 5.14), from which analysis similar conclusions can however be drawn. In Figure 5.14, the Br-richest compositions are obtained for Nicaragua tephra MIs (Kutterolf et al., 2013), which also display the highest B/S ratios (S contents for the Nicaragua eruptions have been derived from Metzner et al. 2012).

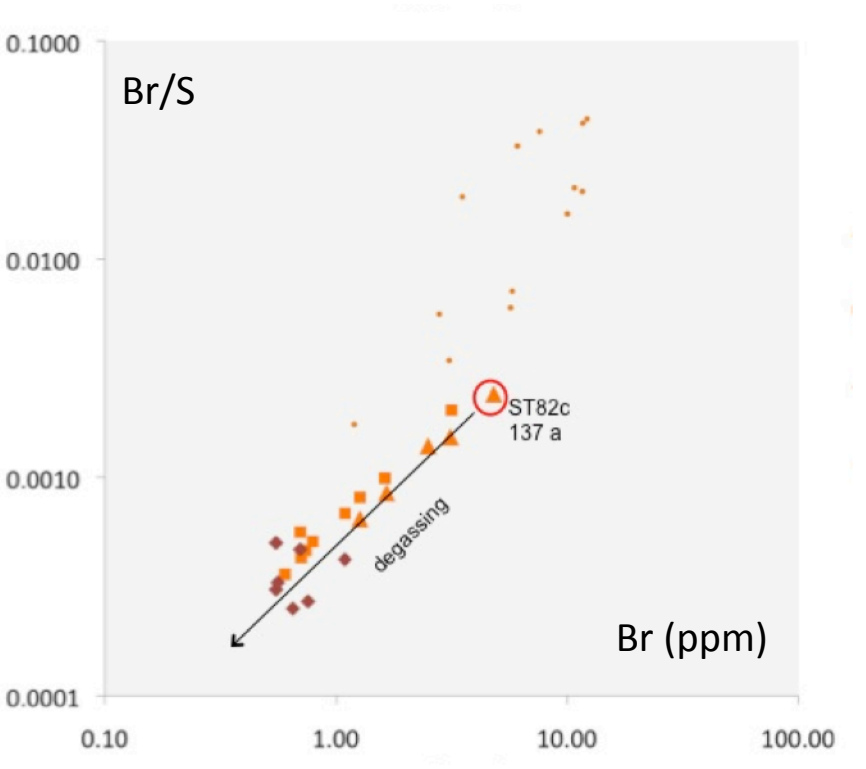

Figure 5.14: Br/S ratios vs Br for melt inclusion from (Stromboli and Etna (this study) compared to those from Nicaragua (Kutterolf et al., 2013).

Among the Etna-Stromboli dataset, MI ST 137a (the "primitive magmatic pole") stands at the Br-rich end of the MI populations. Bromine-depleted (low Br/S) MIs are very likely to result from preferential Br degassing, relative to S. The key information and conclusive argument emerging from this section is that of a large volatile of bromine during magmatic processes occurring at subaerial basaltic systems. This is clearly reminiscent of the high vapour-affinity of bromine, suggested for felsic volcanism based on vapour-melt partition experiments (Bureau et al., 2003, 2010), but remains in stark contrast with the experimental results for mafic (Etna) melts, discussed in chapter 4. Clearly, there is still much to do on the way to a full understanding of bromine behaviour in basaltic systems. Still, the mass of information obtained here will guide development of simple model to interpret S-Cl-Br compositions, ad discussed in the next chapter.

Chapter 6

Bromine degassing model

6.1: Bromine degassing model

The large variability of volcanic S-Cl-Br gas compositions (Fig. 6.1), and the linear array of data in Figure 6.2, from S-rich to S-poor (and halogen-rich) compositions, require the existence of a mechanism through which bromine is fractionated relative to sulphur during volcanic degassing. The relatively constant Cl/Br ratios in volcanic gases would be suggestive, instead, for that little inter-halogen fractionation takes place during degassing; a fact which, if proved, would be reminiscent of the relatively constant Cl/F ratios in volcanic gases that led Aiuppa (2009) to suggest that vapour/melt partition coefficients of the two elements only differ by a factor ~4 or so (with F being less "gas-loving" than Cl).

A rigorous quantitative modelling of volcanic gas compositions requires knowledge of volatile solubilities, vapour-melt partition coefficients, and diffusivities over the range of P-T-X conditions experienced by magmas upon their ascent, storage, and eruption. Such quantitative information is only partially available for Cl (Webster et al., 1999; Signorelli and Carroll, 2000; Webster and De Vivo, 2002; Alletti et al., 2009), and totally missing for fluorine and bromine, at least for mafic compositions. Aiuppa et al (2002) and Aiuppa (2009) responded to such limited availability of experimentally- or theoretically-derived degassing parameters for halogens by introducing an empirical degassing model that describes quantitatively the evolution of the magmatic gas phase (in the SO_2-HCl-HF system) that is exsolved with increasing extents of degassing of a basaltic magma. The model is based on the assumption that a Rayleigh-type open-system degassing model (Aiuppa et al., 2002), with constant S, Cl and F melt-vapour partition coefficients, is suitable to simulate the relatively shallow exsolution of halogens from basaltic magmas (Métrich et al., 2001; Spilliaert et al., 2006; Edmonds et al., 2009). Based on the accepted sequence of volatile solubility in basaltic magmas (S<Cl<F; Carroll and Webster, 1994), Aiuppa (2009) demonstrated that transition from S-rich to halogen-rich and S-depleted compositions at volcanoes can be attributed to an earlier selective S partition into the gas phase, and to a later release of more soluble Cl and F in the final stages of volcanic degassing.

The aim of this section is to extend the Aiuppa (2009) model approach to bromine, and to explore in particular if, steaming from results of determinations of bromine contents in Etna and Stromboli MIs (chapter 5) and of the preliminary experimental determinations of bromine partition coefficients (chapter 5), a simple model can be developed to account for the

variability of S-Cl-Br compositions of volcanic gases.

Following Aiuppa et al. (2002) and Aiuppa (2009), the model we propose here makes use of a set of two Rayleigh-type open system equations to calculate the evolving S/Cl and S/Br (molar) ratios in the magmatic gas phase produced upon increasing extents of degassing of a silicate melt.

The adopted model relations are:

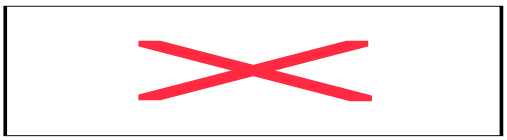

(1)

$$\left(\frac{S}{Br}\right)_{gas} = \left(\frac{S}{Br}\right)_{melt_0} \cdot \frac{D_s}{D_{Br}} \cdot R^{\left(1-\frac{D_{Br}}{D_s}\right)} \qquad (2)$$

where $\left(\frac{S}{Cl}\right)_{gas}$ and $\left(\frac{S}{Br}\right)_{gas}$ are the molar volatile ratios in the gas phase, $\left(\frac{S}{Cl}\right)_{melt_0}$ and $\left(\frac{S}{Br}\right)_{melt_0}$ are the original volatile ratios in the parental (un-degassed) melt, D_S, D_{Cl} and D_{Br} are the vapour/melt (molar) partition coefficients for the three volatiles, and R is the residual fraction of sulphur in the melt (ranging from 1 at onset of degassing to 0 as S is totally exhausted from the melt). A similar equation for fluorine was used in the original works of Aiuppa et al (2002) and Aiuppa (2009):

$$\left(\frac{S}{F}\right)_{gas} = \left(\frac{S}{F}\right)_{melt_0} \cdot \frac{D_s}{D_F} \cdot R^{\left(1-\frac{D_F}{D_s}\right)} \qquad (3)$$

Averaged compositions of primitive melt inclusions are generally taken as proxies of pre-eruptive volatile contents, and allow therefore to estimate $\left(\frac{S}{Cl}\right)_{melt_0}$ and $\left(\frac{S}{Br}\right)_{melt_0}$. Here, we use the composition of the most Forsteritic (Fo 89.9) MI from Stromboli (sample ST82c 137 a in Table 5.3) as representative of the original (pre-eruptive) volatile content in mafic magmas. This samples shows among the highest bromine contents in our dataset (4.8 ppm), and it is also characterised by high H_2O (2.9 wt%), S (0.2 wt %) and Cl (0.17 wt. %) contents, typical of primitive (e.g., un-degassed) MIs from magmas form the Italian volcanic province (Métrich et al., 2004, 2009). With these numbers, $\left(\frac{S}{Cl}\right)_{melt_0}$ and $\left(\frac{S}{Br}\right)_{melt_0}$ can be evaluated at 1.32 and 1000, respectively.

The ratios of partition coefficients (e.g., D_S/D_{Cl}, D_S/D_{Br} and D_S/D_F) are not independently and fully constrained. However, Aiuppa et al., (2002) proposed a novel procedure to derive the ratios between partition coefficients, which involved combining relations (1) and (3) into equation (4), which establishes the dependence between $\left(\frac{S}{Cl}\right)_{gas}$ and $\left(\frac{S}{F}\right)_{gas}$ as:

$$\ln\left(\frac{S}{Cl}\right)_{gas} = \ln\left(\frac{S}{Cl}\right)_{melt_0} + \ln\frac{D_s}{D_{Cl}} + \frac{(1-D_{Cl}/D_S)}{(1-D_F/D_S)}\cdot\left[\ln\left(\frac{S}{F}\right)_{gas} - \ln\left(\frac{S}{F}\right)_{melt_0} - \ln\frac{D_s}{D_F}\right] \quad (4)$$

In a $\log\left(\frac{S}{Cl}\right)_{gas}$ vs. $\log\left(\frac{S}{F}\right)_{gas}$ scatter plot, equation (4) takes the form of straight line, which slope and intercept - both function of the ratios between partition coefficients - can be derived by a linear best-fit procedure applied to suites of volcanic gas (S/Cl and S/F ratios) data. Aiuppa (2009) used a set of volcanic gas measurements from Etna to estimate the ratio of (molar) partition coefficients D_S/D_{Cl} and D_S/D_F as of 9 and 36, respectively. He also

showed that the range of globally available volcanic gas compositions can be satisfactorily reproduced using the same vapour-melt partition coefficients. In this study, a value of 9 was therefore substituted to D_S/D_{Cl} in equation (5), which arises from combination of (1) and (2):

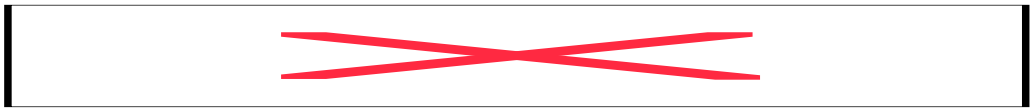

(5)

Finally, D_S/D_{Br} was estimated by a best-fit procedure similar to that of Aiuppa (2009), but applied to the Etna-Stromboli volcanic S-Cl-Br gas dataset of figure 6.2 (Etna volcanic gas samples are by far the largest in the dataset, and those for which the procedure can therefore be considered more realistic). These calculations show that good fit between model (equation 5) and natural (Etna/Stromboli volcanic gas samples) compositions is obtained for a D_S/D_{Br} of ~25 (on a molar basis) ((see green line in Figs. 6.1 and 6.2).

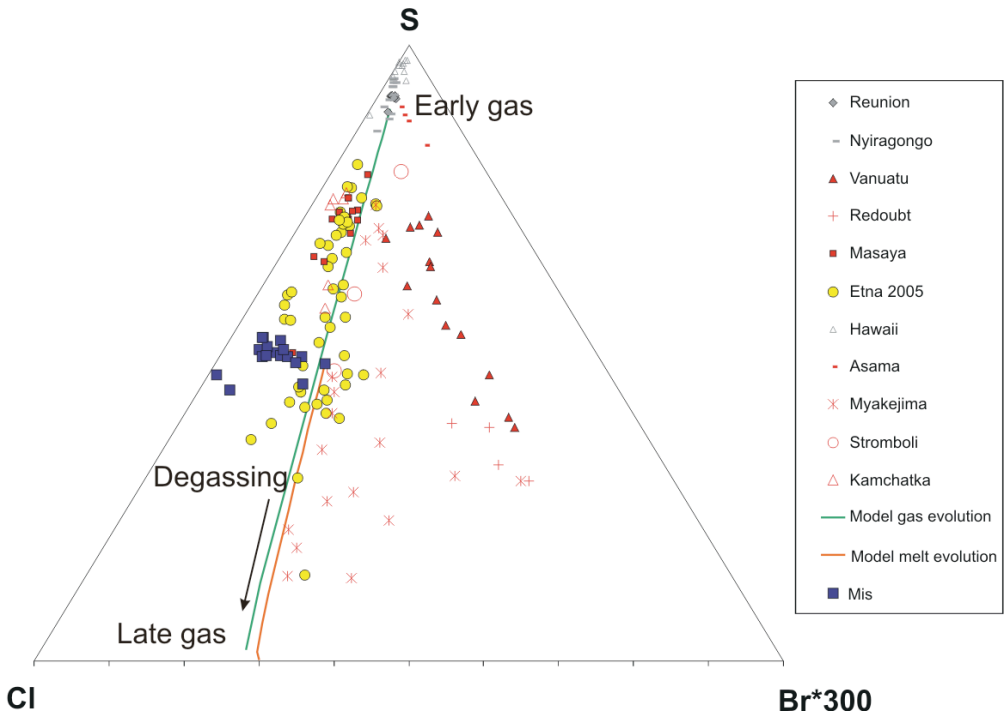

Figure 6.1: S-Cl-Br triangular diagram showing the variability of volcanic S-Cl-Br gas compositions.

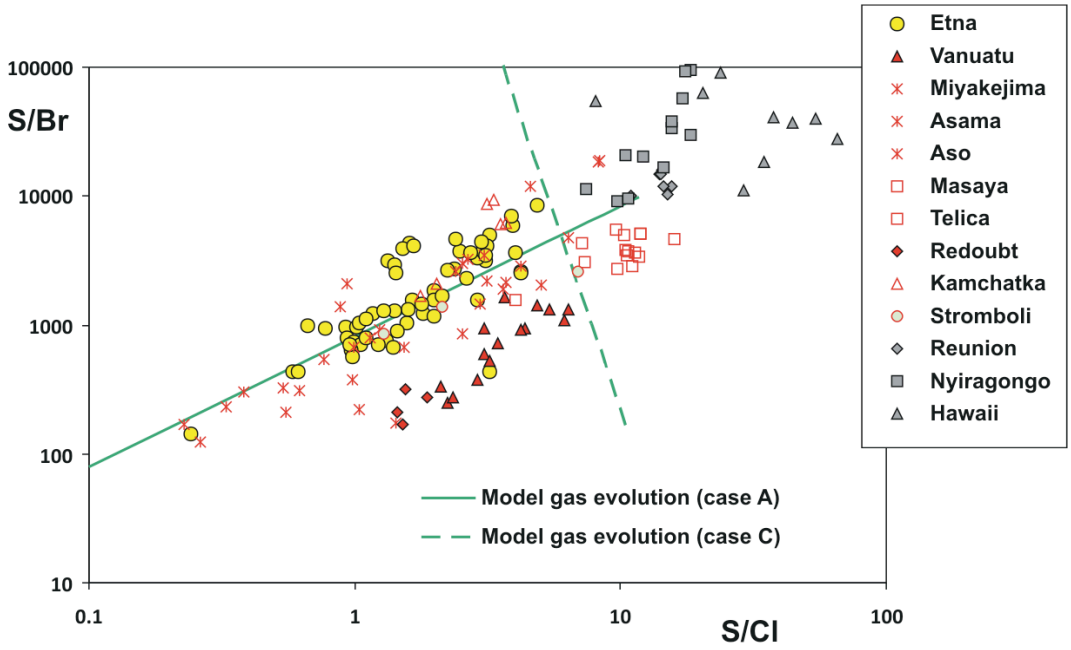

Figure 6.2: Linear array of data in S/Br vs S/Cl plot.

The calculations above indicate that a Rayleigh-type open system model is a potentially sound degassing model to describe, and numerically simulate, the range of S-Cl-Br compositions observed in this study. However, two main sets of problems emerge.

Firstly, with the D_S/D_{Cl} and D_S/D_{Br} taken above (9 and 25), a D_{Cl}/D_{Br} of 2.5 (or ~ 1 on a weight basis) can be obtained. The Cl partitioning coefficient between Etnean basaltic melt and an hydrous fluids was experimentally determined by Alletti et (2009), who demonstrated a negative dependence between $D_{Cl}^{v/m}$ and pressure (at NNO redox conditions), from 11–14 (on a weight basis) at 1-25 MPa, down to 6 (on a weight basis) at 200 MPa. If an average weight/weight $D_{Cl}^{v/m}$ of ~10 is taken as representative of Etna/Stromboli volcanism, than a $D_{Br}^{v/m}$ of the same order of magnitude (~10 on weight basis) is required for equation (5) to hold (e.g., for a good fit between modelled – relation 5 – and gas data to be observed in Figure 6.2). However, a similarly high vapour/melt partition coefficient for Br seems to be

unsupported by our experimental determinations, pointing instead to a very high Br affinity for melt ($D_{Br}^{v/m}$ <1; chapter 5).

Secondly, but not less importantly, the above procedure – given the contrasts of partition coefficients detailed above - predicts that model residual melts should evolve towards more S-poor and halogen-rich compositions throughout the degassing path (e.g., upon increasing extents of degassing; see red curve in figure 6.1): this is the opposite behaviour as seen in natural melts (e.g., melt inclusions), in which bromine appears to deplete much faster than S or Cl over the magmatic degassing path.

In order to illustrate this second argument further, we present below the results of a model (fig. 6.3) in which the above procedure is reversed, e.g., in which the Rayleigh-type open system model was used in the attempt to fit the melt inclusions data, rather than the gas samples.

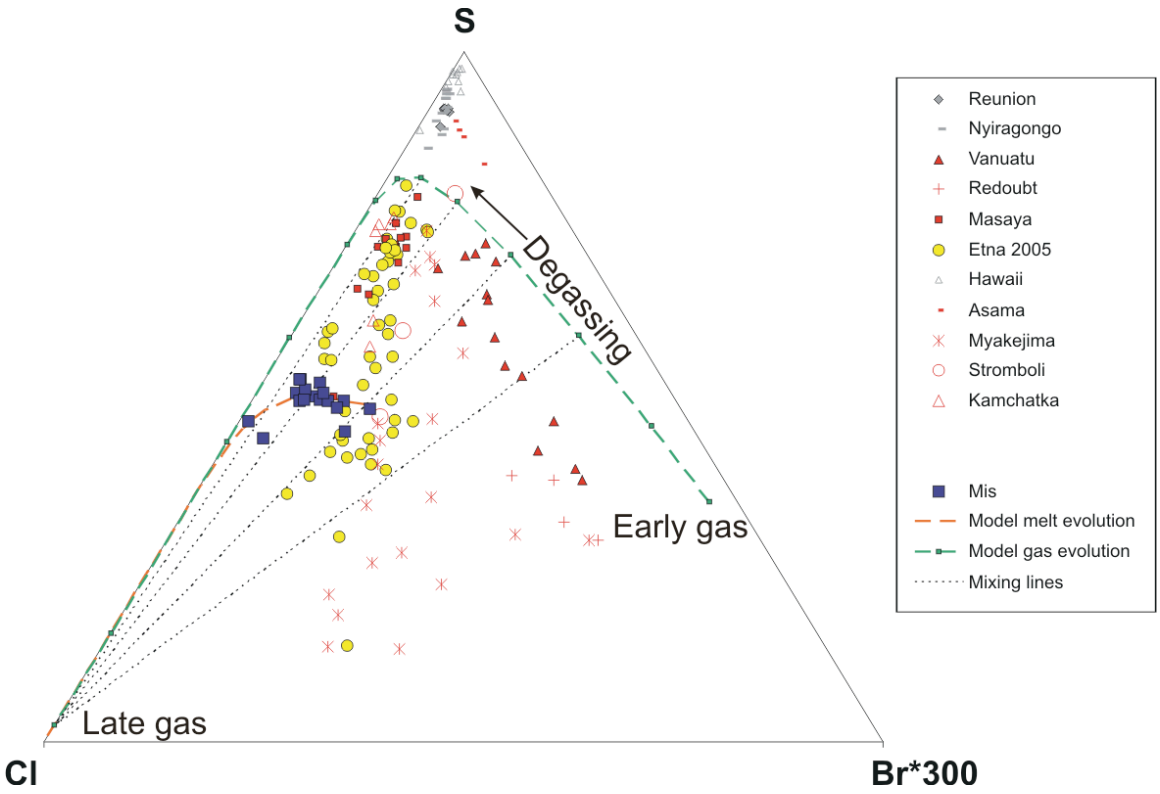

Figure 6.3: Degassing model for S-Cl-Br following a Rayleigh-type open system model

In practical terms, using the same values as above for $\left(\frac{S}{Cl}\right)_{melt_0}$ (1.32), $\left(\frac{S}{Br}\right)_{melt_0}$ (1000) and D_S/D_{Cl} (9) – we used a best-fit routine to calculate the D_S/D_{Br} ratio for which the best agreement is obtained between model melt compositions (orange dotted curve in fig. 6.3) and MI compositions. From this, we obtain that the best agreement between model and observations (gas) is observed for a D_S/D_{Br} ratio of 0.45. This much lower ratio (than obtained previously in the case described in fig. 6.1) would be suggestive of a much larger vapour affinity of bromine ($D_{Br}^{v/m} \sim 500$ for a $D_{Cl}^{v/m}$ of ~10) relative to sulphur ($D_S^{v/m}$ of ~90).

In such conditions, while Br remains a minor component of the magmatic gas phase during the entire degassing path (molar fractions from 10^{-20} to 10^{-4}), the modelled gas compositions would evolve from Br-richer (e.g., S/Br molar ratio of only 160) in the early gas formed at onset of degassing (R =1) toward a more Br-depleted and Cl-richer compositions in the residual gases (the gas separated from a degassed, Br-depleted melt) (see fig. 6.3). This early (deep) degassing history for bromine would agree well with recent analysis of Bobrowski and Giuffrida (2012), who suggested an early Br exsolution (relative to S) from Etna's magmas based on the analysis of temporal variations of BrO/SO_2 ratios in volcanic gases. Figure 6.3 shows that only a few of the Etna gas samples (essentially the most S-rich) would remain accounted for by this modelling (compare volcanic gas samples with the green dashed line dashed line fig. 6.3). There is, however, plenty of evidence on mafic volcanoes, from for instance analysis of systematic of H_2O-CO_2-SO_2 (Aiuppa et al., 2007, 2010; Shinohara et al., 2008) and noble gases (Paonita et al., 2012) in volcanic gases (from both Etna and Stromboli), that surface gas emissions are more likely to result from mixing between deep CO_2-rich gas, rising from deep magma storage zones (e.g., from pressures of 200 MPa or more; Métrich et al,., 2009), and CO_2-poorer, more evolved (e.g., ^{3}He depleted relative to ^{4}He) gas released by shallow residual magmas ponding on the upper parts of the plumbing system (e.g., the shallow conduits). To test if this mechanism can in some way control the variability of S-Cl-Br compositions of volcanic gases, a set of mixing lines between shallow gas and a suit of early (deep?) vapours was calculated, being illustrated in figure 6.3 by the dashed black lines. It is manifest from the figure that this process is well in the conditions to reproduce the compositional features of volcanic gases from Etna/Stromboli, and elsewhere.

Even in this case, however, the problem with the partition experiments remain (chapter 5), or becomes even larger (a very large volatility of Br ($D_{Br}^{v/m} \sim 500$) is in stark contrast with our experimental results). One obvious corollary of the above discussion is that the mechanism of Br release upon magma ascent and degassing remain a puzzling matter. To estimate the range and variability of Br partition coefficients in a range of P-T-X conditions remain central to solve the issue: the <1 $D_{Br}^{v/m}$ partition coefficients, as qualitatively estimated in this study (chapter 5), remain in obvious disagreement with suggestions arising from both volcanic gas (requiring a $D_{Br}^{v/m}$ of ~10) and MI (pointing to far larger $D_{Br}^{v/m}$ of ~500) datasets. The additional conclusion is data Br behaviour is likely to be far more complex than a simple Rayleigh-type open system model, which uses constant ratios between partition coefficients (e.g., P-T-X independent solubility contrasts between S, Cl, and Br), could describe. It cannot be excluded that a combination of an high-pressure degassing history, in which Br is highly partitioned in the gas (to account for the rapid Br depletion upon magma degassing, as captured by MIs), followed by a more shallow degassing step in which Br becomes far less volatile, at least relative to S (to account for the S-Cl-F systematic of volcanic gas samples; Figs. 6.2, 6.2), would probably consistent with the entirety of the line of evidences and observations obtained here. To simulate such a complex degassing history, however, a far better knowledge of Br partition coefficients than available here would certainly be required. We still believe, however, that the degassing history depicted by figure 6.3 is, that present level of our knowledge, the best interpretative scenario for Br behaviour in mafic magmatic systems.

Chapter 7
Summary and conclusions

With this study we have provided new insights on bromine behaviur as a new useful tool to scientific community for a better understanding of the role of halogen in volcanic systems.

A quantitative knowledge of the mechanism controlling Br degassing from subaerial volcanism was impossible due to the uncertaines in quantifying parameters that are still largely unknown as bromine solubility, diffusivity and vapour/melt partitioning coefficients as a function of temperature, pressure and melt composition and starting bromine concentration into the melt.

The main goal of this study was to define a quantitative degassing model to interpret bromine behaviour during degassing path in basaltic volcanic systems. This aim was achieved through three different complementary approaches: first one was aimed to gain informations about bromine content in gas phase by filter-packs technique; second one was aimed to measure starting bromine content in a set of olivine-hosted melt inclusions from Etna and Stromboli volcanoes by synchrotron radiation; finally, third purpose was to investigate bromine fluid/melt partitioning coefficient ($D_{Br}^{fluid/melt}$) in a set of H_2O-Br bearing synthetic glasses produced by IHPV in order to understand the distribution of bromine between these two phases and the link between

In order to measure Br contents in melt inclusions a preliminary step was to produce a good suite of reference material for basaltic composition, which have not obtained since so far. So, the first important goal achivied in this study was the creation of the first set of synthetic standard glasses that we used to quantified Br in melt inclusion by XRF - synchrotron.

Measurements on melt inclusions from Etna and Stromboli obtained by synchrotron analysis range from < 0.5 to 6.2 ppm with the highest values found in Stromboli MIs set. In any case the majority of the samples from the whole set of melt inclusions have less than 0.5 ppm Br.

These results permitted to achieve first important consideration about bromine behaviour during degassing path. First of all, relations between bromine content with differentiation index (CaO/Al_2O_3; K_2O; Fo-hosted olivine) strongly support a degassing scenario in which MI 137a from sample ST82c is the pole representative of the most-primitive (un-degassed) magmas at Stromboli, which, during the degassing path, would evolve towards a late Br-depleted melt. These considerations are supported by relations between Br with other volatiles (Cl; S; H_2O) that are consistent with a strongly affinity of bromine for the fluid phase which would mean its high partitioning into the magmatic gas phase upon decompression of

magmas.

These considerations are also supported by data from a set of melt inclusions from felsic systems (Nicaragua) investigated by Kutterolf et al., 2013 who found a very similar behaviour of Br. Infact, a comparisons between volatile abundances (Br, Cl, S) in the melt inclusions analysed in this study (Etna and Stromboli volcanoes) and the corrisponding information avaiable in the literature for magmas and MIs taken in different context and geodynamic settings, show an evident difference between the Br behaviour trend in MIs compared to submarine basalts (MORB, OIB, BABB) determinated by several authors. Infact, while the latter show constant Br/Cl ratios supporting a coherent behaviour of Br and Cl in these magmas and the absence of any strong fractionation processes, on the contrary, MIs analysed in this study, together with MIs from Nicaragua, show an antithetic trend consisting in a substantial Br depletion at virtually constant Cl, implying a fractionation between these two species. This fact is evidently due to an earlier (pre-eruptive) more extensive Br degassing relative to more soluble that confirms the higher bromine affinity for volatile phase during magmatic processes occurring at subaerial basaltic systems.

Unexpectedly, this scenario described since so far is in stark contrast with our melt-fluid experiments for mafic (Etna) compositions that, instead, support a poorly volatile nature of bromine. Partitioning experiments, performed in our work were aimed to investigate the affinity of bromine for the melt or for the fluid phase. Results seem to support an unexpected high partitioning of Br in the melt phase showing a $D^{melt/fluid} > 1$. This is in contrast not only with observation deriving from melt inclusions analysis but also with the common idea of an increasing affinity for the fluid phase for volatile elements with strong incompatible feature and large ionic radius as Br. Even if these results give just a preliminary and approximate estimation and they have to be verified by further experiments, however this study confirms the complexity of interaction between a basaltic melt and its coexisting fluid phase and highlights the extremely need in increasing efforts to expand knowledge concerning Br behaviour.

The informations obtained from melt inclusions and from partitioning experiments were used to extends the Aiuppa (2009) model approach to bromine. Starting with composition of the most forsteritic MI from Stromboli as representative of the original (pre-eruptive) volatile content in mafic magmas, we developed a simple model (Raylegh-type open system model) to interpret S-Cl-Br compositions that could explain the large variability of volcanic S-Cl-Br gas

compositions and so, the mechanism through which bromine is strongly fractionated relative to sulphur during volcanic degassing. Model we proposed predicts that gas composition would evolve from Br-richer in the early gas formed at onset of degassing (R=1) towards a more Br-depleted and Cl-richer compositions in the residual gases, highlighting an early (deep) degassing history for Br. Also, in order to explain the large variability of S-Cl-Br composition of volcanic gases, a set of mixing lines between shallow gas and a suit of early (deep) vapours was calculated. The final model well reproduced the compositional features of volcanic gases from Etna and Stromboli, and elsewhere, even if problem with partitioning experiments remains.

These considerations highlight that the mechanism of Br release upon magma ascent and degassing remain a puzzling matter. So, our interpretation and results requires further investigation, aimed both to collect additional measurements on MIs, and to perform other partitioning experiments in order to constrain bromine behaviour as better as possible, during magma ascent. However, since no no experimental data on $D_{Br}^{m/f}$ in basaltic melts have ever been obtained so far, this work could be considered an important strarting point for a better understanding of bromine behaviour in volcanic systems.

References

- Aiuppa, A., 2009. Degassing of halogens from basaltic volcanism: insights from volcanic gas observations. Chem. Geol. 263, 99–109 (this issue). doi:10.1016/ j.chemgeo.2008.08.022.

- Aiuppa, A., Bellomo, S., D'Alessandro, W., Federico, C., Ferm, M., Valenza, M., 2004c. Volcanic plume monitoring at Mount Etna by diffusive (passive) sampling. J. Geophys. Res. 109, D21308. doi:10.1029/2003JD004481.

- Aiuppa, A., Federico, C., 2004. Anomalous magmatic degassing prior to the 5th April 2003 paroxysm on Stromboli. Geophys. Res. Lett. 31, L14607. doi:10.1029/2004GL020458.

- Aiuppa, A., Federico, C., Franco, A., Giudice, G., Gurrieri, S., Inguaggiato, S., Liuzzo, M., McGonigle, A.J.S., Valenza, M., 2005. Emission of bromine and iodine from Mount Etna volcano. Geochem. Geophys. Geosyst. 6, Q08008. doi:10.1029/2005GC000965.

- Aiuppa, A., Federico, C., Giudice, G., Guerrieri, S., Paonita, A., Valenza, M., 2004a. Plume chemistry provides insights into mechanisms of sulfur and halogen degassing in basaltic volcanoes. Earth Planet. Sci. Lett. 222, 469–483.

- Aiuppa, A., Federico, C., Paonita, A., Pecoraino, G., Valenza, M., 2002. S, Cl and F degassino as an indicator of volcanic dynamics: the 2001 eruption of Mount Etna. Geophys. Res. Lett. 29–11. doi:10.1029/2002GL015032.

- Alletti, M., Aiuppa, A., Baker, D.R., Freda, C., 2006. Fluid/melt partitioning coefficients of chlorine in basaltic melt. Geophys. Res. Abstr. 8 1607-7962/gra/EGU06-A-08823.

- Alletti, M., Baker, D.R., Freda, C., 2007. Halogen diffusion in a basaltic melt. Geochim. Cosmochim. Acta 71, 3570–3580.

- Alletti, M., Baker, D.R., Scaillet, B., Aiuppa, A., Moretti , R., Ottolini, L., Chlorine partitioning between a basaltic melt and H2O–CO2 fluids at Mount Etna. Chemical Geology 263 (2009) 37–50

- Arevalo R. J. and McDonough W. F. (2010) Chemical variations and regional diversity observed in MORB. Chem. Geol. 271, 70– 85.

- Arrowsmith, P., (1987) Laser ablation of solids for elemental analysis by inductively coupled

plasma mass spectrometry, Analytical Chemistry, 59: 1437-1444.

- Baker, D.R., Alletti, M., 2012, Fluid saturation and volatile partitioning between melts and hydrous fluids in crustal magmatic systems: The contribution of experimental measurements and solubility models: Earth-Science Reviews 114 (2012) 298–324

- Baker, D.R., Balcone-Boissard, E., 2009. Halogen diffusion in magmatic systems: our current state of knowledge. Chem. Geol. 263, 82–88 (this issue). doi:10.1016/ j.chemgeo.2008.10.010.

- Balcone-Boissard, H., Villemant, B., and Boudon, G., 2010, Behavior of halogens during the degassing of felsic magmas: Geochemistry Geophysics Geosystems, v. 11, doi:10.1029/2010GC003028.

- Becker, J.S., Pickhardt, C. and Dietze, H.-J., 2000. Laser ablation inductively coupled plasmamass spectrometry for determination of trace elements in geological glasses. MikrochimicaActa, 135: 71-80.

- Bertagnini A, Métrich N, Francalanci L, Landi P, Tommasini S, Conticelli S (2008) Volcanology and magma geochemistry of the present-day activity: constraints on the feeding system. In: Learning from Stromboli.

- Bertagnini, A., Métrich, N., Landi, P., Rosi, M., 2003. Stromboli volcano (Aeolian Archipelago, Italy): an open window on the deep feeding system of steady state basaltic volcano. J. Geophys. Res. 108, 1–15.

- Bobrowski, N., Hönninger, G., Galle, B., Platt, U., 2003. Detection of bromine monoxide in a volcanic plume. Nature 423, 273–276.

- Bobrowski, N., von Glasow, R., Aiuppa, A., Inguaggiato, S., Louban, I., Ibrahim, O.W., Platt, U., 2007. Reactive halogen chemistry in volcanic plumes. J. Geophys. Res. 112, D06311. doi:10.1029/2006JD007206.

- Boichu, M., Oppenheimer, C., Roberts, T.J., Tsanev, V., Kyle, P., 2011. On bromine, nitrogen oxides and ozone depletion in the tropospheric plume of Erebus volcano (Antarctica). Atmospheric Environment 45, 3856–3866.

- Bureau, H., Foy, E., Raepsaet, C., Somogyi, A., Munsch, P., Simon, G., Kubsky, S., 2010. Bromine cycle in subduction zones through in situ Br monitoring in diamond anvil cells. Geochimica et Cosmochimica Acta 74, 3839–3850.

- Bureau, H., Keppler, H., Metrich, N., 2000. Volcanic degassing of bromine and iodine: experimental fluid/melt partitioning data and applications to stratospheric chemistry. Earth. Planet. Sci. Lett 183, 51–90.

- Bureau, H., Keppler, H., Métrich, N., 2000. Volcanic degassing of bromine and iodine: experimental fluid/melt partitioning data and applications to stratospheric chemistry. Earth and Planetary Science Letters 183, 51–60.

- Bureau, H., Metrich, N., 2003. An experimental study of bromine behaviour in watersaturated silicic melts. Geochim. Cosmochim. Acta 67, 1689–1697.

- Bureau, H., Métrich, N., 2003. An experimental study of bromine behaviour in watersaturated silicic melts. Geochimica et Cosmochimica Acta 67, 1689–1697.

- Burgess, R., Layzelle, E., Turner, G., and Harris, J.W., 2002, Constraints on the age and halogen composition of mantle fl uids in Siberian coated diamonds: Earth and Planetary Science Letters, v. 197, p. 193–203, doi:10.1016/S0012-821X (02)00480-6.

- Chen, Z.X, Doherty, W., and D.C. Gregoire (1997) Application of laser sampling microprobe inductively coupled plasma mass spectrometry to the in situ trace element analysis of selected geological materials, Journal of Analytical Atomic Spectrometry, 12: 653-659.

- Craig, C.A., Jarvis, K.E. and Clarke, L.J., 2000. An assessment of calibration strategies for the quantitative and semi-quantitative analysis of calcium carbonate matrices by laser ablationinductively coupled plasma-mass spectrometry (LA-ICP-MS). Journal of Analytical Atomic Spectrometry, 15: 1001-1008.

- Cromwell, E.F. and Arrowsmith, P., 1995. Semiquantitative Analysis with Laser Ablation Inductively Coupled Plasma Mass Spectrometry. Analytical Chemistry, 67: 131-138.

- D'Oriano, C., Da Pelo, S., Podda, F., Cioni, R., Laser-Ablation Inductively Coupled Plasma Mass Spectrometry (LA-ICP-MS): setting operating conditions and instrumental performance. Per. Mineral. (2008), 77, 3, 65-74

- Deruelle B., Dreibus G. and Jambon A. (1992) Iodine abundances in oceanic basalts: implications for Earth dynamics. Earth Planet. Sci. Lett. 108, 217–227.

- Di Carlo, I., Pichavant, M., Rotolo, S.G., Scaillet, B., 2006. Experimental crystallization of a high-K arc basalt: the Golden Pumice, Stromboli Volcano (Italy). J. Petrol. 47, 1317–1343.

- Ducreux-Zappa, M., and J.-M. Mermet (1996) Analysis of glass by UV laser ablation inductively coupled plasma atomic emission spectrometry. Part1. Effects of the laser parameters on the amount of ablated material and the temporal behaviour of the signal for different types of laser, Spectrochimica Acta, 51B: 321-332.

- Durrant, S.F. (1999) Laser ablation inductively coupled plasma mass spectrometry achievmenets, problems, prospects. Journal of Analytical Atomic Spectrometry 14, 1385-1403.

- Finnegan, D.L., Kotra, J.P., Hermann, D.M., Zoeller,W.H., 1989. The use of 7LiOH-impregnated filters for the collection of acidic gases and analysis by instrumental neutron activation analysis,. Bull. Volcanol. 51, 83–87.

- Francalanci, L., Tommasini, S. & Conticelli, S. (2004). The volcanic activity of Stromboli in the 1906^1998 period: mineralogical, geochemical and isotope data relevant to the understanding of Strombolian activity. Journal of Volcanology and Geothermal Research 131, 179^211.

- Fryer, S.E. Jackson B.J. and H.P. Longerich (1995) The design, operation and role of the laserablation microprobe coupled with an inductively coupled plasma-mass spectrometer (LAMICP- MS) in the Earth Sciences, Canadian Mineralogist, 33: 303-312.

- Gerlach, T.M., 2004. Volcanic sources of tropospheric ozone-depleting trace gases. Geochem. Geophys. Geosyst. 5, Q09007. doi:10.1029/2004GC000747

- Gerlach, T.M., Graeber, E.J., 1985. Volatile budget of Kilauea Volcano. Nature 313, 273–277.

- Gunther, D. and Heinrich C.A. (1999a) Enhanced sensitivity in laser ablation-ICP mass spectrometry using helium-argon mixtures as aerosol carrier. Journal of Analytical Atomic Spectrometry 14, 1363-1368.

- Gunther, D, H.P. Longerich, S.E. Jackson and L. Forsythe (1996) Effect of sample orifice on dry plasma inductively coupled plasma mass spectrometry (ICPMS) background, sensitivities and limit of detection using laser ablation sample introduction, Fresinius Journal of Analytical Chemistry, 355: 771-773.

- Gunther, G., Audetat, A., Frischknecht R., and Heinrich C., A. (1998) Quantitative analysis of major, minor and trace elements using laser ablation inductively coupled plasma mass spectrometry, Journal of Analytical Atomic Spectrometry, 13: 263-270.

- Gunther, D., Horn, I. and Hattendorf, B., 2000. Recent trends and evelopments in laser ablation- ICP-Mass Spectromety. Fresenius J. Anal. Chem., 368: 4-14.

- Halmer, M.M., Schmincke, H.U., Graf, H.F., 2002. The annual volcanic gas input into the atmosphere, in particular into the stratosphere: a global data set for the past 100 years. Journal of Volcanology and Geothermal Research 115, 511–528.

- Heinrich, C.A., Pettke, T., Halter, W.E., Aigner-Torres, M., Audetat, A., Gunther, D., Hattendorf, B., Bleiner, D., Guillong, M., Horn, I., 2003. Quantitative Multi-Element Analysis of Minerals, Fluid and Melt Inclusions by Laser-Ablation Inductively-Coupled-Plasma Mass-Spectrometry. Geochimica et Cosmochimica Acta 67, 3473–3497.

- Iacono-Marziano, G., Paonita, A., Rizzo, A., Scaillet, B., Gaillard, F., 2010. Noble gas solubilities in silicate melts: new experimental results and a comprehensive model of the effects of liquid composition, temperature and pressure. Chemical Geology 279, 145–157.

- Jacques Roux, J., and Lefevre, A., A fast-quench device for internally heated pressure vesselsEur J Mineral, April 1992, v. 4, p. 279-281

- Jambon, A., Deruelle, B., Dreibus, G. and Pineau, F., 1995. Chlorine and bromineabundance in MORB: The contrasting behaviour of the Mid-Atlantic Ridgeand East Pacific Rise and implications for chlorine geodynamic cycle. Chem.Geol., 126(2): 101-117.

- Kamenetsky V. S. and Kamenetsky M. B. (2010) Magmatic fluids immiscible with silicate melts: examples from inclusions in phenocrysts and glasses, and implications for magma evolution and metal transport. Geofluids 10, 293–311.

- Kamenetsky V., Clocchiatti R., (1996). Primitive magmatism of Mt. Etna: insights from

mineralogy and melt inclusions. Earth Planet. Sci. Lett. 142, 553 - 572.

- Kelly, P.J., Kern, C., Tjarda, R.J., Lopez, T., Werner C., Aiuppa A., Rapid chemical evolution of tropospheric volcanic emissions from Redoubt Volcano, Alaska, based on observations of ozone and halogen-containing gases (2012). Journal of Volcanology and Geothermal Research Volume 259, 1 June 2013, Pages 317–333

- Kendrick M. A. (2012) High precision Cl, Br and I determinations of mineral standards using the noble gas method. Chem. Geol., doi:10.1016/j.chemgeo.2011.11.021.

- Kendrick M. A., Scambelluri M., Honda M. and Phillips D. (2011) High abundances of noble gas and chlorine delivered to the mantle by serpentinite subduction. Nat. Geosci, 4, 807–812.

- Kendrick, M.A., Kamenetsky, V.S., Phillips, D., Honda, M., 2012. Halogen systematics (Cl, Br, I) in Mid-Ocean Ridge Basalts: A Macquarie Island case study. Geochimica et Cosmochimica Acta 81 (2012) 82–93

- Kendrick, M.A., D. Woodhead, J., S. Kamenetsky V., Tracking halogens through the subduction cycle. Geology, published online on 18 September 2012 as doi:10.1130/G33265.1

- L. Kinsley, J.M.G. Shelley and S.M. Eggins (1997) Processes affecting laser ablation sampling of materials for analysis by ICP-MS, RSES - Annual report, 137.

- Lee, C., Kim, Y.J., Tanimoto, H., Bobrowski, N., Platt, U., Mori, T., Yamamoto, K., Hong, C.S. 2005. High ClO and ozone depletion observed in the plume of Sakurajima volcano, Japan. Geophys. Res. Lett. 32, 21 809. doi:10.1029/2005GL023 785.

- Lesne, P., Scaillet, B., Pichavant, M., Iacono-Marziano, G., Beny, J.M.. The H2O solubility of alkali basaltic melts: an experimental study. Contrib Mineral Petrol DOI 10.1007/s00410-010-0588-x

- Longerich, H.P., S.E. Jackson, B.J. Fryer and D.F. Strong (1993) The laser ablation microprobe-inductively coupled plasma-mass spectrometer, Geoscience Canada, 20: 21-27.

- Malyshev, O.B., Cox, M.P., Design modelling and measured performance of the vacuum system of the Diamond Light Source storage ring. Vacuum 86 (2012) 1692e1696

- Mank, A.J.G. and P.R.D. Mason (1999) A critical assessment of laser ablation ICP-MS as an analytical tool for depth analysis in silica-based glass samples. Journal of Analytical Atomic Spectrometry 14, 1143-1153.

- Martin, J.B., Gieskes, J.M., Torres, M. Kastner, M., Bromine and iodine in Peru margin sediments and pore fluids: Implications for fluid origins, Geochim. Cosmochim. Acta 57 (1993) 4377^4389.

- Mather, T., Witt, M.L.I., Pyle, D.M., Quayle, B.M., Aiuppa, A., Bagnato, E., Martin., R.S., Sims, K.W.W., Edmonds, M., Sutton, A.J., Ilyinskaya, E.. Halogens and trace metal emissions from the ongoing 2008 summit eruption of Kīlauea volcano, Hawaii. Geochimica et Cosmochimica Acta, Volume 83, 15 April 2012, Pages 292-323.

- Menez, B., Philippot, P., Bonnin-Mosbah., M., A. Simionovici, F., Gibert. Analysis of individual fluid inclusions using Synchrotron X-Ray Fluorescence microprobe: progress toward calibration for trace elements. Geochimica et Cosmochimica Acta, Vol. 66, No. 4, pp. 561–576, 2002

- Metrich, N., Allard, P., Spilliardet, N., Andronico, D., Burton, M., 2004. 2001 flank eruption of the alkali- and volatile-rich primitive basalt responsible for Mount Etna's evolution in the last three decades. Earth Planet. Sci. Lett. 228, 1–17.

- Metrich, N., Bertagnini, A., Landi, P. & Rosi, M. (2001). Crystallisation driven by decompression and water loss at Stromboli volcano (Aeolian Islands). Journal of Petrology 42, 1471^1490.

- Métrich, N., Bertagnini, A., Landi, P., Rosi, M., 2001. Crystallization driven by decompression and water loss at Stromboli volcano (Aeolian Islands, Italy). J. Petrol. 42, 1471–1490.

- Métrich, N., Bertagnini, A., Landi, P., Rosi, M., Belhadj, O., 2005. Triggering mechanism at the origin of paroxysms at Stromboli (Aeolian Archipelago, Italy): The 5 April 2003 eruption. Geophys. Res. Lett. 32, L10305. doi:10.1029/2004GL022257.

- Métrich, N., Rutherford, M.J., 1992. Experimental study of chlorine behavior in hydrous silicic melts. Geochim. Cosmochim. Acta 56, 607–616.

Metrich, N., Allard, P., Bertagnini, A., Di Muro, A. Comment on 'Conduit convection, magma mixing, and melt inclusion trends at persistent degassing volcanoes' by Fred Witham, published in Earth Planetary Science Letters (2011) 301, 345–352. Earth and Planetary Science Letters, Volume 306, Issues 3–4, 15 June 2011, Pages 306-308

- Metzner, D., Kutterolf, S., Toohey, M., Timmreck , C., Niemeier, U., Freundt, A., Kruger, K., Radiative forcing and climate impact resulting from SO2 injections based on a 200,000-year record of Plinian eruptions along the Central American Volcanic Arc. Int J Earth Sci (Geol Rundsch) DOI 10.1007/s00531-012-0814-z

- Muramatsu, Y, Wedepohl, K.H., The distribution of iodine in the earth's crust, Chem. Geol. 147 (1998) 201^216.

- Muramatsu, Y., Fehn, U., Yoshida, S., Recycling of iodine in fore-arc areas: evidence from the iodine brines in Chiba, Japan. Earth and Planetary Science Letters 192 (2001) 583^593

- Newsom, H.E., 1995. Composition of the solar system, planetes, meteorites, and major terrestrial reservoirs. Global Earth Physics, A Handbook of Physical Constants, AGU Reference Shelf, vol. 1. American Geophysical Union, Washington.

- Oppenheimer, C., Tsanev, V.I., Braban, C.F., Cox, R.A., Adams, J.W., Aiuppa, A., Bobrowski, N., Delmelle, P., Barclay, J., McGonigle, A.J.S., 2006. BrO formation in volcanic plumes, Geochim. Cosmochim. Acta 70, 2935–2941.

- Palme, H. and O'Neill, H.S.C., 2003. Cosmochemical estimates or Mantle Composition. In: H. Holland and K.K. Turekian (Editors), Treatise on Geochemistry. Elsevier, New York, pp. 1-38.

- Paonita, A., Noble gas solubility in silicate melts: a review of experimentation and theory, and implications regarding magma degassing processes, ANNALS OF GEOPHYSICS, VOL. 48, N. 4/5, August/October 2005

- Perkins, W.T. Pearce N.J. and Jeffries T.E. (1993) Laser ablation inductively coupled plasma mass spectrometry: a new technique for the determination of trace and ultra-trace elements in silicates, Geochimica et Cosmochimica Acta, 57: 475-482.

- Perkins, W. T. & Pearce, N. J. G., 1995. Mineral microanalysis by laserprobe inductively

coupled plasma mass spectrometry. In: Potts, P. J., Bowles, J. F. W., Reed, S. J. B. & Cave, M. R. (eds.) Microprobe Techniques in the Earth Sciences. Chapman & Hall, London, pp. 291-3

- Pettke, T., Heinrich, C.A., Ciocan, A.C., Gu□nther, D., 2000. Quadrupole mass spectrometry and optical emission spectroscopy: detection capabilities and representative sampling of short transient signals from laser-ablation. Journal of Analytical Atomic Spectrometry 15 (9), 1149–1155.

- Pichavant, M., Di Carlo, I., Le Gac, Y., Rotolo, S. G. & Scaillet, B. (2009). Experimental constraints on the deep magma feeding system at Stromboli volcano, Italy. Journal of Petrology 50, 601^624, doi:10.1093/petrology/egp014.

- Ping, D., Halogen-element (F, Cl and Br) behaviour in apatites, scapolite, and sodalite: an experimental investigation with field applications. Unpub. Ph.D. diss., Univ. of Saskatchewan, 234 pp.

- Pyle, D.M, Mather, T.A, 2009, Halogens in igneous processes and their fluxes to the atmosphere and oceans from volcanic activity: A review: Chemical Geology 263 (2009) 110–121

- Pyle, D.M., and Mather, T.A., 2009, Halogens in igneous processes and their fl uxes to the atmosphere and oceans from volcanic activity: A review: Chemical Geology, v. 263, p. 110–121, doi:10.1016/j.chemgeo.2008.11.013.

- Roedder E., (1984). Fluid inclusions. Reviews Mineral. 12.

- Rosciglione A., Evidences of Enriched Mantle (EM-2) source contribution to Etnean magmas: a comprehensive study on fluid and melt inclusions of 2001-2006 eruptions. Unpub. Ph.D. diss., Univ. Di Palermo.

- Schilling, J.-G., Unni, C.K., Bender, M.L., 1978. Origin of chlorine and bromine in the oceans. Nature 273, 631–636.

- Schilling, J.G., Bergeron, M.B., Evans, R., 1980. Halogens in the mantle beneath the North Atlantic. Philosophical Transactions of the Royal Society of London A297, 147–178

- Schroeder, E., M. Hamester, and M. Kaiser (1998) Properties and characteristics of a laser ablation ICP-MS system for the quantitative elemental analysis of glasses. Applied Surface Science 129, 292-298.

- Seo, J.H., Guillong, M., Aerts, M., Zajacz, Z., Heinrich, C.A., 2011. Microanalysis of S, Cl, and Br in Fluid Inclusions by LA-ICP-MS. Chemical Geology 284, 35–44.

- Sheppherd T.J, and S.R. Chenery (1995) Laser ablation ICP-MS elemental analysis of individual fluid inclusions: An evaluation study, Geochimica Cosmochimica Acta, 59: 3997-4007.

- Shinohara, H., Ilyama, J.T., Matsuo, S., 1989. Partition of chlorine compounds between silicate melt and hydrothermal solutions: partition of NaCl–KCl. Geochim. Cosmochim. Acta 53, 2617–2630.

- Signorelli, S., Carroll, M.R., 2000. Solubility and fluid-melt partitioning of Cl in hydrous phonolitic melts. Geochim. Cosmochim. Acta 64, 2851–2862.

- Signorelli, S., Carroll, M.R., 2001. Experimental constraints on the origin of chlorine emissions at the Soufriere Hills volcano, Montserrat. Bull. Volcanol. 62, 431–440.

- Smith, J.V., 1981. Halogen and phosphorus storage in the Earth. Nature 289, 762–765.

- Spillaert, N., Metrich, N., Allard, P., 2006b. S–Cl–F degassing pattern of water rich alkali basalt: modelling and relationship with eruption styles of Mount Etna volcano. Earth Planet. Sci. Lett. 248, 772–786.

- Symonds, R.B., Rose, W.I., Bluth, G.S., Gerlach, T.M., 1994. Volcanic gas studies, methods, results and applications. Reviews in Mineralogy and Geochemistry 30, 1–66.

- Taylor, T. S.E. Jackson, H.P. Longerch and J.D. Webster (1997) In situ trace-element analysis of individual silicate melt inclusions by laser abaltion microprobe-inductively coupled plasma-mass spectrometry (LAM-ICP-MS), Geochimica et Cosmochimica Acta, 61: 2559- 2567.

- von Glasow, R., Bobrowski, N., Kern, C., 2009. The effects of volcanic eruption on atmospheric chemistry. J. Volcanol. Chem. Geol. 263, 131–142. doi:10.1016/

j.chemgeo.2008.08.020.

- Wallace, P.J., 2005. Volatiles in subduction zone magmas: concentrations and fluxes based on melt inclusion and volcanic gas data. Journal of Volcanology and Geothermal Research 140, 217–240.

- Webster, J.D., De Vivo, B., 2002. Experimental and modeled solubilities of chlorine in alumosilicate melts, consequences of magma evolution, and implications for the exsolution of hydrous chloride melt at Mt. Somma–Vesuvius. Am. Mineral. 87, 1046–1061.

- Webster, J.D., Kinzler, R.J., Mathez, A., 1999. Chloride and water solubility in basalt and andesite melts and implications for magmatic degassing. Geochim. Cosmochim. Acta 63, 729–738.

- Webster, J.D., Sintoni, M.F., De Vivo, B., 2009. The partitioning behavior of Cl, S, and H2O in aqueous vapor- ± saline liquid saturated phonolitic and trachytic melts at 200 MPa. Chem. Geol. 263, 19–36

- Wehrmann, H., 2005. Volatile degassing and plinian eruption dynamics of the mafic Fontana Tephra, Nicaragua. Unpub. Ph.D. diss., Univ. of Kiel, Germany, 125 pp.

- Witt, M.L.I., Fisher, T.P., Pyle, D.M., Yang, T.F., Zellmer, G.F. Fumarole compositions and mercury emissions from the Tatun Volcanic Field, Taiwan: Results from multi-component gas analyser, portable mercury spectrometer and direct sampling techniques. Journal of Volcanology and Geothermal Research, Volume 178, Issue 4, 30 December 2008, Pages 636-643.

- Yoon, Y.Y., Kim, T.S., Chung, K.S., Lee, K.Y. and Lee, G.H., 1997. Application of laser induced plasma spectroscopy to the analysis of rock samples. The Analyst, 122: 1223-1227.

Acknowledgements

Several people were of great help and support during the course of this study, without whom this thesis would not have been possible.

First of all, I wish to thank my tutor, Alessandro Aiuppa, for his limitless support and encouragement during these years.

I am deeply grateful also to my co-tutor Dr. Antonio Paonita for sharing his knowledge and scientific experience.

A great and special thanks is for Giada Iacono Marziano who patiently spent a lot of time with me during my period at the CNRS – ISTO of Orléans (France). I am also in debt with all the staff of the ISTO laboratories for hosting me, giving scientific supports and friendship (Bruno Scaillet, Marina Alletti, Ida Di Carlo and many others).

Credit is due to all those who helped with the analytical work:

- Lorenzo Brusca and Sergio Bellomo (INGV-Palermo) for their support during LA-ICP-MS analyses;
- Nicole Metrich (IGG – Paris) and Emanuela Gennaro (University of Palermo) for their precious help with melt inclusions;
- David Pyle, Tamsin Mather, Kim Berlo (Department of Earth Sciences – University of Oxford) and Tina Geraki (Diamond Light Source) for supporting me during Synchrotron analysis;

Also, I wish to thanks the whole staff of INGV of Palermo for the great opportunity they gave me to grow up in these years.

I am grateful also to all the professors of the DiSTeM of University of Palermo for the formation and influences they gave me before and during my research project.

And, for sure, strong thanks to my family and friends.